NTNU
Norwegian University of
Science and Technology

Use of Realistic Geomodels and Synthetic Ultra-Deep Directional Resistivity Inversion in the Pre-job Planning of a Horizontal Oil Production Well

Palak Arora

Petroleum Geosciences
Submission date: June 2016
Supervisor: Erik Skogen, IPT
Co-supervisor: Frank Antonsen, Statoil ASA

Norwegian University of Science and Technology
Department of Petroleum Engineering and Applied Geophysics

NTNU – Trondheim
Norwegian University of
Science and Technology

Use of Realistic Geomodels and Synthetic Ultra-Deep Directional Resistivity Inversion in the Pre-job Planning of a Horizontal Oil Production Well

Palak Arora

CONFIDENTIAL

June 2016

Supervisor: Erik Skogen, NTNU

Co-Supervisor: Frank Antonsen, Statoil ASA

Norwegian University of Science and Technology

Department of Petroleum Engineering and Applied Geophysics

ABSTRACT

The aim of this thesis is to test a workflow to improve subsurface understanding by building and updating realistic geomodels for a horizontal well in the Norwegian Continental Shelf (NCS). The focus is on pre-job planning for a well placement job based on logging while drilling (LWD) and surface seismic survey, where the ultra-deep electromagnetic (GeoSphere tool by Schlumberger) measurements link the LWD measurements to the seismic.

By using the Compound Earth Simulator (CES) software, developed by Statoil ASA, a set of realistic geomodel scenarios are constructed based on the offset well information, the existing geological concept and seismic data interpretation. The synthetic ultra-deep resistivity inversion images are generated, by forward and 1D inverse modelling, and are then studied for potential pre-drilling scenarios. This summarizes the pre-job planning phase.

These geomodels assist in the evaluation of the uncertainty before drilling. A better understanding of the subsurface and reservoir conditions by these pre-job models and their inversions, assist in the interpretation of features such as the top of reservoir, fluid contacts, flooding in layers and formation structures at the time of drilling and therefore, improve real time geosteering decisions. Any variations in the expected geological features that may be encountered at the time of drilling can be compensated for, more swiftly, with these pre-job models available on different scenarios. Thus, make the operations robust and achieve optimized well placement.

Acknowledgement

I would like to express my sincere gratitude to my supervisor, Erik Skogen, for his continuous support not only during this thesis work but also, throughout my two years in Norway.

I am very grateful to my co-supervisor, Frank Antonsen, Statoil ASA, for introducing me to the deep directional electromagnetic measurements. His expertise, understanding, generous guidance and support made it possible for me to work on this topic.

I sincerely thank Maria Emilia Teixeira De Oliveira and Per Atle Olsen for their continuous guidance and cooperation throughout the duration of this project.

I would like to acknowledge Gunnar Digranes, Hans Petter Normann, Kristine Hermanrud, Odd Arve Solheim, Steen Agerlin Petersen, Stein Ottar Stalheim, the ST RCM department at Statoil ASA and Abby Han Men, Dzevat Omeragic, Jean Seydoux and Valery Polyakov at Schlumberger, for their inputs, encouragement and insightful comments at various stages in this project.

I would also like to thank the Norwegian University of Science and Technology and Statoil ASA for giving me the opportunity to carry this research.

This would not have been possible without the support of my family and friends who are the pillars of strength in my life.

Table of Contents

List of Figures

Abbreviations

1D	One Dimensional
2D	Two Dimensional
3D	Three Dimensional
BCU	Base Cretaceous Unconformity
BHA	Bottom Hole Assembly
CDP	Common Depth Point
CES	Compound Earth Simulator
DOI	Depth of Investigation
EM	Electromagnetic
Fm	Formation
GOC	Gas-Oil Contact
GR	Gamma Ray
kHz	Kilo Hertz
LWD	Logging while Drilling
m	meter
MD	Measured Depth
MSL	Mean Sea Level
NCS	Norwegian Continental Shelf

NPHI	Neutron Porosity Log
NTNU	Norwegian University of Science and Technology
Ohmm	Ohm meter
OWC	Oil-Water Contact
Ref	Reference
RHOB	Bulk Density Log
Rt	True Formation Resistivity
Sc.	Scenario
Sw	Saturation of water
T-R	Transmitter-Receiver
TVD	True Vertical Depth
TVDSS	True Vertical Depth Subsurface
TWT	Two-way Travel time
UB-LB	Upper Brent – Lower Brent

1 Introduction

This technical work was carried out as a part of the course curriculum of the Masters in Petroleum Geoscience course at the Department of Petroleum Engineering and Applied Geophysics, Norwegian University of Science and Technology (NTNU), Norway. It was carried out in cooperation with the Statoil Research Centre in Trondheim, Norway.

The objective of this thesis is to test a workflow for building and updating realistic geomodels along a highly deviated wellbore. It is based on logging while drilling (LWD) and surface seismic survey, where the ultra-deep electromagnetic measurements play a key role to link LWD-measurements to larger scale structures and, therefore, also seismic. These deep measurements provide reservoir scale imaging during drilling and therefore a more extensive understanding of the reservoir is possible.

The geomodels assist in the evaluation of the uncertainty in the area. By creating various geomodel scenarios, proper planning for geosteering and well placement can be achieved.

The focus in this thesis is detailed pre-job planning for a well placement job. The pre-job planning phase involves the development of a set of realistic geomodel scenarios based on the offset well information, the existing geological concept and seismic data interpretation. This is done by using the Compound Earth Simulator[1] (CES) software.

[1] for more explanation of the software, refer chapter 4

A synthetic ultra-deep resistivity inversion image is generated for each realistic geomodel by using the WebGS[2] software. This resistivity profile is studied for potential pre-drilling scenarios, and with variations in the realistic geomodel other anticipated scenarios can be tested. These have been discussed in detail.

The work was carried out for a particular well placement job in the Visund-asset on the Norwegian Continental Shelf (NCS). A similar workflow has been tested on a couple of wells and is still under development.

This study will highlight the importance of the pre-job planning phase. Pre-job planning phase geomodel scenarios provide information on the geological conditions that may be encountered during drilling. A study and analysis of potential scenarios can make the operations more robust. It will keep the drilling team prepared for multiple scenarios that they may face at the time of drilling. Hence it will assist in faster decision making and optimized well placement.

The results from the semester thesis titled *Software Simulations of an Ultra Deep Resistivity Tool using Synthetic Geo-models, December 2015, NTNU* have also been used in this study to interpret the resistivity inversion profiles (Arora P., 2015).

It is important to have a good understanding of the background information available, related to the task, and of the previous study done in the area. This marks the importance of a good literature study and therefore Information Retrieval has been discussed in a chapter in the Appendix.

[2] for more explanation of the software, refer chapter 4

Chapters 2 and 3 give background information about the geology of the Visund field, the stratigraphic column and information about the well A-16 H to be drilled. Subsequent chapters explain the used software, the methodology and various scenarios for this study, ending with the results, discussions and conclusions.

The workflow followed during pre-job planning phase is given in figure 1.

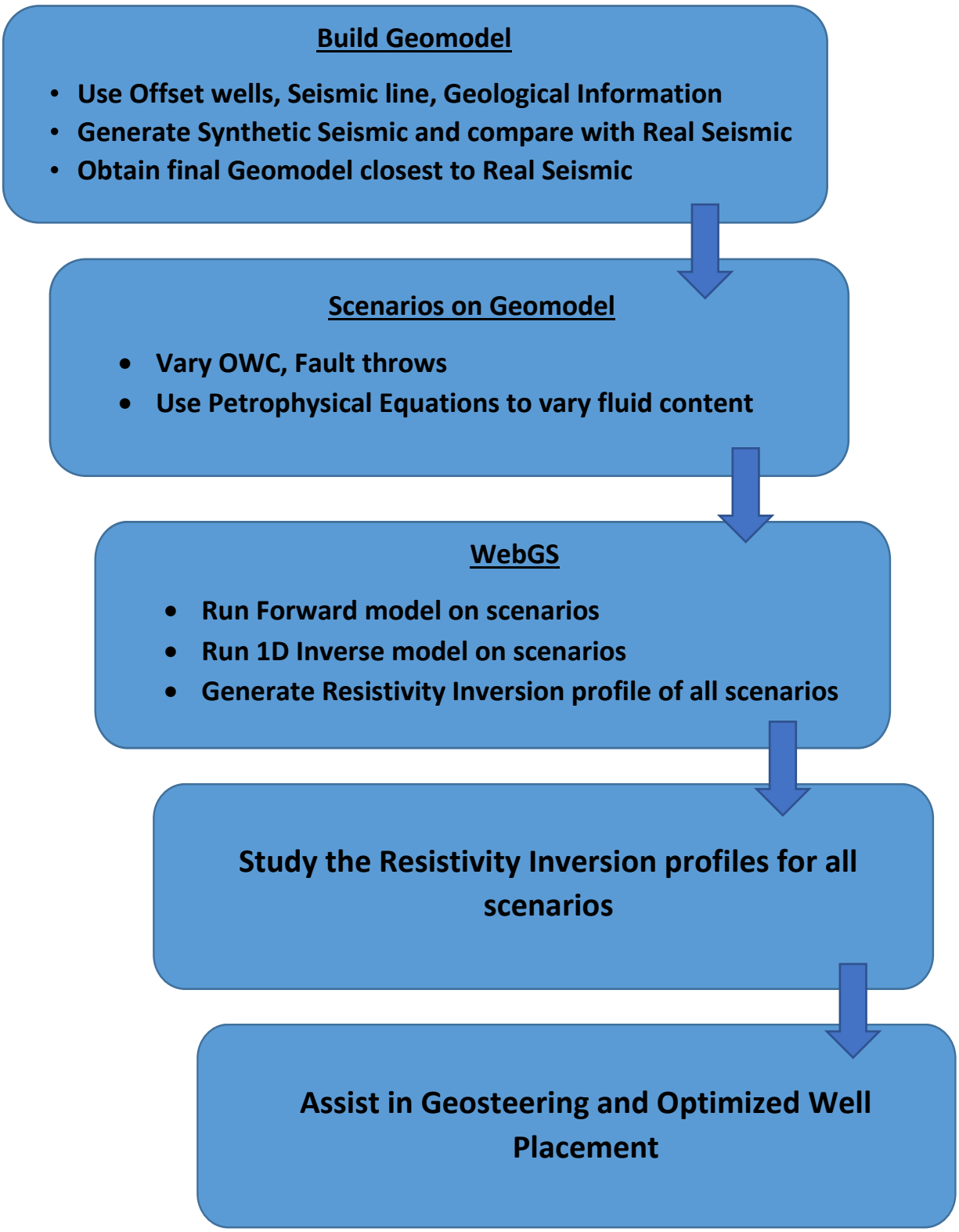

Figure 1: *Conceptual workflow, for the pre-job planning phase (as followed in this study)*

2 Background of the Visund field

The Visund field is an oil field located to the east of the Snorre field and lies in the northern part of the North Sea on the eastern flank of the Tampen Spur region (figure 2). The Visund field contains oil and gas in several tilted fault blocks. The pressure and liquid systems are varying. The reservoirs are in the Middle Jurassic sandstones in the Brent Group and Lower Jurassic and Upper Triassic sandstones in the Statfjord and Lunde Formations (Norsk Petroleum AS).

The depth to the Brent reservoir is approximately 2900 m from the MSL. The oil column is 40 m - 100 m and the gas column is 110 m. The water depth is about 335 m (Offshore Technology).

The production from the Visund field started on April 21st, 1999 (Statoil ASA). Oil in the Brent reservoirs is mainly produced by pressure maintenance from gas injection and water injection (Norsk Petroleum AS).

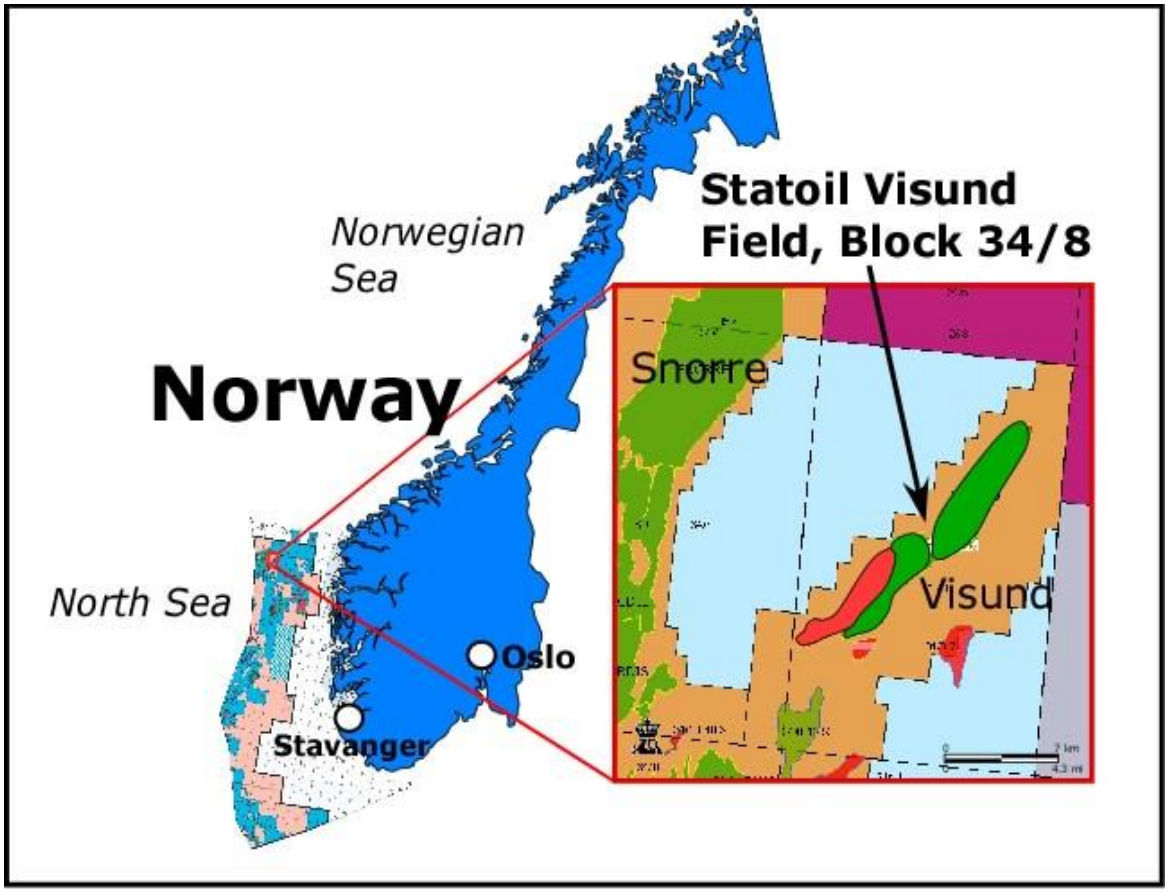

Figure 2: *Map showing the location of the Visund field (Statoil ASA)*

2.1 Geological Background

The northern North Sea is a rift basin, which stretches from the East Shetland Platform to the Øygarden Fault Zone, covering an area of about 40,000 km^2. It includes three main regions (figure 3), the East Shetland Basin and Tampen Spur in the west, the North Viking Graben and the Horda Platform in the east (Glennie and Underhill, 1998).

The North Sea rift basin is itself part of the north-west European continental shelf. The basin is characterized by a prolonged history of extension that began in the Devonian with the extension of the thickened crust formed during the Caledonian Orogeny (Zanella and Coward, 2003). Subsequently, the basin was subjected to Permo-Triassic and mid-late Jurassic intracontinental lithospheric extensional phases, which were followed by thermal subsidence and cooling to produce the North Sea Sedimentary Basin (Færseth et al. 1997). These two extensional events have mainly resulted in the present-day structural configuration of the North Sea (Zanella and Coward, 2003).

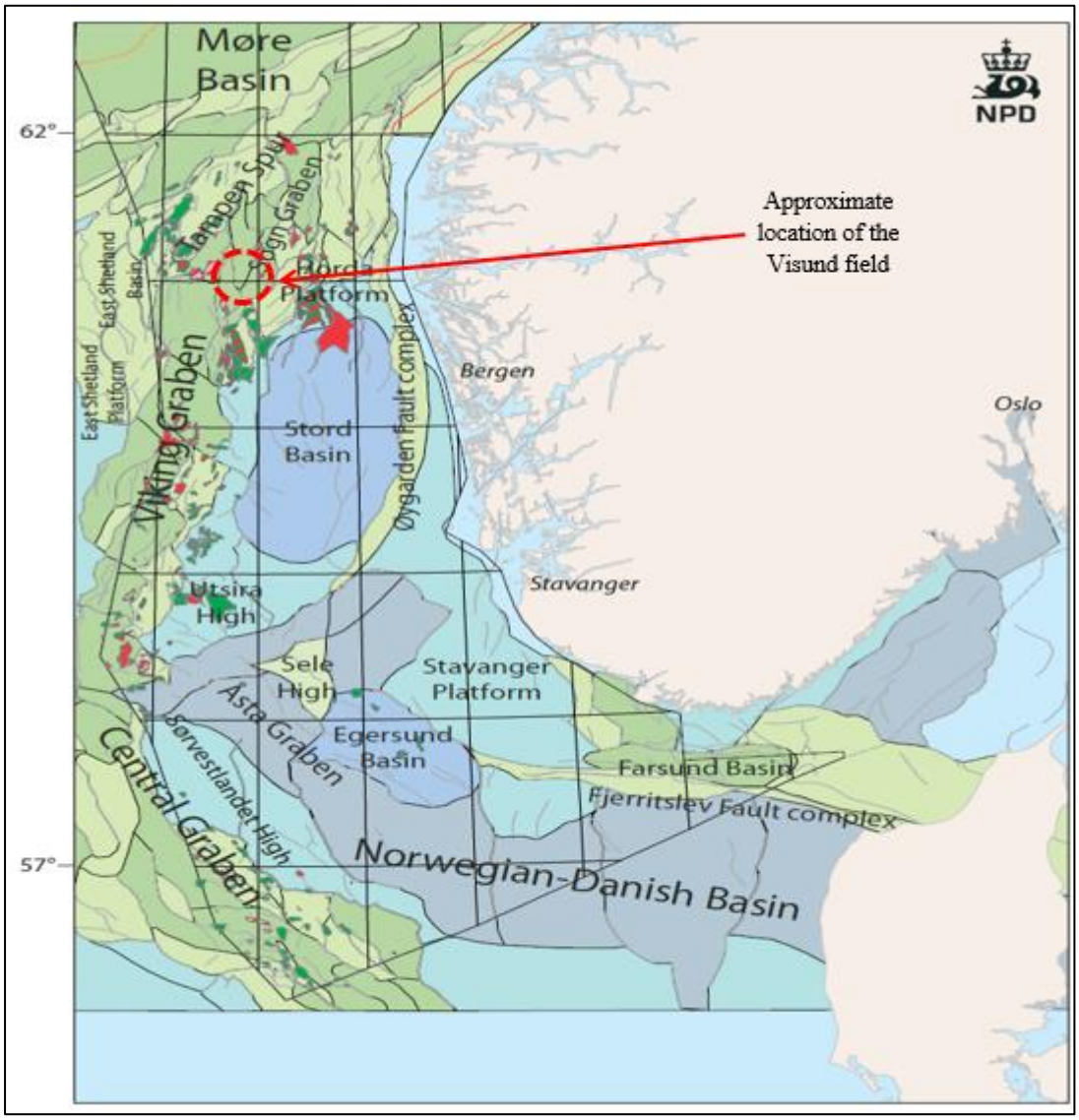

Figure 3: *Geological Map of the Northern North Sea (www.npd.no)*

The Visund field is located in the northern part of the North Sea on the eastern flank of the Tampen Spur region. In the northern Tampen area, lower shoreface deposits have been interpreted to occur in front of wave dominated upper shoreface deposits. To the South of these upper shoreface deposits, a southwest to northeast oriented, laterally extensive bay-fill succession is interpreted.

These were deposited from Early to Middle Jurassic period. The facies associations in the Visund field represent a variety of shallow marine, marginal marine and non-marine environments that may be classified into wave dominated shoreline, back barrier lagoonal and delta plain deposits (Visund field study, Statoil ASA).

2.2 Stratigraphic Column

A part of the stratigraphic column of the Visund field mainly focussing on the Viking, Brent, Dunlin, Statfjord and Lunde Groups is shown in figure 4. Some of these groups have been discussed in detail in the following sections.

2.2.1 The Lunde Group

The Lunde formation is a fluvial deposit. It is dominated by relatively thick floodplain and meandering and sinuous channels with limited lateral and vertical connectivity. There is an uncertainty in the prediction of sand bodies and paleosols and coal deposits are found (Concept Selection Report, Statoil ASA).

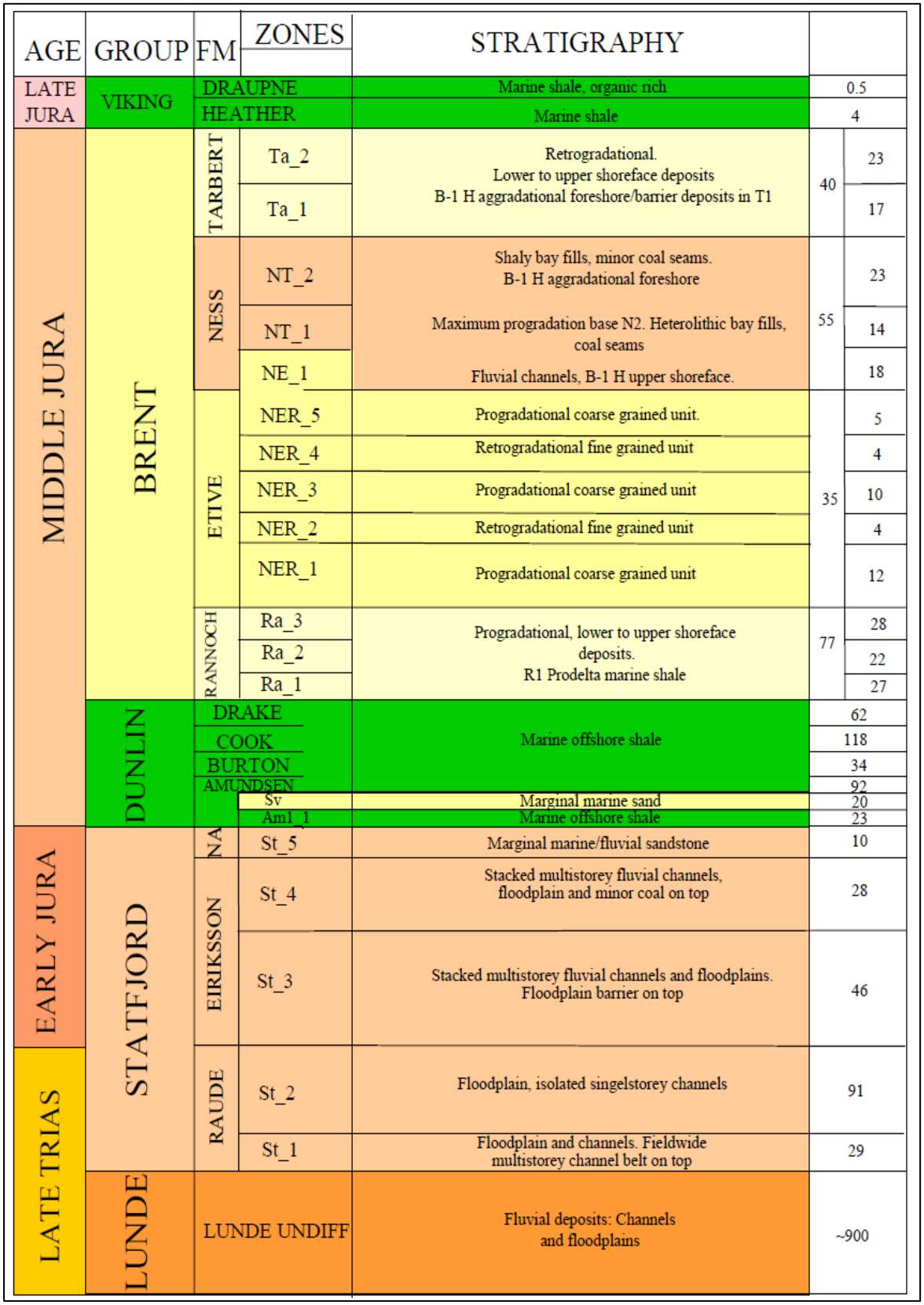

Figure 4: *Stratigraphy information of the Visund field (Statoil ASA)*

2.2.2 The Statfjord Group

The depositional environment is similar to the Upper Lunde formation for the Lower Statfjord formation. There exists limited communication and uncertainty in the prediction of sand bodies.

The Upper Statfjord formation is characterised by amalgamated channels and relatively thin floodplains. It demonstrates good reservoir properties with good lateral reservoir connectivity. Minor coal depositions are also present (Concept Selection Report, Statoil ASA).

2.2.3 The Dunlin Group

In the Visund field, the sandstones and lean marine shales of the Dunlin Group overlies the Statfjord Formation. It consists of the Amundsen, a thin Burton, Cook and Drake formations. The Dunlin group is mainly composed of thin and lean marine shales and marginal marine sand (Faleide et al., 2010).

2.2.4 The Brent Group

A variation in the sediment types overlying flooding surfaces is common in the Visund field and reflects the proximal (south) to distal (north) facies relationship in this field (Brent Study, Statoil ASA).

The Rannoch formation comprises of a single, upward shallowing wave dominated shoreface succession overlain by distributary mouthbar deposits. The succession is thick and has no major flooding surfaces and indicates normal regression under rising relative sea level conditions. But the abrupt influx of medium grained sandstones in the overlying Etive distributary mouthbar and tidal inlet succession is sharp implying forced regression under conditions of falling relative sea level. The Rannoch-Etive succession has northwards oriented sediment transport routes and shoreline progradation directions as indicated by the lateral facies variability and northwards thinning of mouthbar deposits (Brent Study, Statoil ASA).

The Ness formation is dominated by lagoonal and bay fill deposits present towards the southern part of the field. These overlie coal seams. The water depth at the time of deposition has deepened northwards into distributary channels to wave dominated shorefaces belonging to the Etive formation. An east-west oriented coastline existed during this time. The upper Ness is bounded by the development of a regionally extensive lagoon overlying a widespread coal. The top of this unit corresponds to a major transgressive surface at the base of the Tarbert formation.

An abrupt change from lagoonal and bay fill deposits below to a wave dominated lower shoreface and barrier deposits above in the Tarbert is observed. The Tarbert formation consists of a gradually coarsening upward shoreface system and east-west coastline orientation (Brent Study, Statoil ASA).

The progradational and retrogradational development of the Brent delta in the North Sea represents the depositional model for the Brent Group on Visund. The retrogradational phase forms the Upper Brent Group which includes the Upper Ness and the Tarbert Formations. The progradational phase forms the Lower Brent Group which includes the Lower Ness, Etive and Rannoch Formations (Brent Study, Statoil ASA). A summary of this stratigraphic framework is given in figure 4.

2.2.5 The Viking Group

The late Jurassic was characterized by subsidence, rotation and erosion of tilted fault blocks in the Viking Graben (Fraser et al., 2002). Transgression at the same time covered the graben with a thick drape of organic rich argillaceous sediments. These sediments became the Viking Group. The lower and upper shale members are referred to as the Heather and Draupne Formations respectively (Vollset and Dore, 1984).

2.2.6 The Cromer Knoll Group

The latest phase of rifting and erosion of uplifted fault blocks in the late Jurassic-early Cretaceous was followed by a major rise in sea level across the North Sea. Subsequently, Cretaceous sediments were deposited unconformably on late Jurassic sediments of the North Sea. This major unconformity between the Jurassic and Cretaceous is called the Base Cretaceous Unconformity (BCU).

In the northern North Sea, the Lower Cretaceous deposits comprise shallow marine mudstones, calcareous shales and some sands. These belong to the Cromer Knoll Group. These are deposited on top of the Viking group formations.

2.2.7 The Shetland Group

The sea level attained its maximum in the Late Cretaceous and clastic sedimentation ceased. Planktonic carbonate algae then mainly dominated sedimentation. In the Viking Graben area, the carbonates are impure and have been replaced by marls. The Upper Cretaceous comprises mudstones and minor interbedded limestones of the Shetland Group (Adda, W. G., 2012). In the upper part, these limestones are thicker and more frequent, and their thickness and frequency of occurrence, decreases with depth (Concept Selection Report, Statoil ASA).

3 Description of Well 34/8-A-16 H

The work carried out in this thesis is for a particular well placement job in the Visund asset on the NCS. This is the Well 34/8-A-16 H. It was drilled before the commencement of this work. It was a horizontal wellbore trajectory targeting the Brent group in the eastern flank of the Visund field.

3.1 Location

The Brent reservoir in the Visund field comprises three main segments, N1, S1 and N2 (figure 5). These segments represent areas of different reservoir fluid properties and contact relations. The N1 segment has proved to contain oil. The segments are further divided into sub-segments used for volume calculation, e.g. N1A, N1B etc. (Concept Selection Report, Statoil ASA).

The Brent target comprises up to 4 potential stratigraphic reservoirs; the Upper Brent Group in the N1B segment, the Lower Brent Group in N1B, the Upper Brent Group in the N1A segment and the main target with the Lower Brent Group in the N1A segment (Concept Selection Report, Statoil ASA).

N1 is a rotated fault block, down-faulted from the S1 block. The N1A segment is located south of N2 segment and east of N1B segment (Concept Selection Report, Statoil ASA). The well 34/8-A-16 H was planned to be an oil producer from the Brent group in the N1A segment (figure 5).

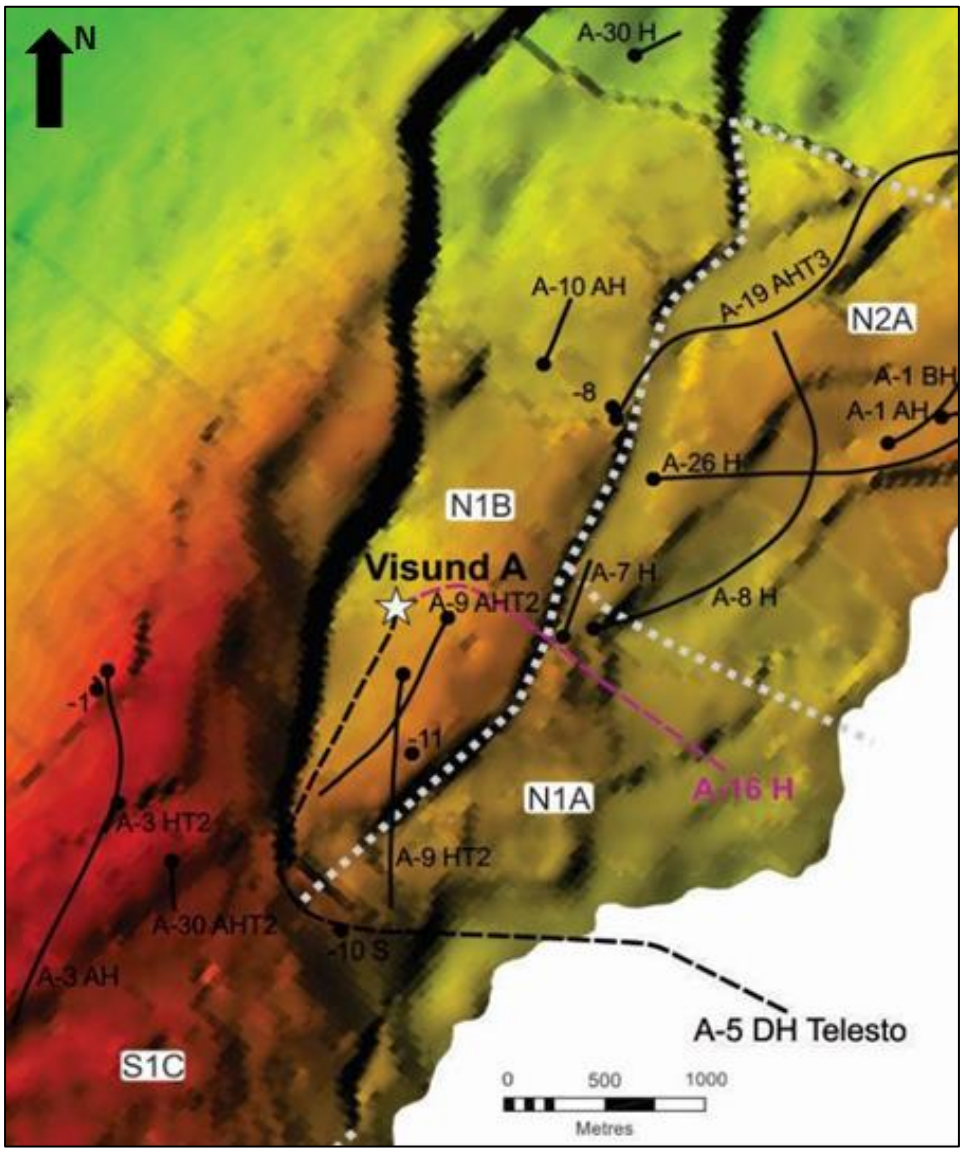

Figure 5: *Map showing location of well A-16 H (Statoil ASA)*

3.2 Well Objective

The main objective of this well was to drill into the Etive formation in the Lower Brent group.

Optimal well placement in relation to fluid contacts was of most importance to maintain a distance, about 7 m, above the oil-water contact.

Another important objective was to keep far from the Draupne (Shale) formation above the Brent group and avoid drilling into it.

Due to these constraints, it was decided to use the deep directional electromagnetic measurements for pro-active geosteering. Apart from the GeoSphere[3] tool, normal LWD measurement tools were also present in the Borehole assembly.

3.3 Deep Directional Resistivity Measurements

The deep directional resistivity tool called GeoSphere was used in this well to map the reservoir top and oil-water contact and to help in well placement in the Lower Brent.

[3] commercial name for the Ultra-Deep reading Resistivity LWD tool by Schlumberger

GeoSphere is an ultra-deep reading resistivity tool developed by Schlumberger. This tool provides reservoir scale imaging while drilling and therefore a more extensive understanding of the reservoir is possible. The main well placement applications for this technology include optimized landing, reduction of pilot wells, horizontal well placement in multilayer reservoirs, refinement of the surface seismic interpretation, and extensive updating of the reservoir model (Seydoux J., et. al, 2014).

The main features of this tool are, depth of investigation in excess of 30 m, deep directional electromagnetic measurements with 3D sensitivity, multi-frequency measurements (six frequencies from 2 kHz to 96 kHz) to accommodate a wide variety of formation resistivities, real time automated stochastic inversions and modular system design tailored for multiple applications (Seydoux J., et. al, 2014).

Very deep azimuthal measurements require multi-spacing and multi-frequency measurements. The DOI is primarily proportional to the distance between the transmitter and receiver antennas and depends on the signal frequency. The tool architecture consists of systems of tilted antenna spaced along a LWD BHA. The tool is configurable with up to three spacings (figure 6). Using the rotation of the tool, nine elementary components (xx, xy, xz, yy, yx, yz, zz, zx, zy) are extracted and combined to produce four types of calibrated phase shift and attenuation measurements. The symmetrized directional measurement is primarily sensitive to boundary proximity. The tilted antenna pair architecture is different from the standard industry LWD propagation or induction resistivity tools consisting of two receivers.

For maximum DOI in low resistivity, a low frequency range is required, i.e. landing in a reservoir with overlying conductive shale. And, the high frequency range is more appropriate for high-resistivity reservoirs and also short spacing measurements that have low DOI (Seydoux J., et. al, 2014).

The results from the semester thesis titled *Software Simulations of an Ultra Deep Resistivity Tool using Synthetic Geo-models, December 2015, NTNU* may also be referred to, to understand the dependence of the depth of investigation of this tool with respect to the resistivity, variation in geology and variations in the frequencies that the tool operates upon (Arora P., 2015).

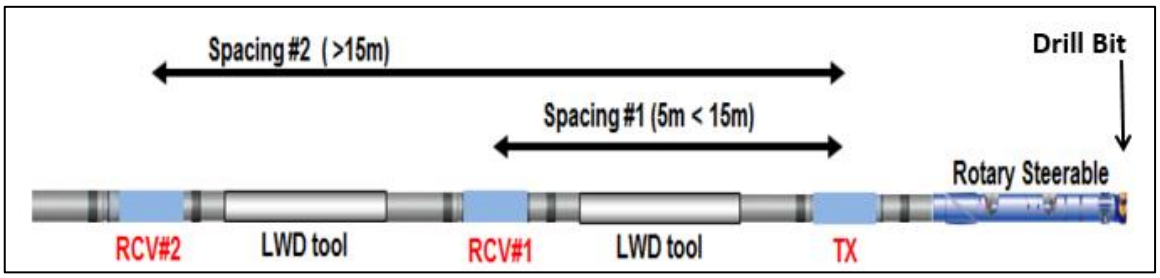

Figure 6: *Tool configuration of the GeoSphere tool which is configurable up to 3 receivers, 2 receivers configuration is shown in this figure (Seydoux J., et.al, 2014)*

3.4 Other information available

The exploration wells, available for this study, in the region are 34/8-1, 34/8-8 and 34/8-11. Well tops, measured depth, TVD, TVDSS, TWT, Easting and Northing coordinates are available from these wells. They also contain the Density, Gamma Ray, Neutron and Resistivity log data.

Two production wells in the region are 34/8-A-7 H and 34/8-A-9 HT2.

A Seismic line in depth (figure 7) is available with information about the estimated regional Gas-Oil contact depth, regional Oil-Water contact depth, faults and horizons. The regional oil-water contact is found at 2944 m and therefore it is expected to be at around 2944 m TVD in the area where this well is planned to be drilled.

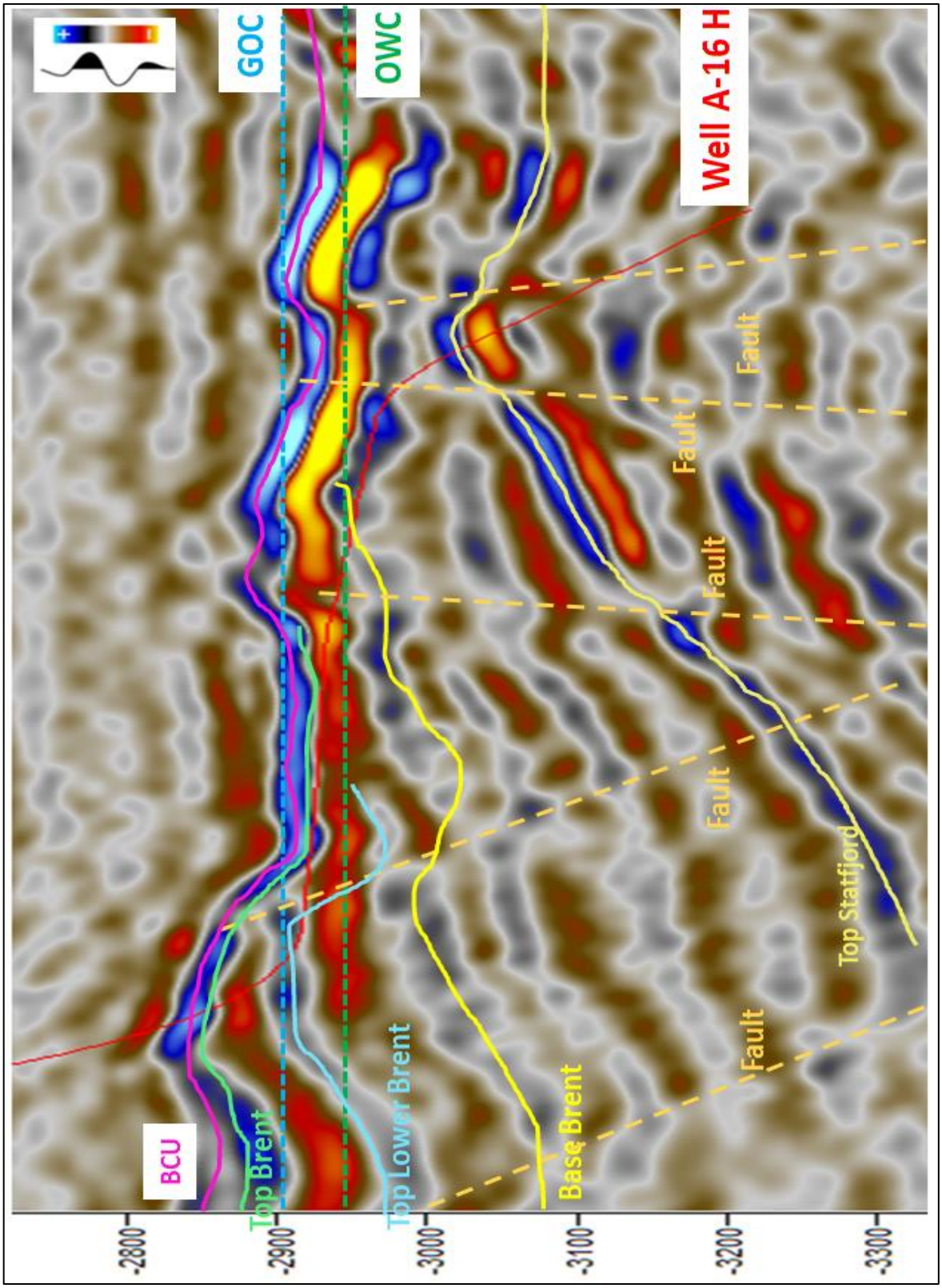

Figure 7: *Seismic Section showing Top and Lower Brent, Statfjord, GOC and OWC positions, Fault locations and Well A-16 H planned trajectory (Statoil ASA)*

4 Software Used

Various software were used in this study for tasks such as building geomodels, generating inversion profiles etc. This chapter will give a brief introduction to them. A flow chart in figure 8 demonstrates the methodology followed in this study and the use of the various software at each step.

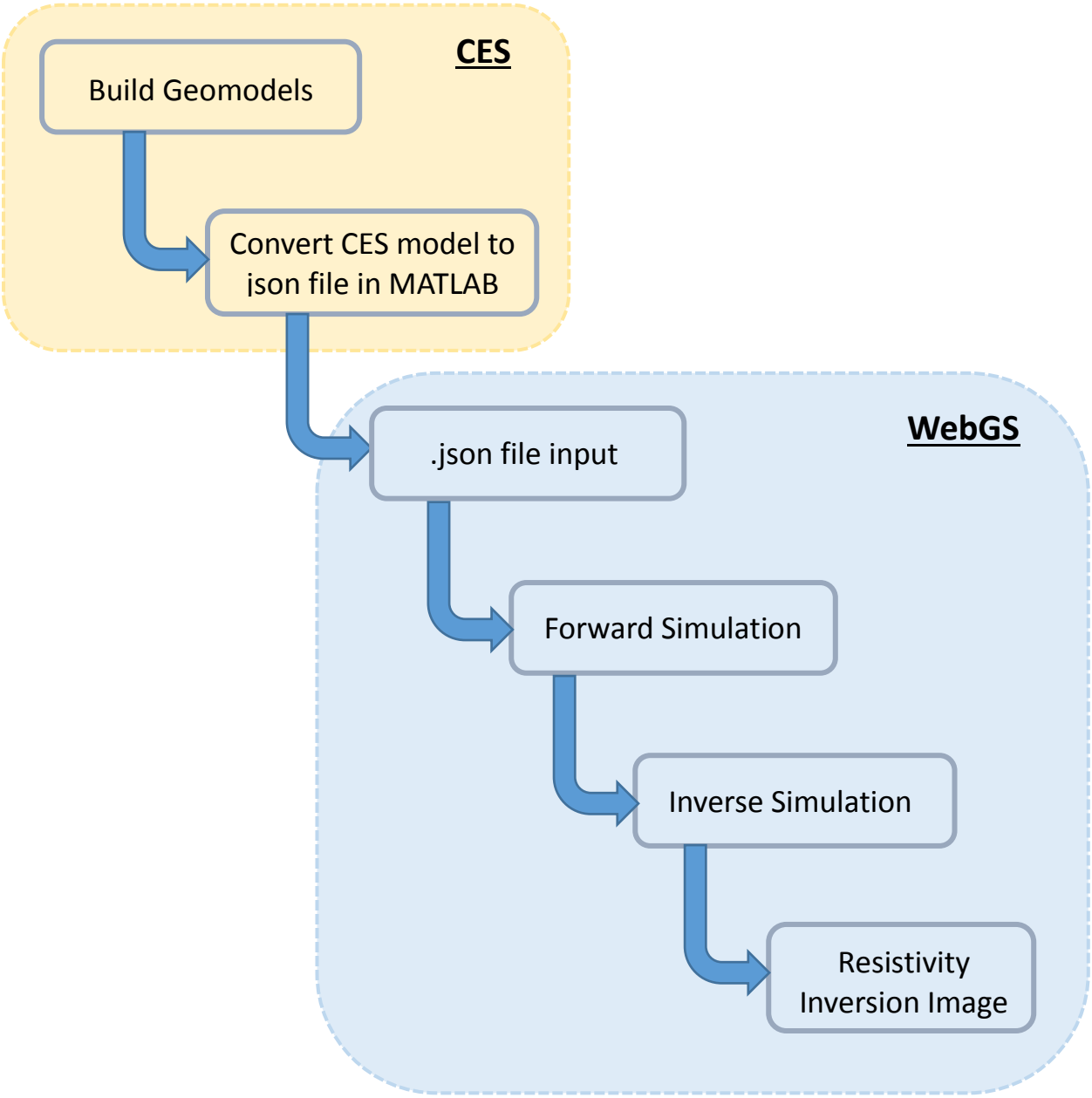

Figure 8: *Schematic diagram showing the methodology followed during the pre-job planning phase and the used software*

4.1 Compound Earth Simulator (CES)

Realistic geomodels for this study were created using the Compound Earth Simulator (CES) software. This software is developed by Statoil ASA and is suitable for creating geomodels. It uses a process based method and focuses on the geological processes in the area. The CES is developed for Structural Restoration, based on Seismic lines or volumes and Model Reconstruction using general information about the geological evolution of the area, the local history gained from the restoration and the well log data (Oliveira et al., 2015). It is a unique tool to build complex models from simple geological processes. It functions via dedicated processes such as fault restoration and reconstruction processes, mapping of layers, erosion surfaces, generation of synthetic seismic etc. (figure 9).

The importance of this process based software is that it updates the entire model on change in a particular geological feature. Hence, it is a powerful tool to make geomodels consistent with the data, honouring the geological history of the area.

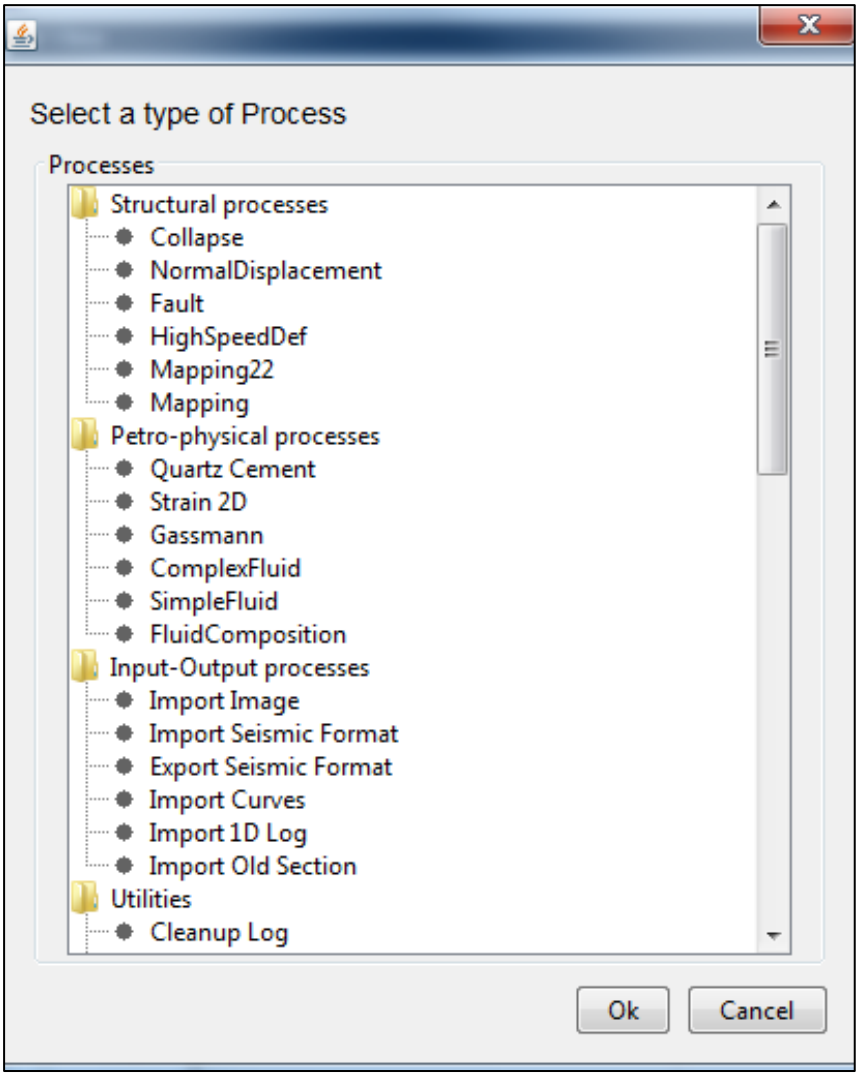

Figure 9: *Various processes in the CES Software that are used for the construction of a Geomodel (Ref. CES Software)*

The realistic geomodels in the CES software were converted to json file format using the MATLAB software. This json file format is the input to the WebGS software for forward and inverse modelling (figure 8).

4.2 The WebGS Software

The deep electromagnetic measurements play an important role in this study. The resistivity inversion profiles for the realistic geomodels were generated using the WebGS software. This software is developed by Schlumberger for forward and inverse simulations on geomodels, to produce a resistivity inversion profile.

The CES resistivity model that has been converted to a .json file format using MATLAB software is input into WebGS and the forward and inverse simulations are run.

The WebGS software allows the user to manually input the tool configuration (transmitter-receiver spacing) and frequencies that are used to run the forward and inverse simulations (figure 10). This is beneficial because the pre-job model inversions can be run and tested on various combinations of transmitter-receiver spacings and frequencies, including the ones to be used real-time at the time of drilling. Thus, the pre-job model inversion results will be consistent and comparable to the real-time inversion results.

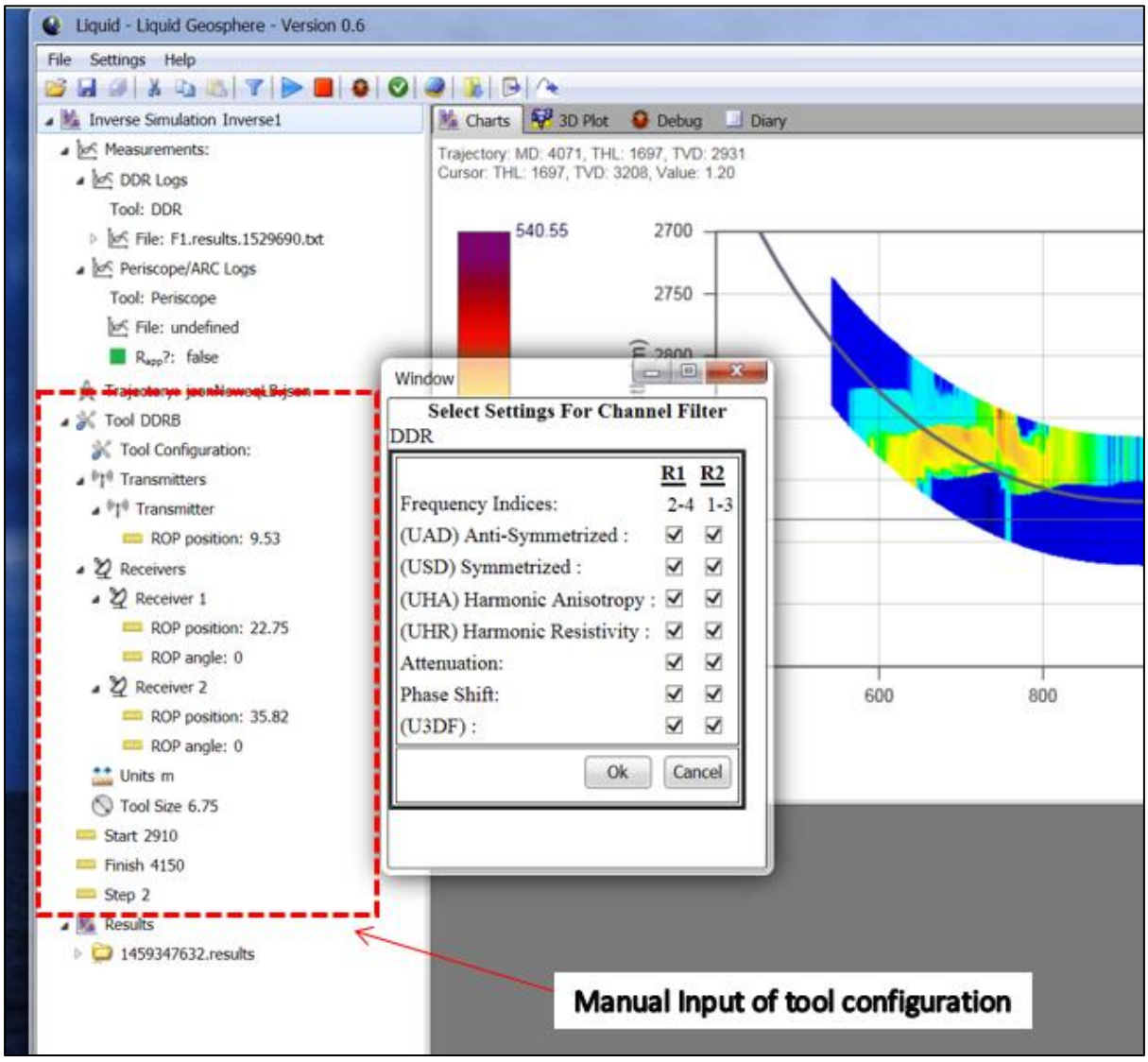

Figure 10: *WebGS interface to produce Resistivity Inversion profiles, manual input of tool configuration and frequencies that each receiver operated upon (Ref. WebGS Software)*

5 Geomodel

This chapter will explain in detail the procedure followed in order to build a realistic geomodel in the Compound Earth Simulator software during the pre-job planning phase. This is also demonstrated by a schematic diagram in figure 11.

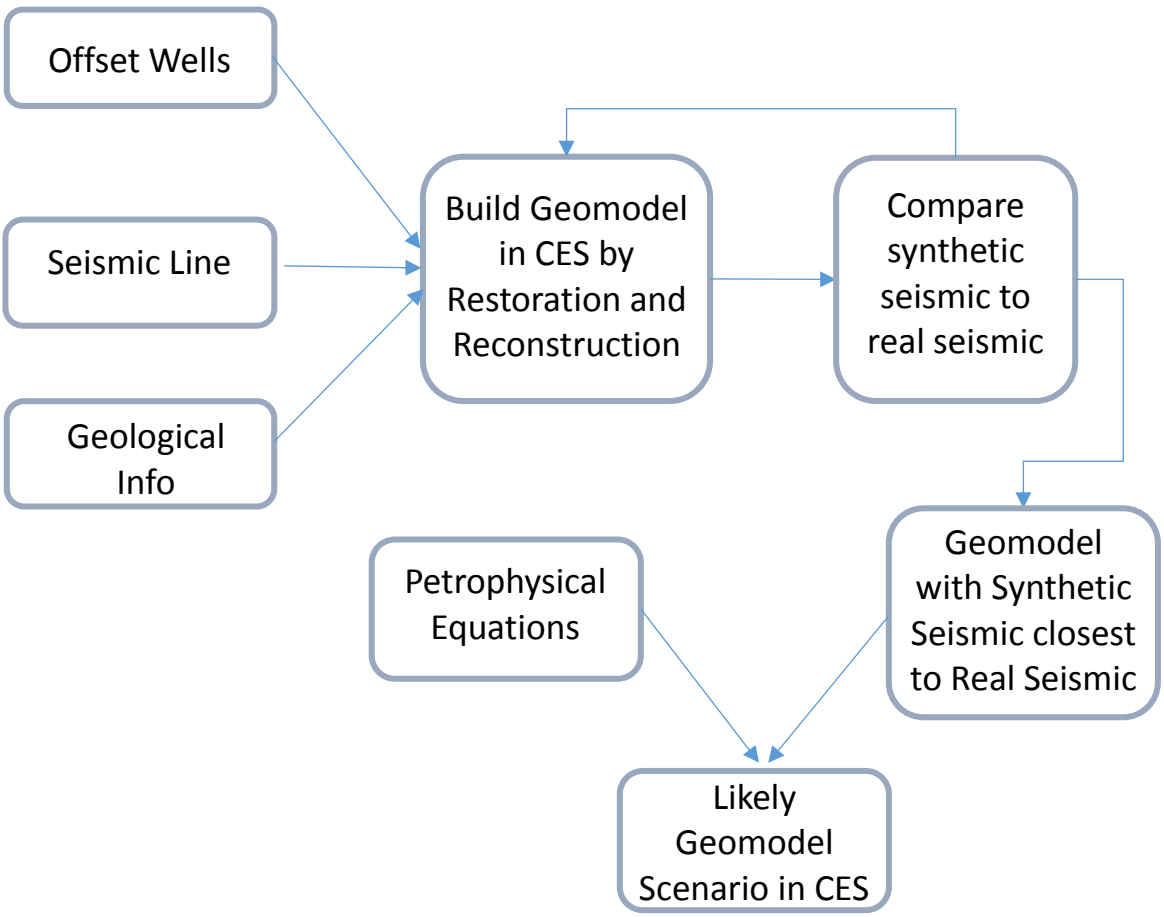

Figure 11: *Schematic overview of the methodology to construct a geomodel in CES during the pre-job planning phase*

5.1 Import Data

The seismic line in depth as a .segy file is imported using the 'Import Seismic' process available in CES. The offset wells, .trj file for trajectory and .log file for the well log information are imported into CES using the 'Import Log' process (figure 12). These are resampled because resampling removes the spikes and other noise in the well logs that may disturb or alter the geomodel. The well tops are marked.

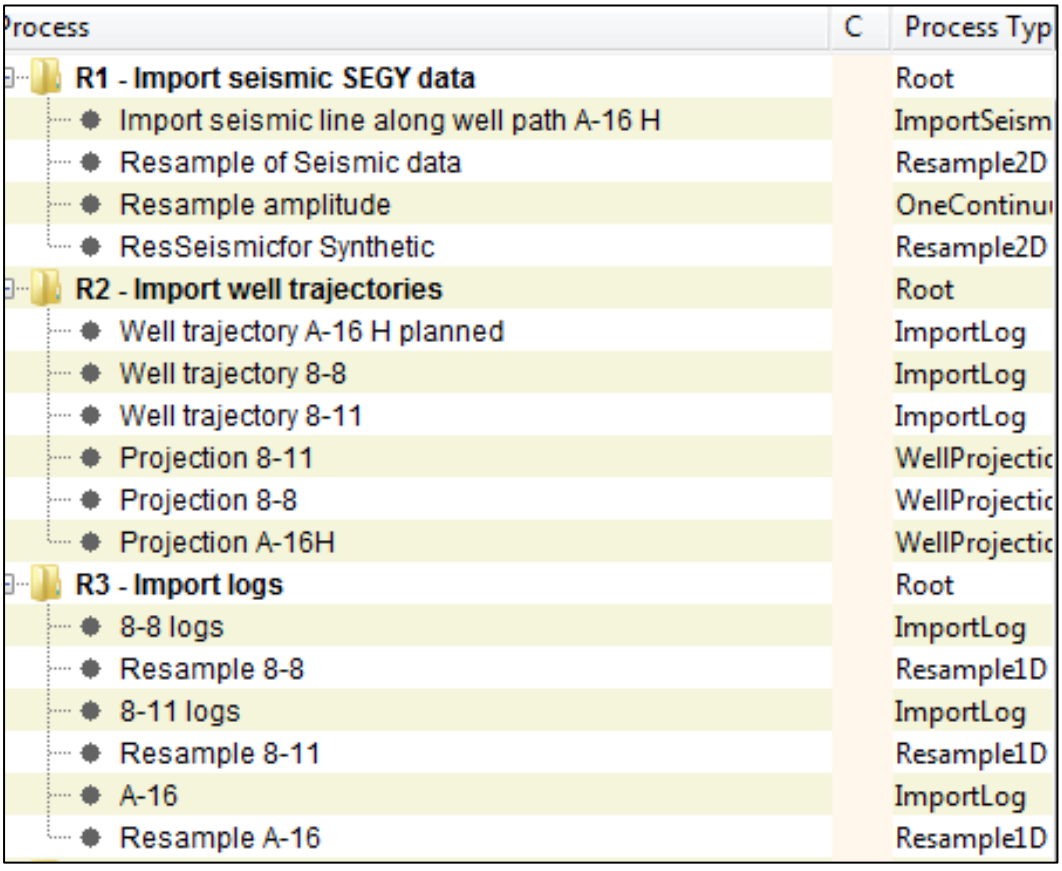

Figure 12: *Import of the Seismic line and Offset Wells (Ref. CES Software)*

5.2 Restoration

The Restoration process reverses the effects of faults, folds, differential subsidence and other structural geological effects with respect to geological time. The present seismic image is used as an input. After the restoration process is complete, the outcome is in pre-reservoir time. This is the state that would have been at the time of deposition. Restoration process can be related to going back in time to the original conditions of a particular stratigraphic unit.

Figure 13 displays the present seismic line with all the horizons and faults marked. These would be removed sequentially in order to restore the seismic to pre-reservoir time. Figure 14 shows the sequence followed during this process.

On the available seismic line, the first layer to be removed during the restoration process was the top of the Shetland group (figure 15). This was so because the concentration was on the Brent group. On the seismic image (figure 13), it can be noted that the Shetland group is the first formation above the Brent group that is clearly identifiable. The Cromer Knoll and Viking groups are not clearly distinguishable due to a lot of noise and irregular features on the seismic. Hence to avoid any errors, Shetland group was removed first and then directly the Brent group level.

This was followed by removal of a small fault and then the removal of the fault F1 (figure 16).

This fault F1 is an important geological structure for this study since the well trajectory crosses this fault and most of the discussions in this study are around the fault F1.

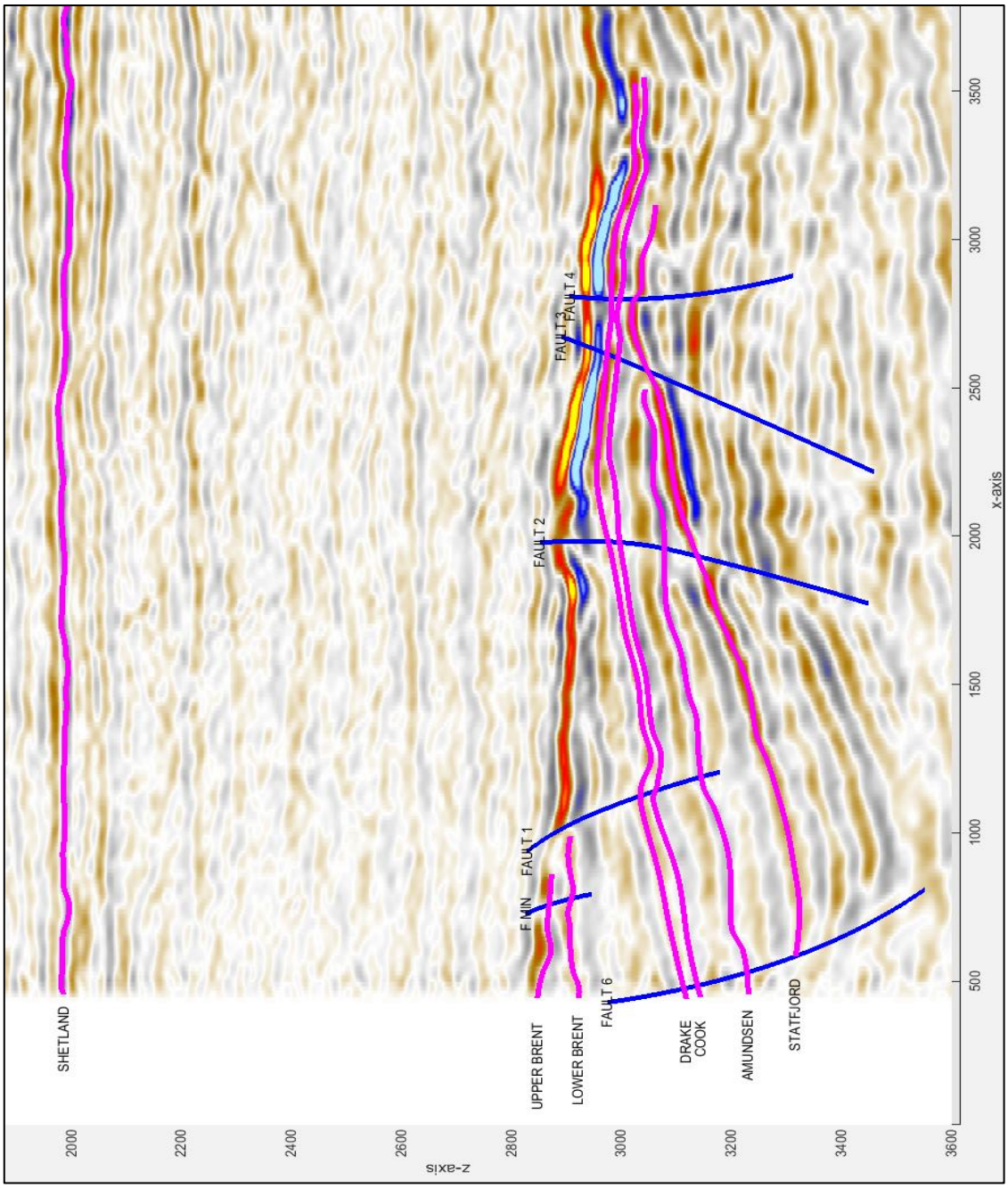

Figure 13: *Seismic line at present geological time displaying faults (in blue) and horizons (in pink) that were removed during the Restoration process (Ref. CES Software)*

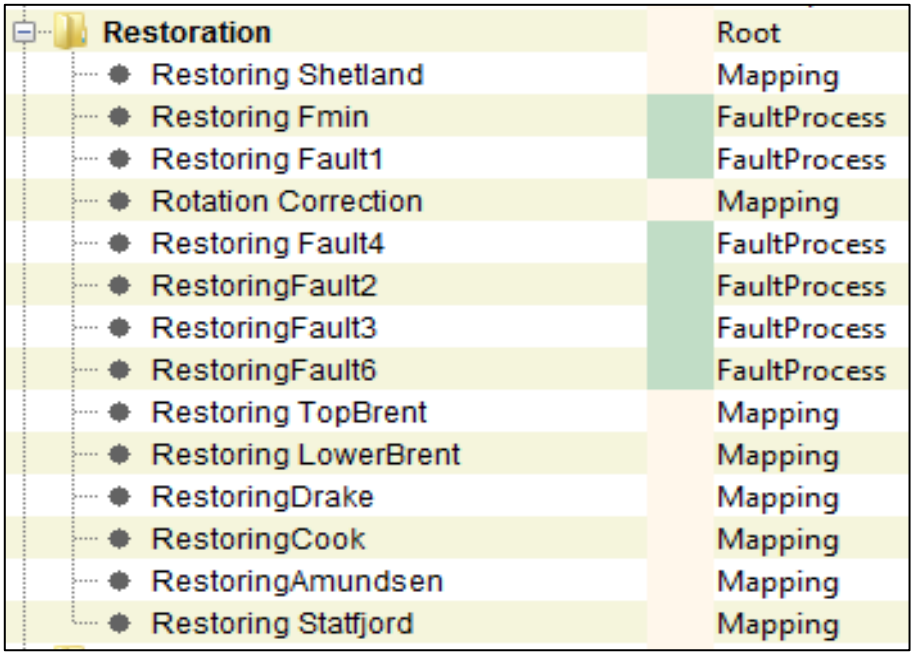

Figure 14: *Restoration process sequence followed in this study (Ref. CES Software)*

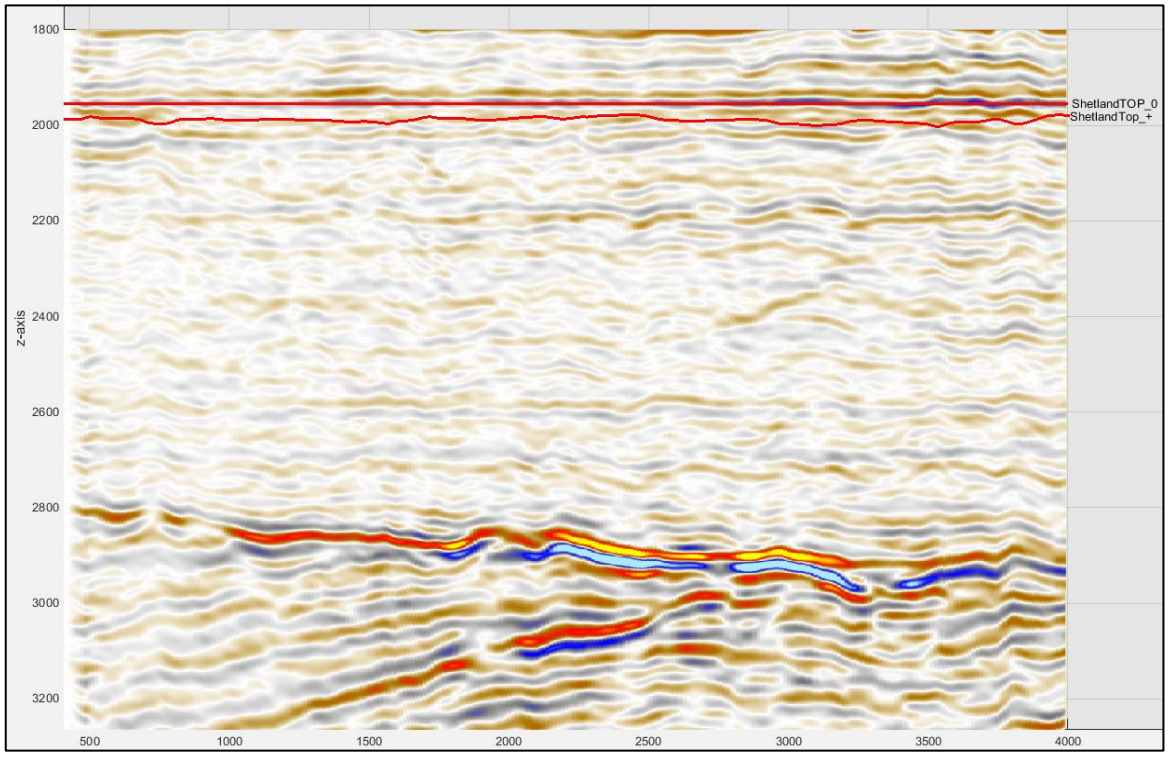

Figure 15: *Seismic line after the removal of the Shetland group during Restoration (Ref. CES Software)*

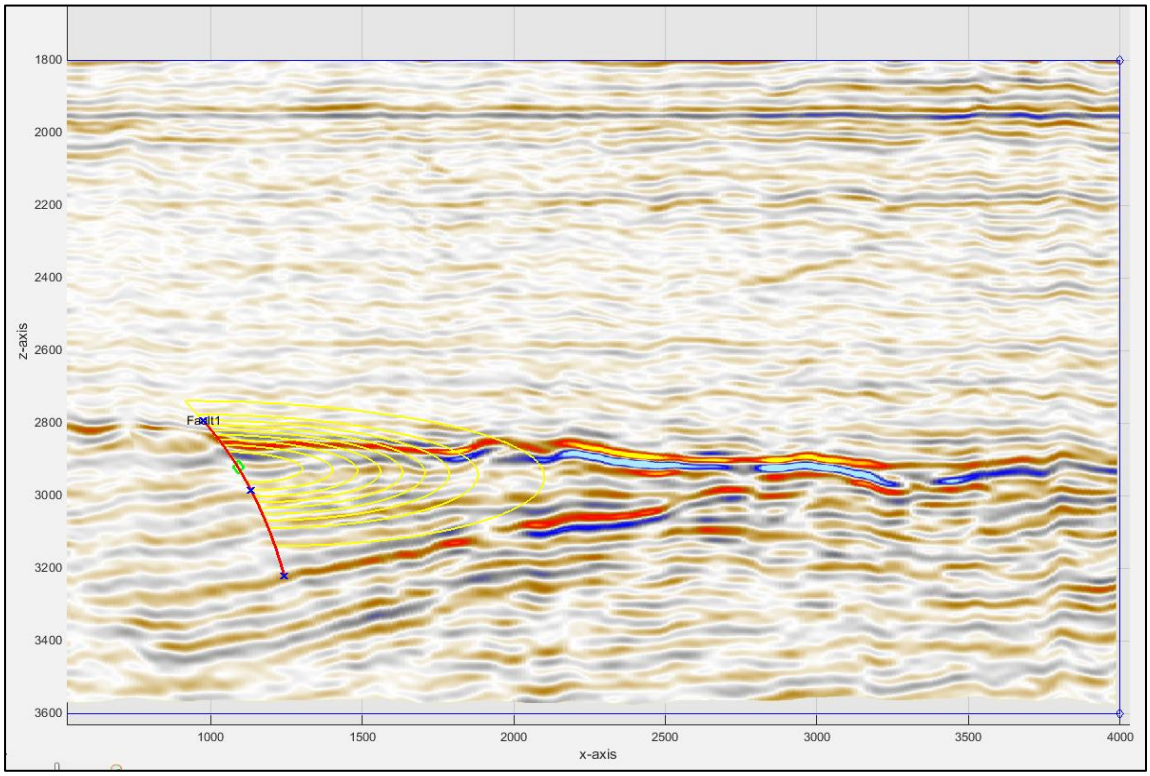

Figure 16: *Removal of Fault F1 during Restoration (Ref. CES Software)*

After the sequence of the results of geological events were removed (figure 14), such as the removal of the other faults, rotation effects inversed and restoration of other layers, the last layer to be removed was the top of the Statfjord group. Once the entire restoration process was completed, the end result on the seismic image is as shown in figure 17.

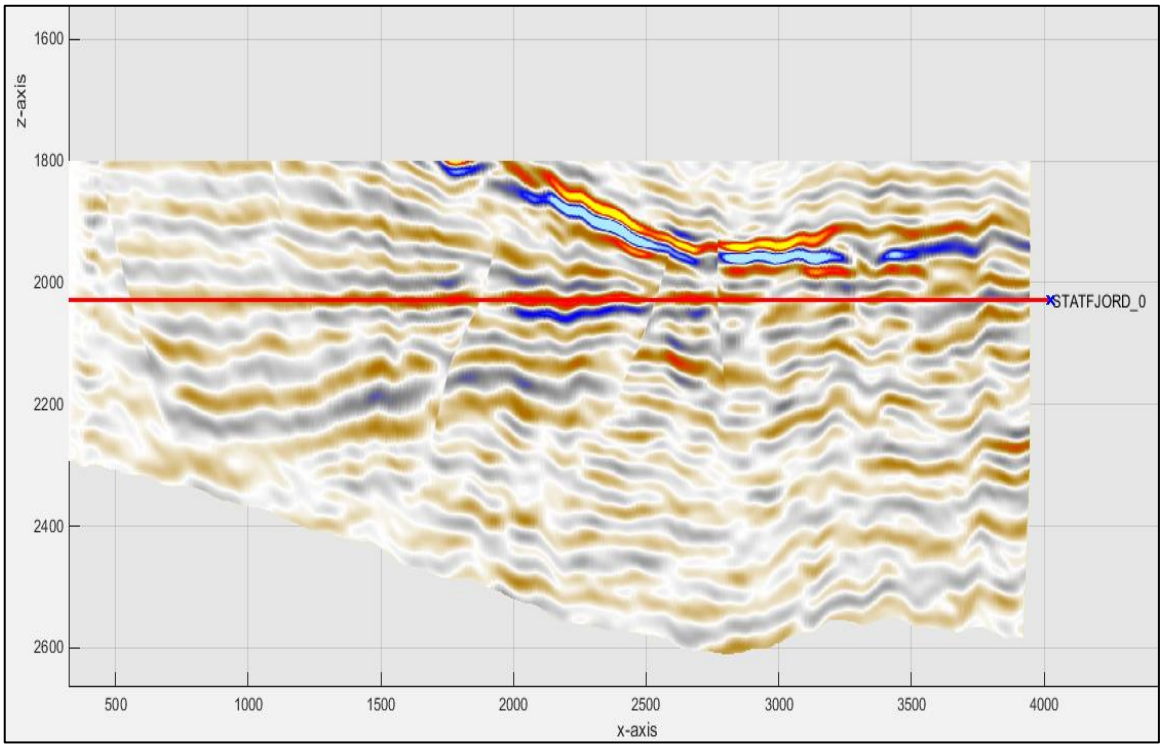

Figure 17: *Restoration process end result (Ref. CES Software)*

5.3 Reconstruction

The reconstruction process uses the horizons marked at the time of the restoration process (section 5.2) for each layer, along with information of well tops from the offset wells in order to create a geomodel. This geomodel includes all the structural features such as faults, layers, erosion surfaces, rotation effects and layers that were interpreted during the restoration process on the seismic line.

The last layer at the time of restoration, i.e. the Statfjord layer, is the starting point for the reconstruction process (figure 18). This is followed by addition of all the other layers, faults, erosional surfaces, rotation effects etc. (figure 19). The end result obtained by the reconstruction process is the realistic geomodel, as seen in figure 20.

Each layer is associated with the horizons marked during restoration and well tops from the offset wells and is populated with the properties (Gamma, Resistivity, Density, Neutron etc.) from the offset wells used.

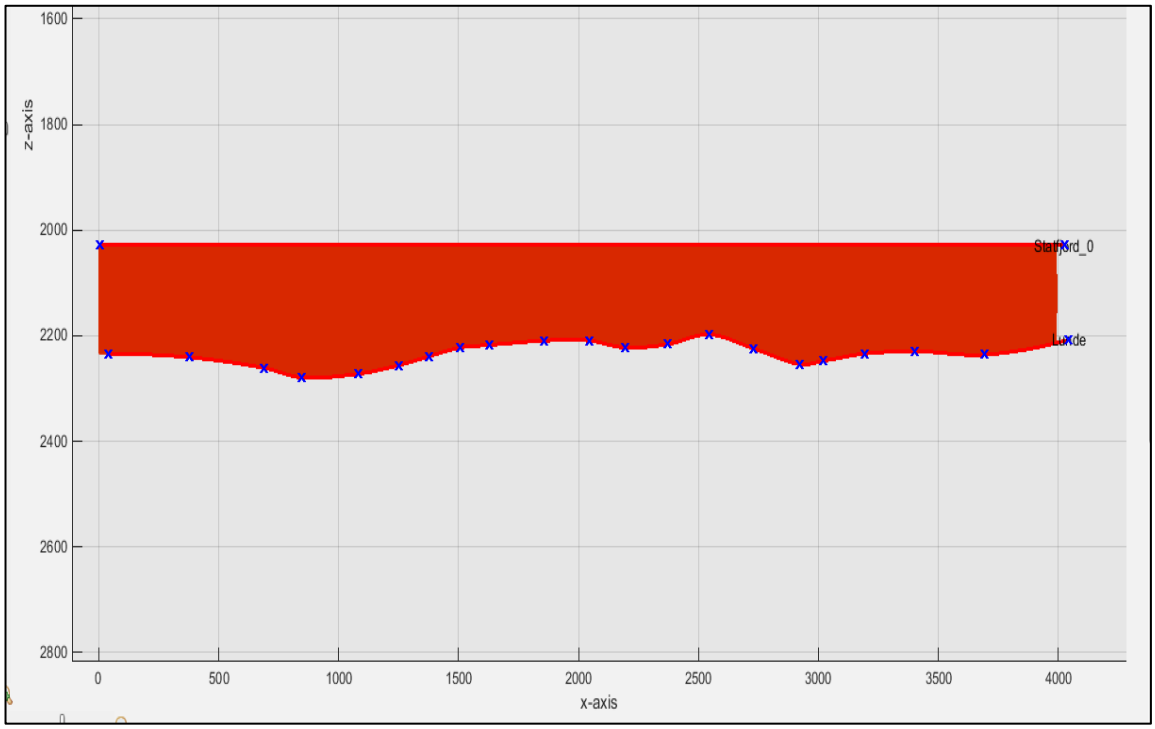

Figure 18: *First step in Reconstruction - the Statfjord layer (Ref. CES Software)*

Reconstruction	Root
Statfjord Recons	Layer
Reconst Statfjord	Mapping
Amundsen Recons	Layer
Recons Amundsen	Mapping
Cook Recons	Layer
ReconsCook	Mapping
Drake Recons	Layer
ReconsDrake	Mapping
Recon LowerBrent	Layer
ReconstBrent	Mapping
TopBrentRecons	Layer
TopBrentRecons	Mapping
ReconsFault6	FaultProcess
ReconsFault3	FaultProcess
ReconsFault2	FaultProcess
ReconsFault4	FaultProcess
Add Rotation	Mapping
Fault1 Recons	FaultProcess
Compartment A	Geom2Cont
Merging Fault1Reconst	ContMerge
Fmin Recons	FaultProcess
Extra Brent	Layer
Viking	Layer
CromerKnoll	Layer
Recons Shetland	Layer
Recons Shetland	Mapping

Figure 19: *Sequence of events during Reconstruction process (Ref. CES Software)*

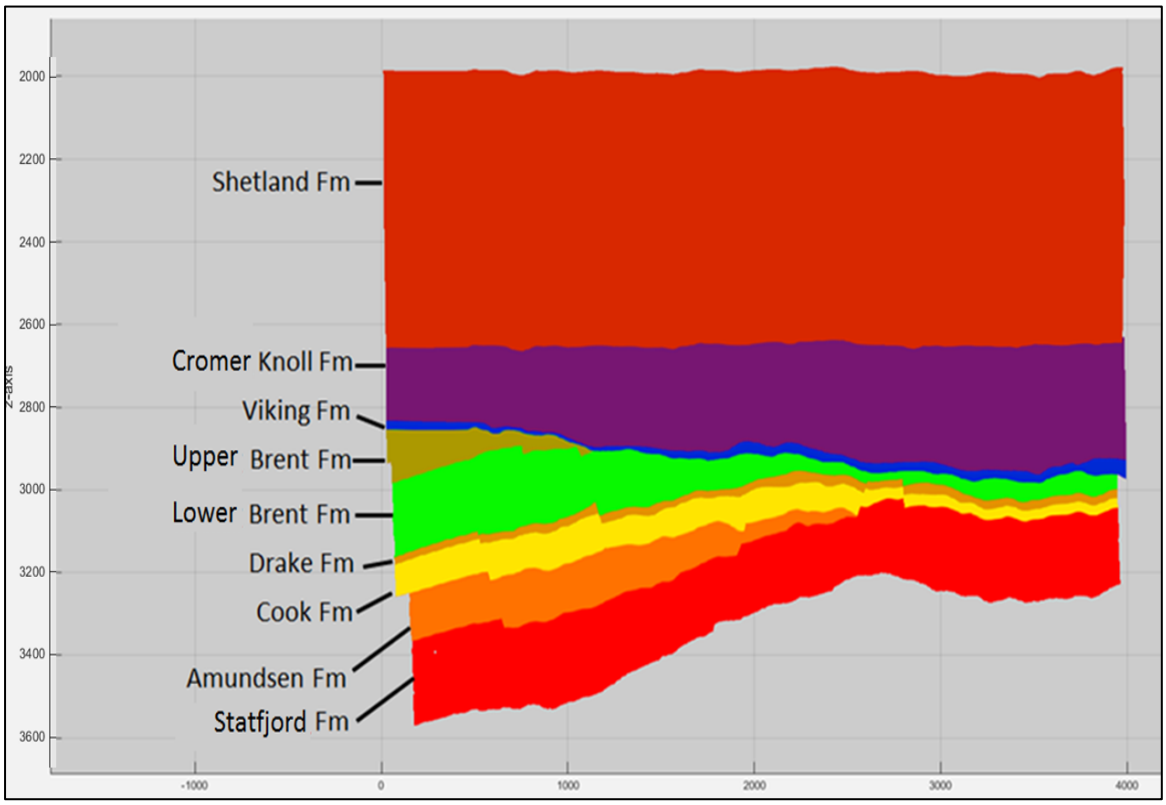

Figure 20: *Reconstruction process end result – the Geomodel (Ref. CES Software)*

An interesting observation is that the reconstruction process takes into account the effect of differential subsidence, compaction and rotation with time. This can be noticed by comparing the position of the Statfjord layer (in red colour) with respect to the z-axis in figures 18 and 20. In the first step of reconstruction (figure 18), the Statfjord layer was deposited at about 2000 m TVD. However, the reconstruction end product in figure 20 shows this layer at about 3200 m TVD. This is based on the positions of the mapped horizons of the formations during the Restoration process. The horizons on the Seismic line are interpreted based on the information from the offset wells and hence, the offset wells also have a direct impact on the Reconstruction process.

5.4 Synthetic Seismic

The geomodel that has been constructed by the Reconstruction process is resampled in x and z axis, to the desired area, which is to be taken into consideration for the study. This resampled model is used to generate a synthetic seismic (figure 21) using an algorithm 'Toxopeus2D' available in CES.

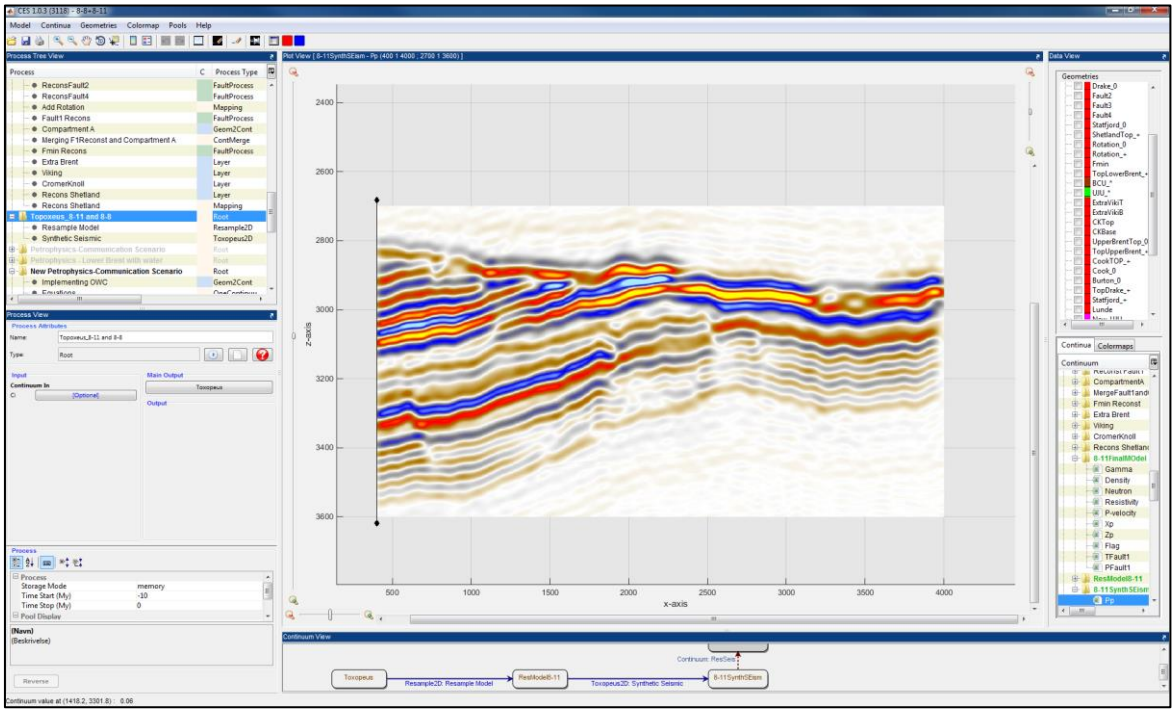

Figure 21: *Synthetic Seismic generated for the realistic geomodel obtained after the Reconstruction process (Ref. CES Software)*

Toxopeus 2D uses a constant or 1D velocity model (overburden velocity) and the migration aperture, CDP distance etc., can be set manually. It follows the approach to filter a model by spatial-resolution and angle filters to simulate migrated and inverted data, respectively. The simulated migrated data show the effects of vertical and horizontal smearing and exhibit a different wavelet stretch for different reflector dips, similar to migrated real data (Toxopeus G. et. al., 2008).

The synthetic seismic, so generated, has to be validated and checked for matching the original seismic line. Hence, the original seismic and the synthetic seismic are put together in one window, and scrolled from the left to right (and vice versa), to compare the positions of reflectors on both of them (figure 22).

In case of any discrepancies, it is believed that the synthetic geomodel generated was not correct and did not match the original geological conditions. Hence, some changes during the restoration and/or reconstruction process need to be made. These can be changes in the sequence of deposition and therefore removal of the stratigraphic layers, fault sequence changes or changes in fault throw or their effect on the surrounding area etc. The restoration and reconstruction processes are run again and a new geomodel is created. The synthetic seismic generated for this new geomodel is checked again by comparing with the original seismic and further changes in the restoration and reconstruction processes are done. It may also be possible that the properties in the synthetic seismic are not a good representation of the properties in that area. Hence, using different offset wells, and therefore varying the properties, may also bring the synthetic seismic match the real seismic better.

This process is repeated until the synthetic seismic matches the original seismic for every reflector. Once this match is achieved, the realistic geomodel is considered to be a good representation of the original geological conditions in the area.

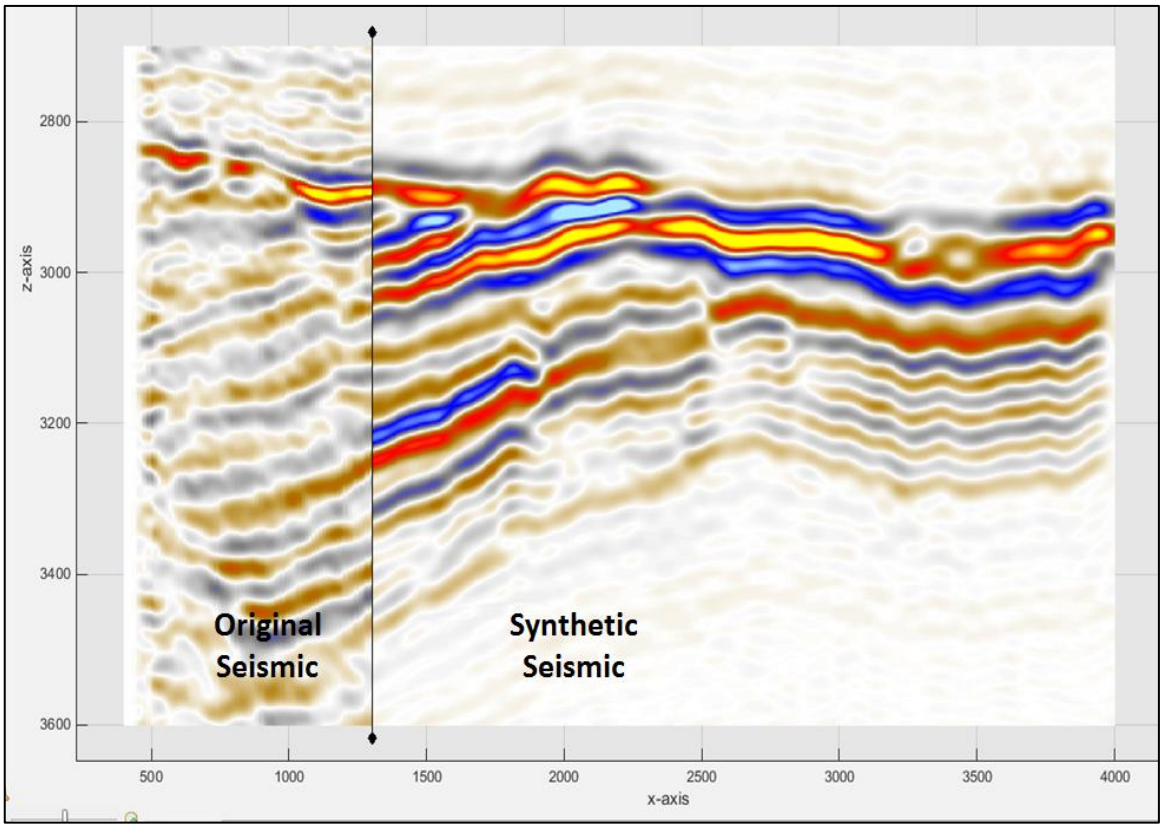

Figure 22: *Comparison between Original Seismic (Left) and Synthetic Seismic, indicating a good match (Right) (Ref. CES Software)*

It is important to understand that a seismic match is necessary, but it is not necessarily sufficient for achieving a realistic geomodel. This means that there are other factors that need to be taken into consideration before it can be stated that the geomodel is a good representation of the real geological conditions. Offset wells may or may not be good representation of the properties. Also, seismic images are relatively coarse and smaller scale structural variations may not be captured on the seismic. There can be more than one geomodels, whose synthetic seismic may match with the original seismic. For example, in this study, the synthetic seismic for two geomodels matched the original seismic. This has been discussed in more details in subsequent chapters.

6 Resistivity Inversion Profile

The deep directional tool in a highly deviated well generates large amount of data, due to multiple depths of investigation, different frequencies and multi-component complex measurements. It is not feasible to handle and interpret these using conventional log interpretation techniques or visual observation of log patterns. Therefore there is a need for an inversion algorithm to interpret the measurements.

An inversion image presents a multilayer formation model around the borehole that includes resistivity and anisotropy, uncertainty estimation, structural dip and orientation. The inversion complements seismic information but with a better spatial resolution (Seydoux J., et. al, 2014).

The WebGS software is used to generate 1D inversion profiles from the geomodels built using the Compound Earth Simulator. These deep directional EM inversion images are powerful tools to increase the understanding of the reservoir. Further development of inverse algorithms from 1D inversions to 2D and 3D inversions has a strong focus in the industry today.

The inversion provides a solution to complex multilayer interpretation by combining the constraints of all the available measurement types at various frequencies and spacings, each of them having its own DOI and sensitivity (Seydoux J., et. al, 2014). The WebGS uses an inversion algorithm based on the deterministic Gauss-Newton optimization approach with box parameter constraints and a line search scheme (Omeragic D., et. al, 2015).

Detailed discussion of the WebGS inversion algorithm is beyond the scope of this work. Figure 23 explains the procedure followed in order to generate an inversion profile in WebGS for a geomodel from CES.

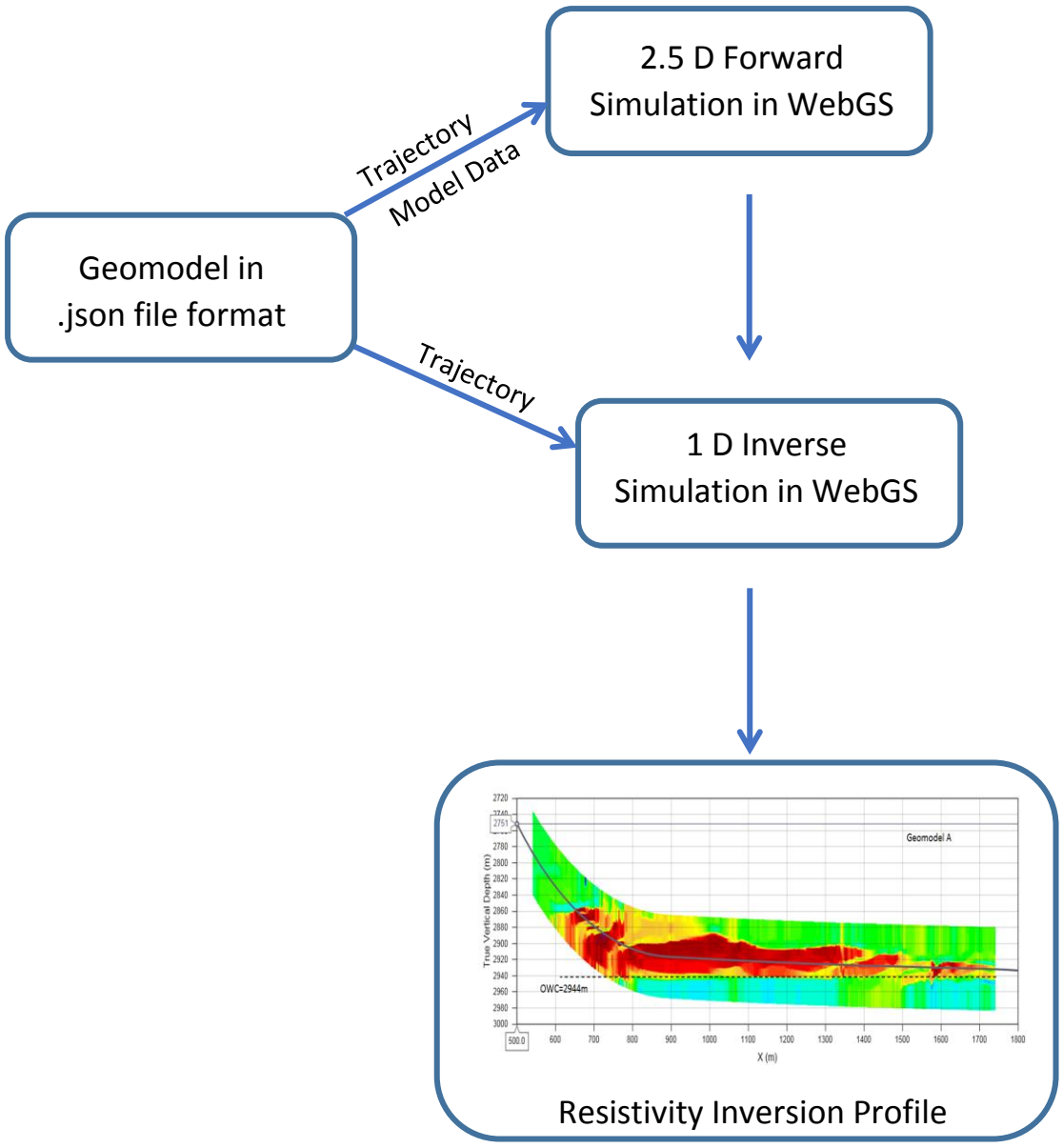

Figure 23: *Schematic overview of the methodology to generate an Inversion profile for a Geomodel*

The tool specifications such as distance between the transmitter and receivers, frequencies used etc. can be manually input into the WebGS software during forward and inverse simulation and therefore make the pre-job inversion images consistent and comparable to those generated real-time.

The details on the tool specifications and other input parameters for the Forward and Inverse Simulations used in this study are available in Appendix D.

A typical resistivity inversion image is shown in figure 24. The inversion image displays the well trajectory and the features around this trajectory. This image is a ‘look around’ image and has the ability to look above and below the well trajectory. However, it is not a ‘look ahead’ image and therefore has limited ability to predict the features ahead of the tool.

The colour scale represents the deep blue and bluish green features on the image depict lower resistivity values and the red or red-yellow features depict higher resistivity values.

The important geological formations and structures can be identified based on resistivity values and this image can be interpreted to steer the well such that it stays in the reservoir sweet zone, away from the oil-water contact, avoid drilling into shales and structurally complex formations and hence lead to an optimized well placement.

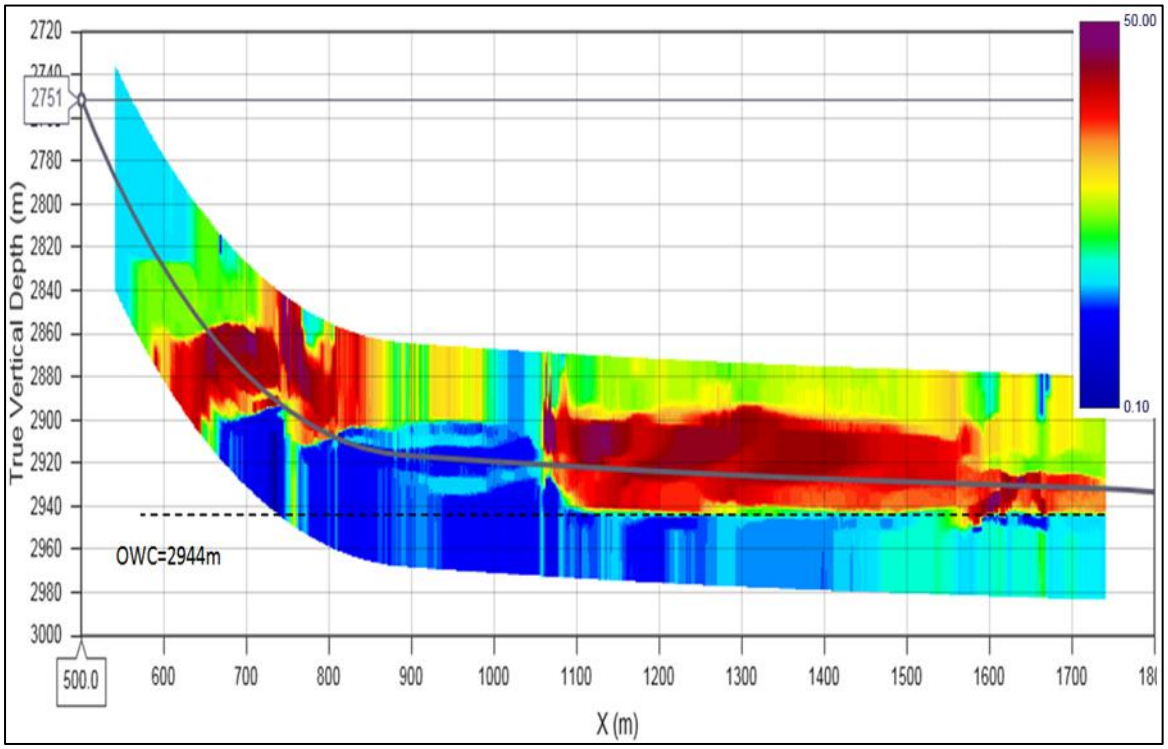

Figure 24: *A typical Resistivity Inversion profile (Ref. WebGS Software)*

7 Offset Wells

During the pre-job planning phase, it is important to consider relevant possibilities of the model, by taking into consideration all the available data.

For building the geomodel in this study, the exploration wells that were available were 34/8-1, 34/8-8 and 34/8-11. Various models, based on difference in lithological content of offset wells used, were considered, namely,

- Model with offset well 34/8-1
- Model with offset well 34/8-8
- Model with offset well 34/8-11
- Model with a combination of offset wells 34/8-8 and 34/8-11

The location of these wells with respect to the well A-16 H is shown in figure 25.

Figures 26, 27 and 28 display the offset well logs namely, Gamma Ray, Resistivity, Neutron and Density for wells 8-1, 8-8 and 8-11 respectively.

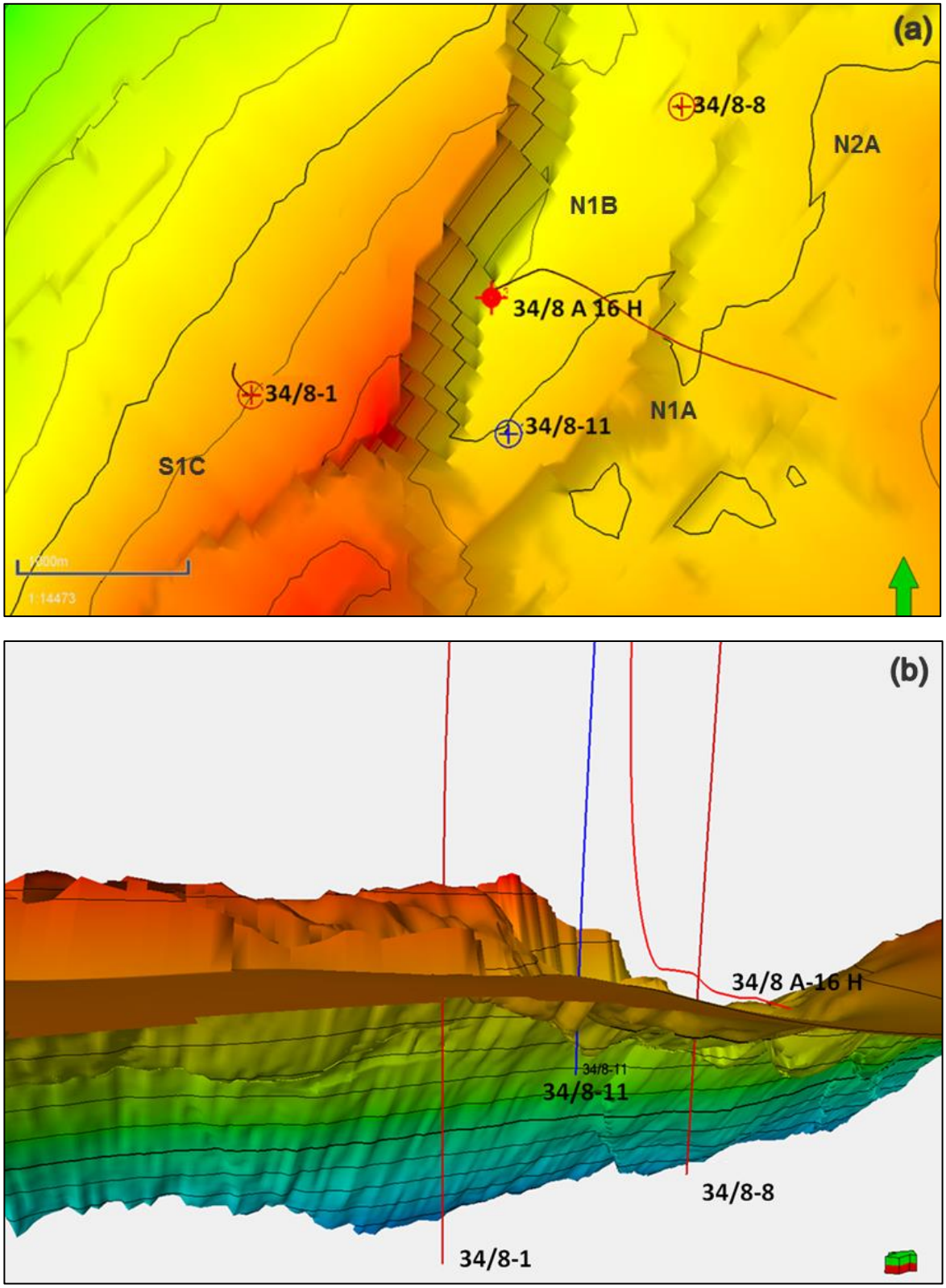

Figure 25: (*a) Location of offset wells 8-1, 8-8 and 8-11 with respect to well A-16 H; (b) 3D view of offset well trajectories with respect to well A-16 H; for the Brent group base surface (Ref. Statoil ASA)*

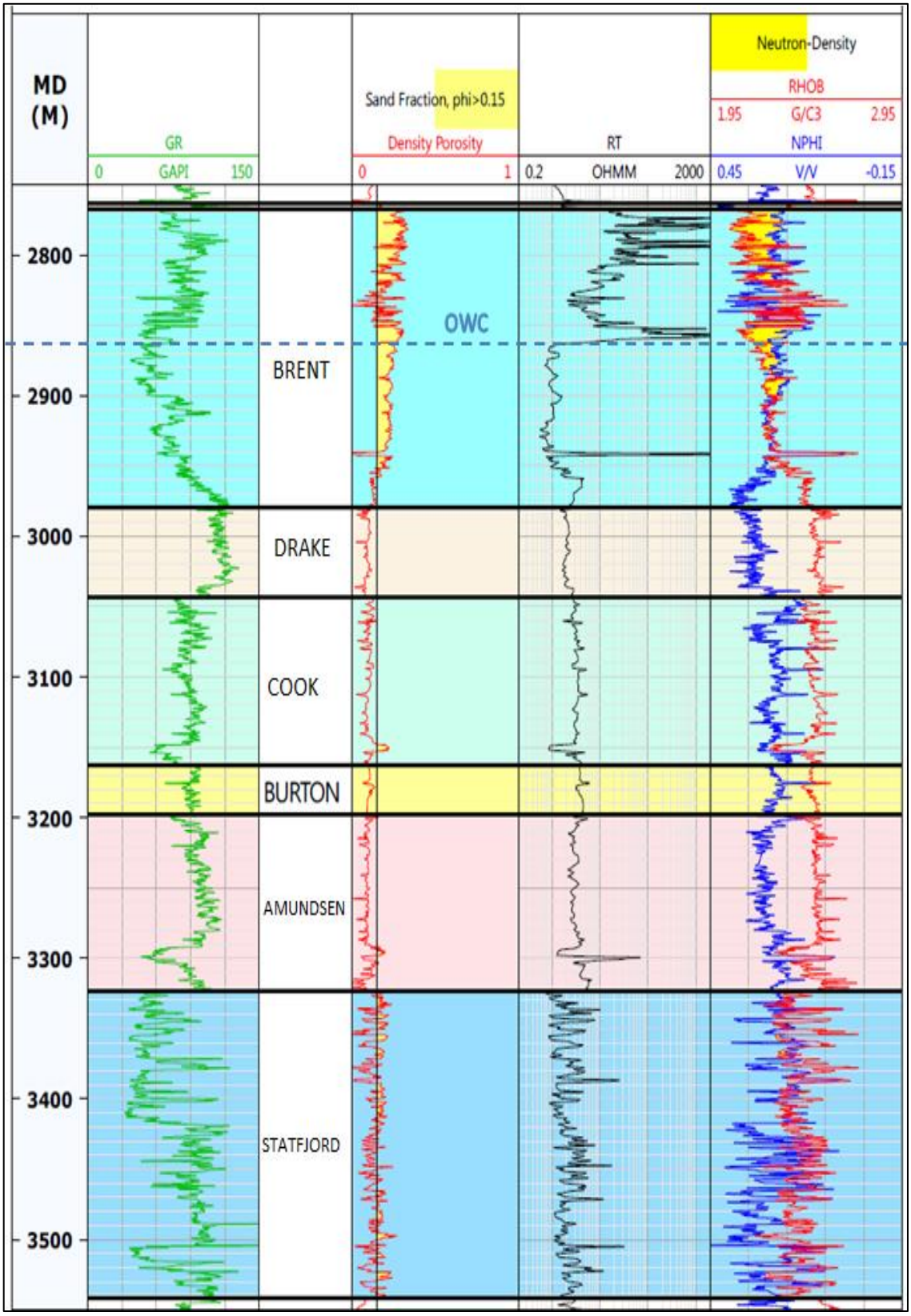

Figure 26: *Offset well 34/8-1, marked with tops of various formations and the OWC as per Statoil ASA interpretation*

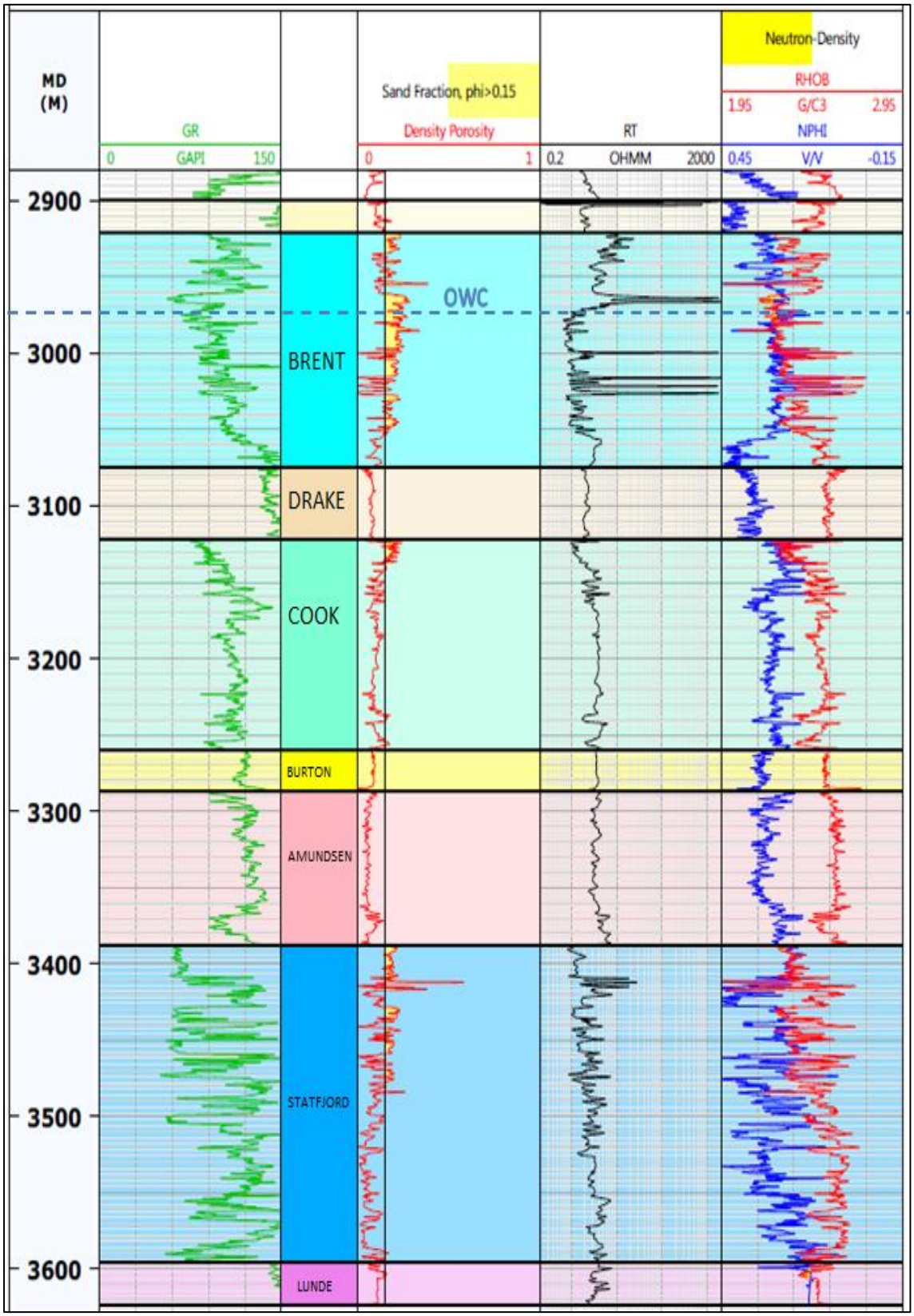

Figure 27: *Offset well 34/8-8, marked with tops of various formations and the OWC as per Statoil ASA interpretation*

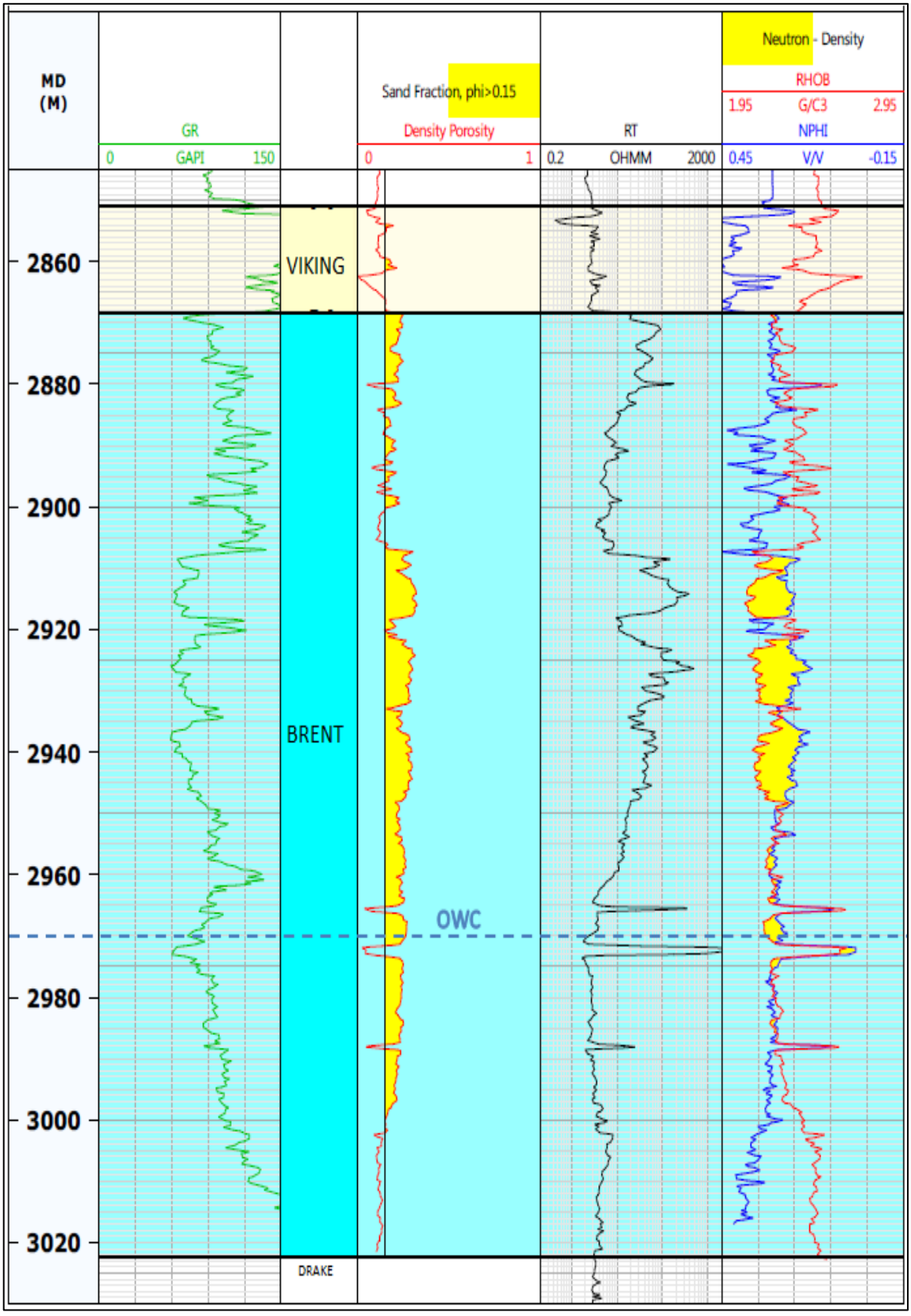

Figure 28: *Offset well 34/8-11, marked with tops of various formations and the OWC as per Statoil ASA interpretation*

7.1 Offset Well 34/8-1

The well 34/8-1 is drilled in the S1C segment and not in the N1 segment as that of well 34/8 A-16 H to be drilled. As can be seen in figure 26, the well 34/8-1 logs show a section of sand filled with hydrocarbons, with high resistivity in the Brent (about 2750 m – 2860 m MD in figure 26).

When this well was used during the reconstruction process in CES to build the geomodel, the reflectors on the synthetic seismic generated (figure 29), did not match the original seismic reflectors (figure 30). This is probably due to different properties in the formations of the wells 34/8-1 and the well 34/8-A 16 H to be drilled. This means that the well 34/8-1 is not a good representative of the N1 segment.

Hence, this model was dropped and was not considered further in this study.

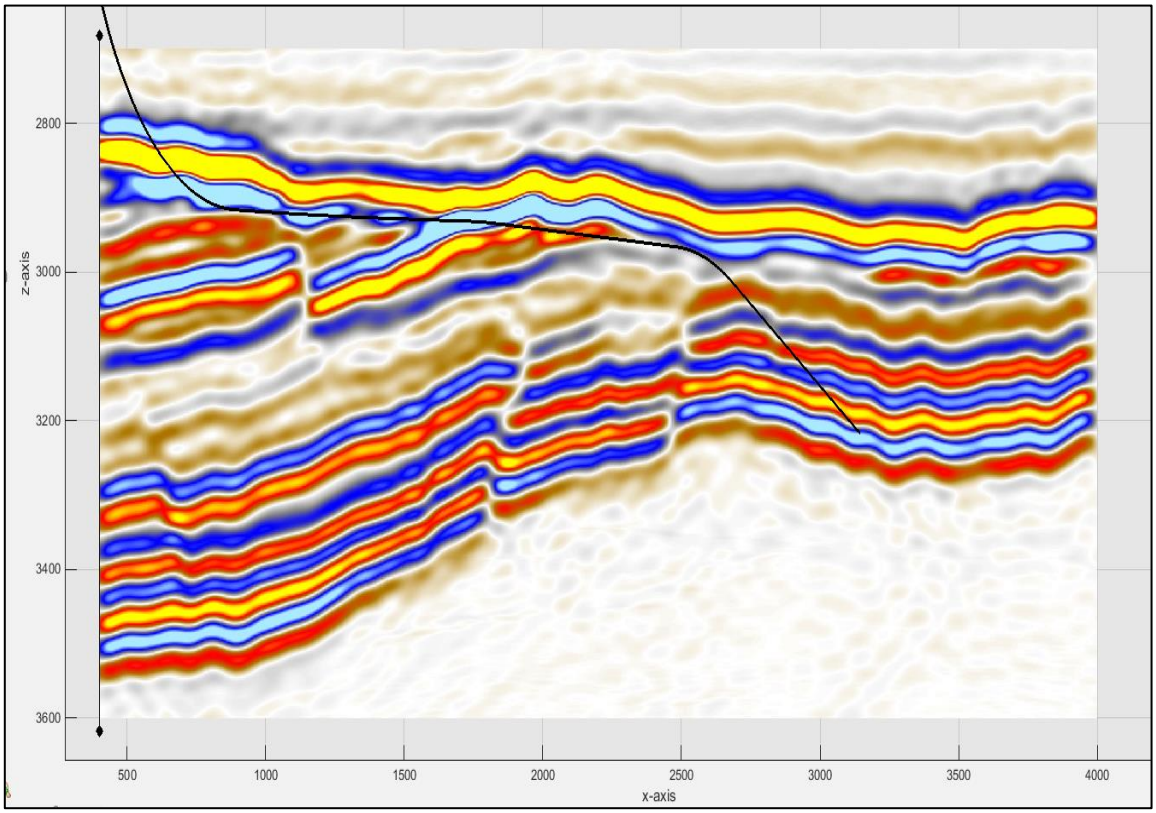

Figure 29: *Synthetic Seismic for the geomodel constructed using offset well 34/8-1, black solid line depicting the trajectory for the well A-16 H (Ref. CES Software)*

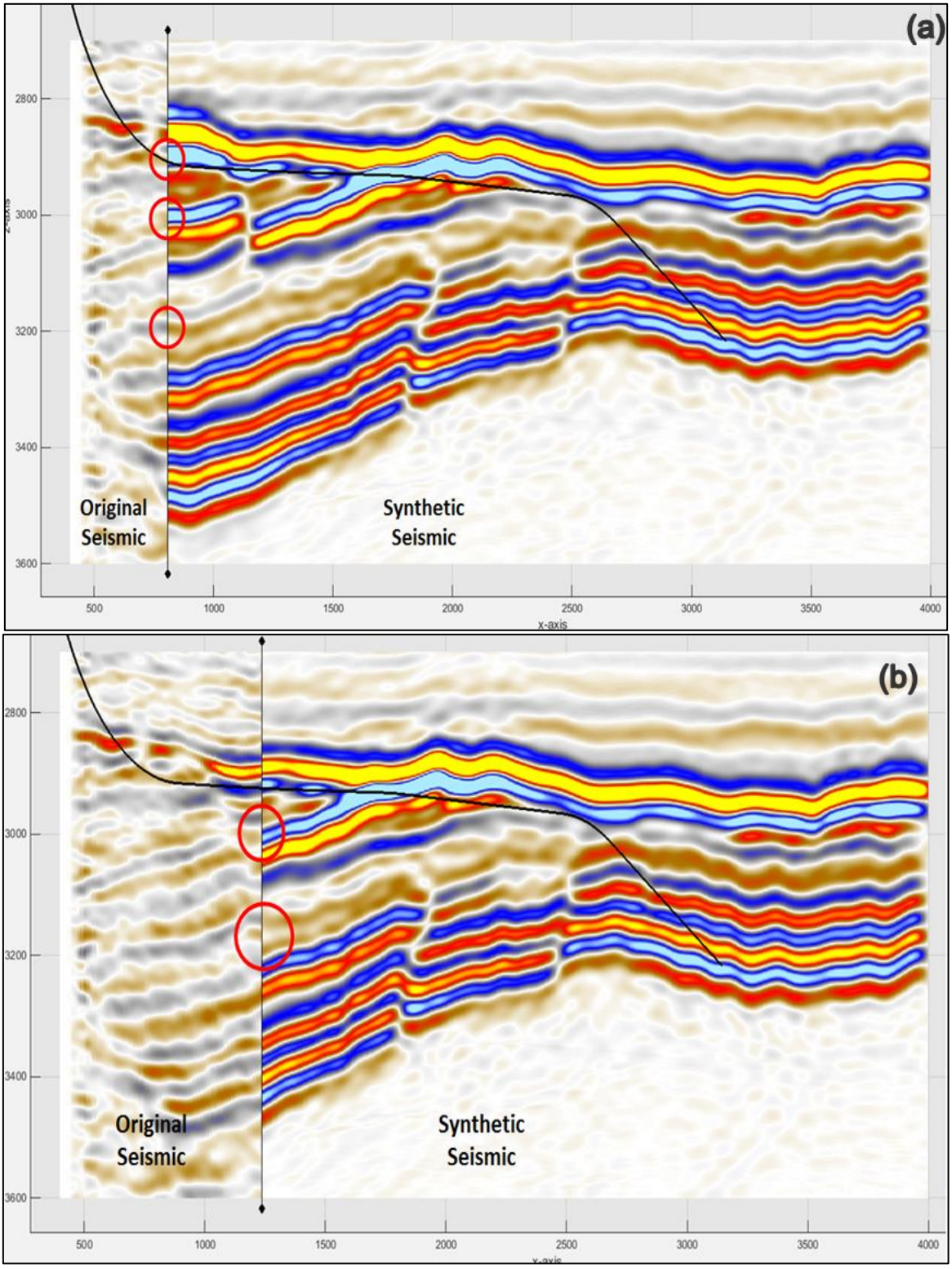

Figure 30: *Synthetic Seismic compared with Original Seismic Image for geomodel built with offset well 34/8-1 at two positions ((a) and (b)) on x axis, red circles showing deviation of reflectors on synthetic seismic from the original seismic (Ref. CES Software)*

7.2 Offset Well 34/8-8

The well 34/8-8 lies in the N1-B segment and is close to the well A-16 H. As can be seen in the log image in figure 27, this well is very shaly throughout its depth. The Brent group in this well is also shaly.

However, the synthetic seismic generated by the geomodel created by using this offset well (figure 31), matches very closely to the original seismic line (figure 32).

Hence, the geomodel generated by using the offset well 34/8-8 was used in this study. The geomodel thus contained the log properties (such as resistivity) from this well.

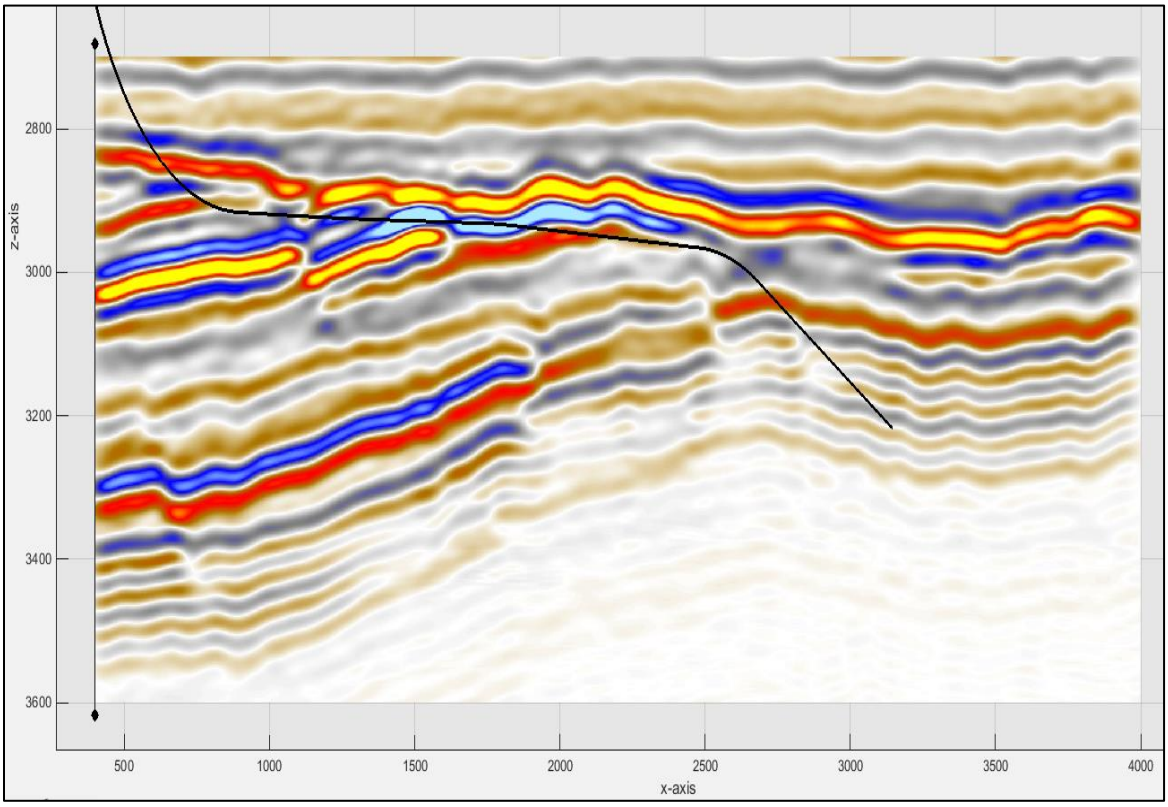

Figure 31: *Synthetic Seismic for the geomodel constructed using offset well 34/8-8, black solid line depicting the trajectory for the well A-16 H (Ref. CES Software)*

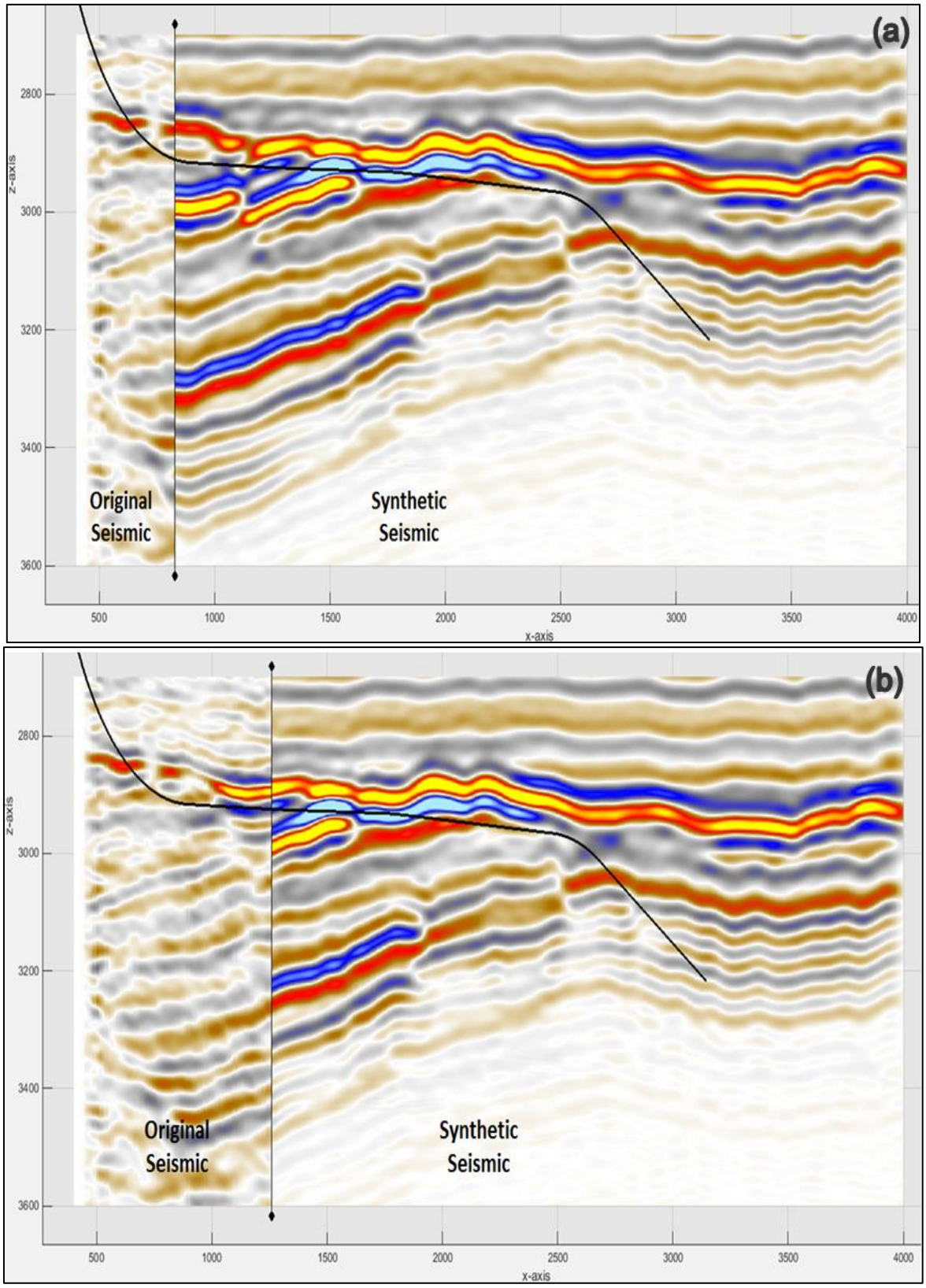

Figure 32: *Synthetic Seismic compared with Original Seismic Image for geomodel built with offset well 34/8-8, at two positions ((a) and (b)) on x axis, reflectors on synthetic and original seismic match (Ref. CES Software)*

7.3 Offset Well 34/8-11

The well 34/8-11 lies closest to the well A-16 H that was to be drilled (figure 25). The logs of this well indicate the presence of hydrocarbons in the sand in the Brent group (about 2910 m – 2950 m MD in figure 28). However, this well is very shallow and is drilled only till the top of the Cook formation.

The geomodel in CES is generated from the Top of the Lunde formation (bottommost layer of the geomodel) till the Top of the Shetland formation (topmost layer of the geomodel). This well falls short to provide information for the formations below the Drake formation. Hence, the geomodel cannot be built by using the well 34/8-11 solely.

7.4 Combination of offset wells 34/8-8 and 34/8-11

The main focus in this study was the Brent group. Since, the well 34/8-11 falls short in depth to make the geomodel, the properties only for the Brent group were taken from the well 34/8-11. Hence, a combination of wells 34/8-8 and 34/8-11 was used to build this geomodel.

In this geomodel, the properties of the well 34/8-11 were used from the Shetland formation till the Lower Brent group. The properties of the well 34/8-8 were used for the Drake formation till the Top of the Lunde formation.

The resultant geomodel from this combination of offset wells was a good representation of the realistic geological conditions in that area. This was because the reflectors on the synthetic seismic (figure 33) matched the reflectors on the original seismic (figure 34).

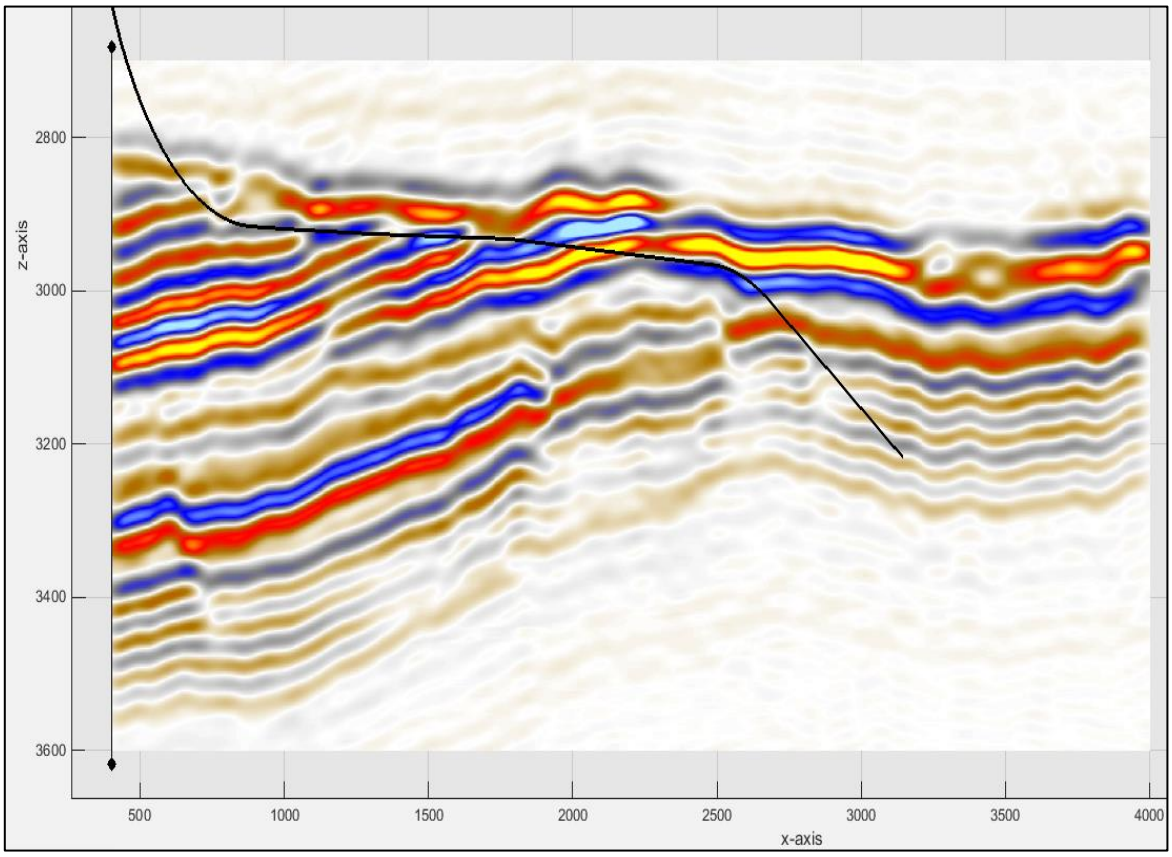

Figure 33: *Synthetic Seismic for the geomodel constructed using a combination of offset wells 34/8-8 and 34/8-11, black solid line depicting the trajectory for the well A-16 H (Ref. CES Software)*

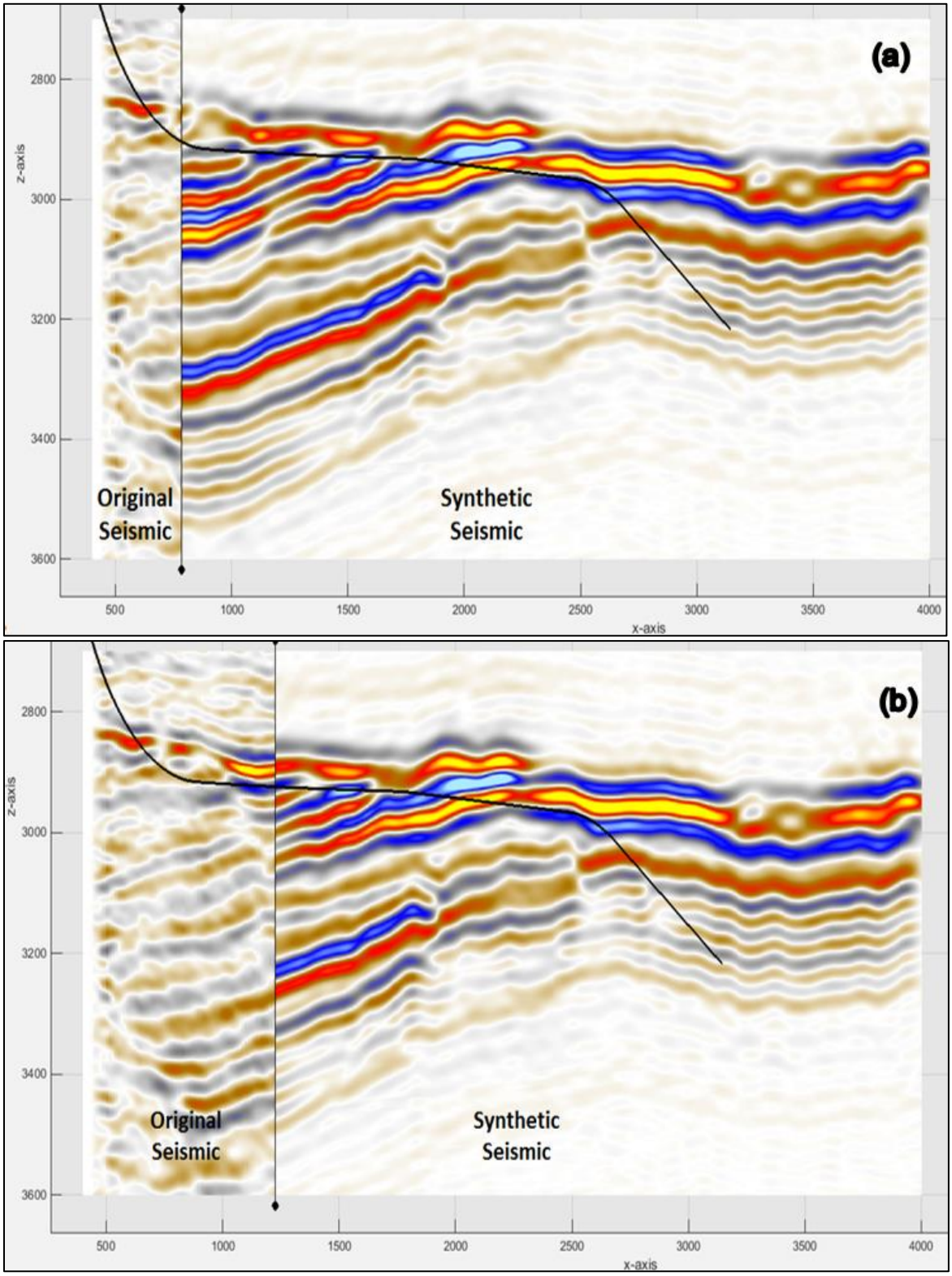

Figure 34: *Synthetic Seismic compared with Original Seismic Image for geomodel built with a combination of offset wells 34/8-8 and 34/8-11, for two positions ((a) and (b)) on the x axis, reflectors on synthetic seismic match the original seismic (Ref. CES Software)*

7.5 Conclusion

Two geomodels were finalized to be used in this study, namely, geomodel built using the offset well 8-8 only and geomodel built with a combination of offset wells 34/8-8 and 34/8-11.

The figure 35 shows the synthetic seismic images obtained from the two geomodels. The Fault F1 is more clearly visible in the synthetic seismic image generated by the geomodel using the offset well 34/8-8 only.

Also, these synthetic seismic images differ in the amplitudes of the reflectors. This difference in amplitude is possibly because the real seismic image is a processed image and has been affected by the overburden and the noise. However, the synthetic seismic generated using the Toxopeus2D process is a very simplified image and it does not include the effects of the overburden, dispersion, migration and noise. Also, the fluid content may not be the same on the synthetic and real seismic images.

However, this is not a sufficient reason to eliminate the possibility of using the geomodel constructed using a combination of offset wells 34/8-8 and 34/8-11, in this study.

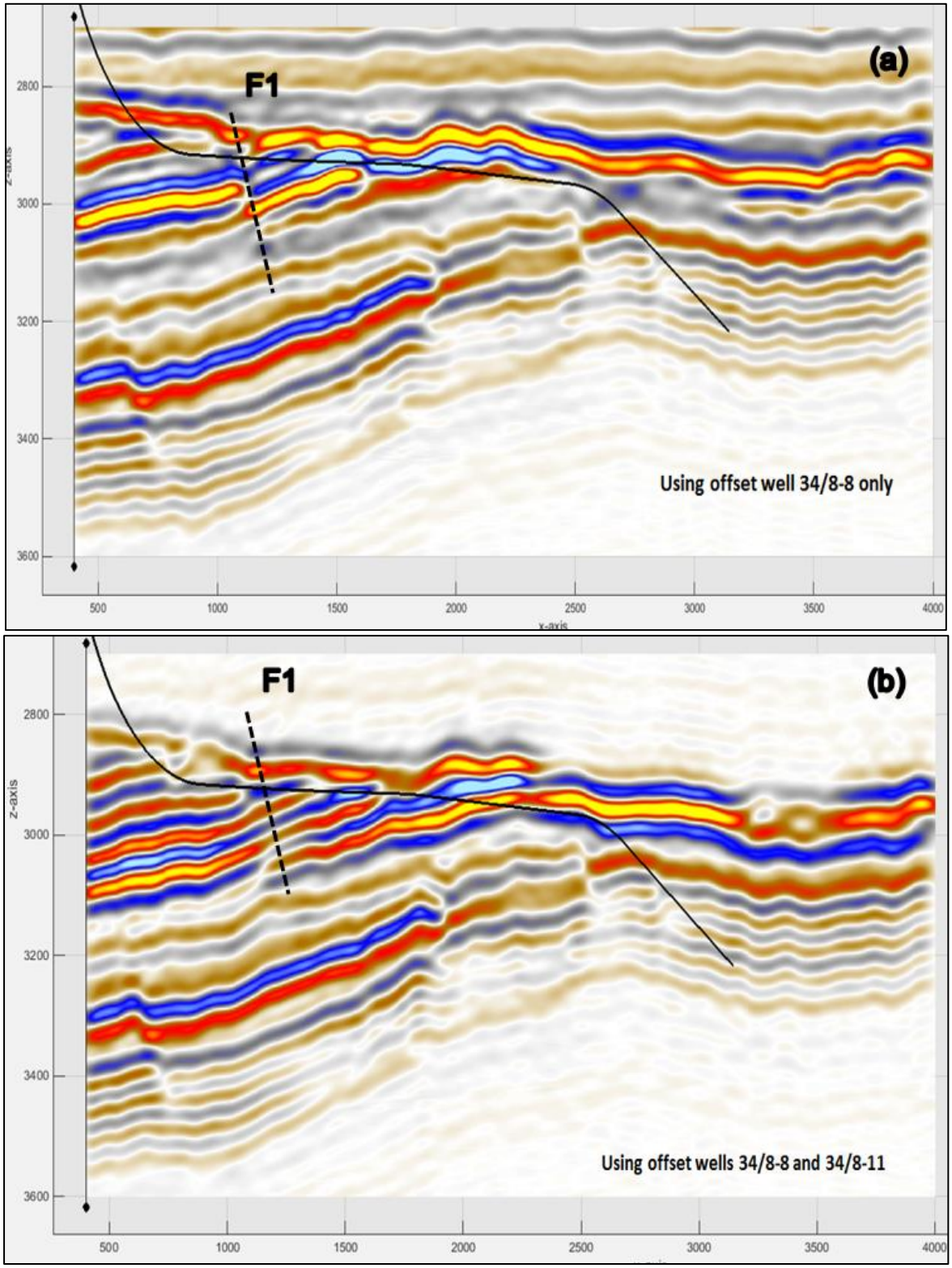

Figure 35: (a) *Synthetic Seismic for the geomodel constructed using offset well 34/8-8 only, fault F1 marked approximately; (b) Synthetic Seismic for the geomodel constructed using a combination of offset wells 34/8-8 and 34/8-11, fault F1 marked approximately (Ref. CES Software)*

The sections ahead in this report discuss the scenarios (Communication scenario and Sealing Fault scenario) built on the geomodels. All these scenarios were made for both the geomodels namely, geomodel using well 34/8-8 only and using a combination of wells 34/8-8 and 34/8-11.

For simplicity, we call the geomodel built using offset well 34/8-8 as **Geomodel A.** The geomodel built using a combination of offset wells 34/8-8 and 34/8-11 is called **Geomodel B**.

8 Pre-job CES Resistivity model Scenarios

Once a geomodel is finalized, various scenarios can be studied on it, with certain variations to investigate the sensitivity to fluid, lithological or structural changes.

As can be seen in figure 36, the planned trajectory (in red solid line) for the well A-16 H passes through the Upper Brent, then into the Lower Brent and crosses the Fault F1. The main focus in this study will be the landing of the well, the heel-section before the main fault F1 and the area around the fault F1.

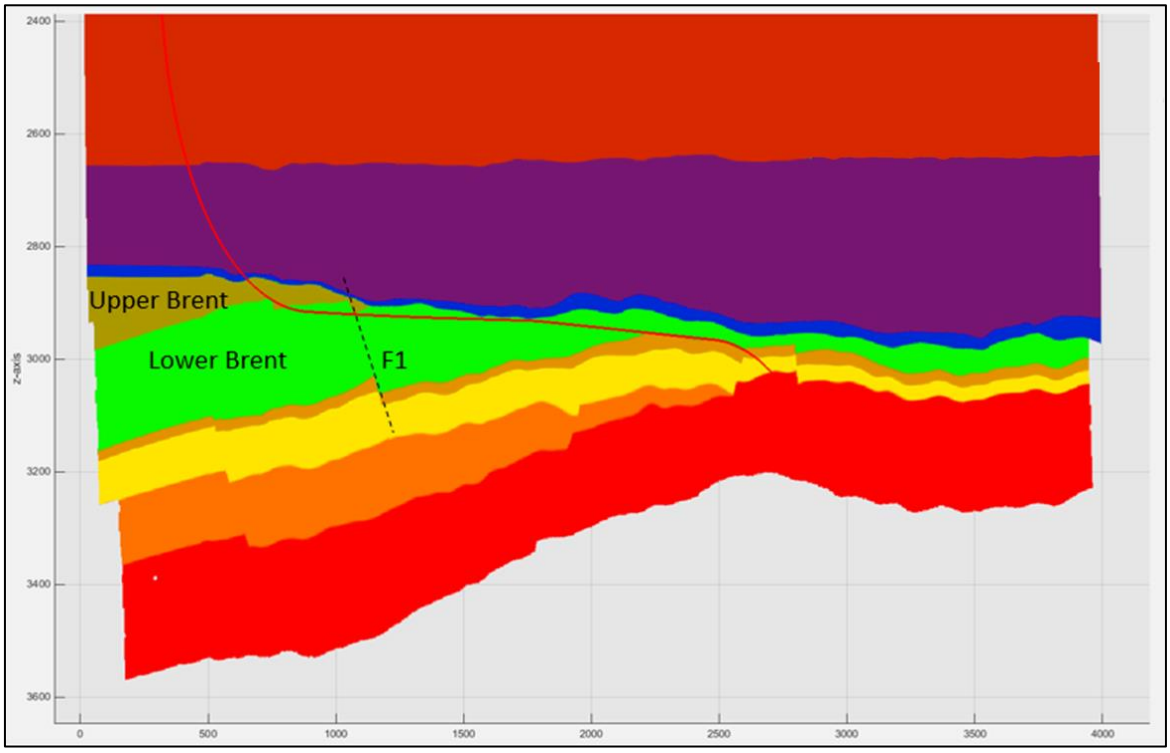

Figure 36: *The Geomodel showing planned trajectory for well A-16 H and location of Fault F1 (Ref. CES Software)*

During the restoration process, the throw of the fault F1 was kept constant at 55 m. This was done to bring the synthetic seismic match with the original seismic line. Some scenarios were built with varied fault throws in order to study the effect of variation on the synthetic seismic. These will be presented in chapter 9.

Petrophysical Model

The CES geomodel comprises of geological layers that have been populated by the properties (such as Gamma, Density, Neutron, Resistivity etc.) from the offset wells. These geomodels have to be converted to resistivity models that would further be used as inputs to the WebGS software to produce resistivity inversion profiles. The scenarios considered in this study were constructed on the geomodel using specific Petrophysical equations (figure 37) resulting in resistivity models. The parameters used in these equations have been derived from regional geological knowledge and were inputs from Statoil ASA's internal Concept Phase Report (Concept Phase Report, Statoil ASA).

```
F 1     por|frac|b|b2=abs(((2.68-Density)/(2.68-0.82)));
        b=1.0*b2;

F 2     K|frac|c|c=10.^(25.64.*por-3.66);

F 3     Sand|frac|s| ina=find(por>0.15);s=ones(size(por));
        s=s-1;s(ina)=1;

F 4     J|frac|d|; d=TOWC_2944.*((K.^0.5)./(por.^0.5));

F 5     Swh2|frac|a| ina=find(TOWC_2944>0.1 & Sand > 0.1);
        a=ones(size(Sand));a(ina)=1.16.*J(ina).^(-0.23);

F 6     Res2|Ohmm|r| ina=find(Sand>0);r=ones(size(Sand));
        nevner(ina)=(por(ina).^1.82).*(Swh2(ina).^2.27);
        r=r.*Resistivity;r(ina)=((0.065)./(nevner(ina)));
```

Figure 37: *Petrophysical equations used during the construction of the scenarios on the geomodel (Ref. MATLAB Software)*

As seen in the figure 37, porosity, permeability, net sand, J function, water saturation and therefore resistivity were calculated, and hence the resistivity model was generated.

The equation used to calculate the porosity (Φ) is given by-

$$\Phi = \frac{\rho_{ma} - \rho_b}{\rho_{ma} - \rho_f}$$

where, ρ_{ma} = 2.68 g/cc, ρ_f = 0.82 g/cc and ρ_b = is the density log response (Concept Phase Report, Statoil ASA).

To calculate the permeability (K), the equation used was (Concept Phase Report, Statoil ASA)-

$$K = 10^{25.64 * (\Phi - 3.66)}$$

Net sand is defined where $\Phi > 0.15$.

The J function was defined by-

$$J = H * \sqrt{\frac{K}{\Phi}}$$

where, J function varies with depth as,

H = (depth of the oil-water contact – true vertical depth)

The saturation of water (S_w) is calculated based on the J function and is given as-

$$S_w = 1.16 * J^{-0.23}$$

In order to calculate the resistivity, the Archie equation is used for the sand with porosity greater than 0.15, i.e. for good reservoir sand.

The Archie equation is given by-

$$S_w{}^n = \frac{R_w}{R_t * \Phi^m}$$

Hence,

$$R_t = R_w * S_w^{-n} * \Phi^{-m}$$

where, m = 1.82, n = 2.27 and R_w = 0.065 Ohmm.

The lower porosity bad reservoir quality sand or shale resistivity is extrapolated from the offset wells.

8.1 Communication Scenario

The Communication scenario was the first scenario to be studied on the geomodel. In this scenario, the communication of fluids was considered to be possible from the left of the fault F1 to the right of the fault (figure 38 and 39).

The oil-water contact is expected to be at 2944 m TVD (refer section 3.4). By applying the Petrophysical equations on the geomodel, it is considered that the layers below 2944 m TVD are filled with water and hence they have water saturation equal to 1.

Figure 38 shows the resultant geomodel in this scenario in terms of water saturation. Note that the resistivity values (figure 39) were used as inputs for the inversion process in WebGS and not the water saturation values. The red solid line shows the planned well trajectory for the well A-16 H.

The boundary between the Upper and Lower Brent (UB-LB Boundary) is marked in a black solid line.

The sand in the Upper and Lower Brent with a porosity value greater than 0.15, i.e. good reservoir sand is given a value of resistivity calculated by the Archie's equation as explained by the Petrophysical model. The lower porosity bad reservoir quality sand or shale resistivity is extrapolated from the offset wells. The figure 39 is a representation of the geomodel in terms of resistivity values.

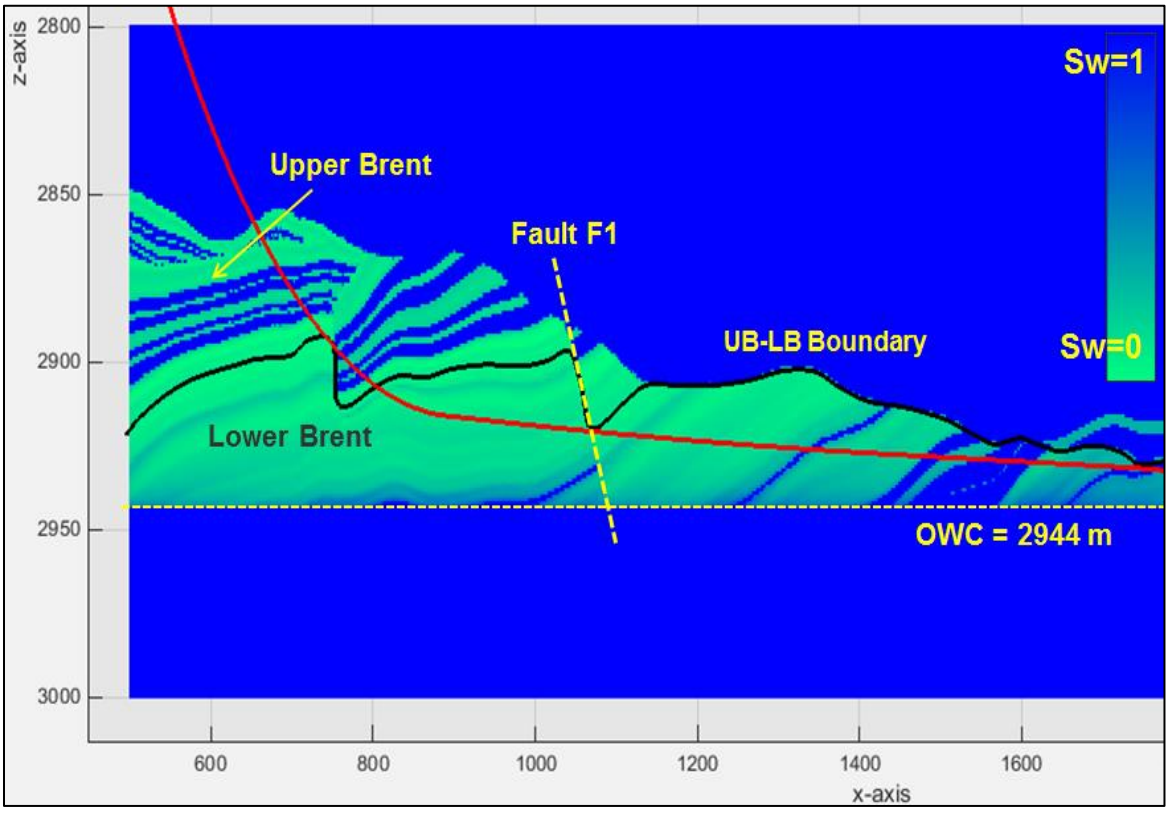

Figure 38: *Geomodel for the Communication scenario, green representing lower water saturation and blue representing water saturated zone, planned well trajectory in red solid line (Ref. CES Software)*

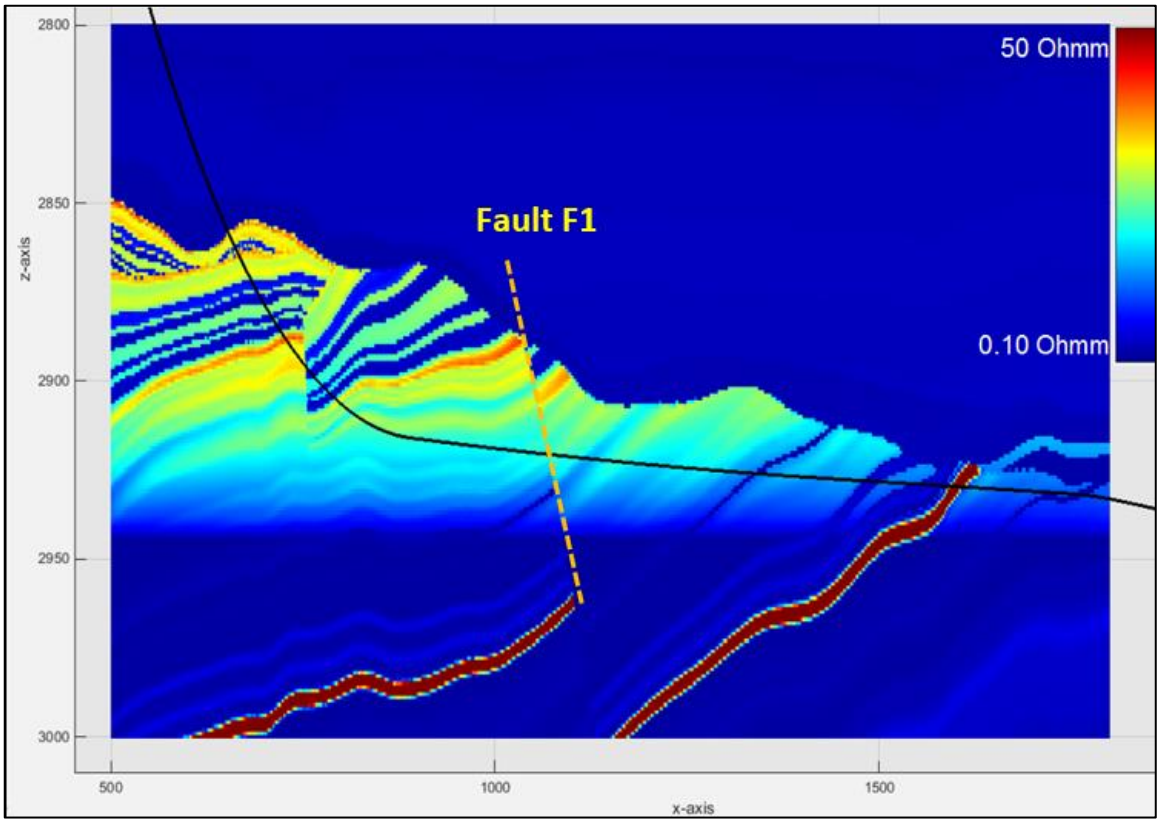

Figure 39: *Geomodel for the Communication scenario in terms of resistivity with blue representing lower resistivity values (water zone) and red representing higher resistivity values, planned well trajectory in black solid line (Ref. CES Software)*

In figure 39, the deep red features (approx. z= 2950 m to 3000 m) do not necessarily represent high resistivity due to the presence of hydrocarbons. These may be a result of cementation in the Lower Brent group. This cementation phenomenon can be supported by the high density and resistivity values in the offset well logs. In figure 27, these can be observed as spikes in the RT and RHOB logs at around 3020 m MD. In figure 28, these can be observed at 2987 m MD.

8.2 Sealing Fault Scenario

The second scenario to be considered is the Sealing Fault scenario (figure 40), where the Lower Brent to the left of the Fault F1 is filled with water. The Upper Brent and the Lower Brent to the right of fault F1 are filled with hydrocarbons.

This scenario was considered because the well 34/8 A-10 AH (figure 5) is a water injector and is present in the same segment N1B, as well 34/8-A-16 H to be drilled. Hence, there could be a possibility of presence of water in the sand and, therefore, to be prepared for such a water flooded situation, this scenario was considered.

Using the Petrophysical equations, the layers below 2944 m TVD were filled with water. The Lower Brent to the left of Fault F1 with porosity greater than 0.15 was filled with water i.e. the water saturation was equal to 1 and that with porosity less than 0.15 was given resistivity values from the offset wells.

The sand in the Upper Brent and in the Lower Brent to the right of fault F1, with porosity greater than 0.15 was given resistivity values calculated from the Archie's equation. The bad reservoir quality sand with lower porosity values and the shale resistivity was extrapolated from the offset wells.

Figure 40 displays the geomodel in this scenario in terms of water saturation. The planned well trajectory is marked in a red solid line and the boundary between the Upper and Lower Brent is marked in black solid line.

The figure 41 is a representation of the geomodel in terms of resistivity values.

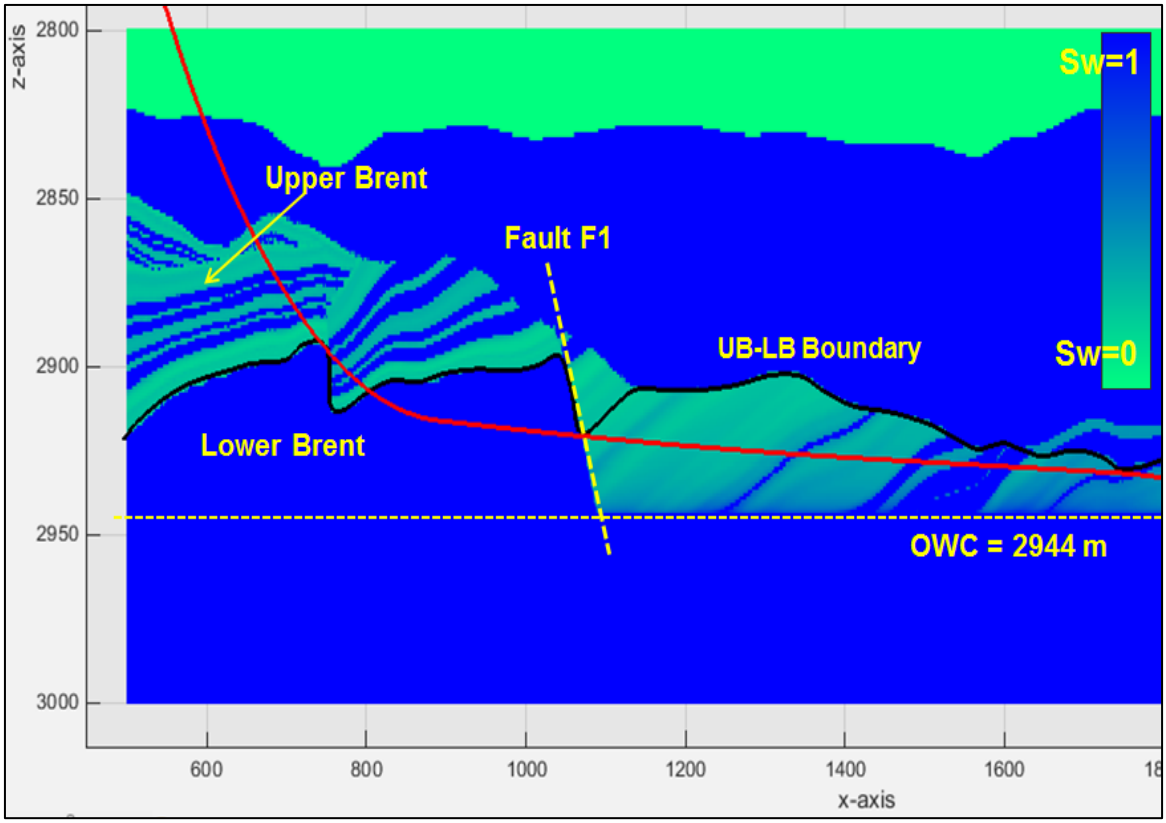

Figure 40: *Geomodel for the Sealing Fault Scenario, green representing lower water saturation and blue representing water saturated zone (Ref. CES Software)*

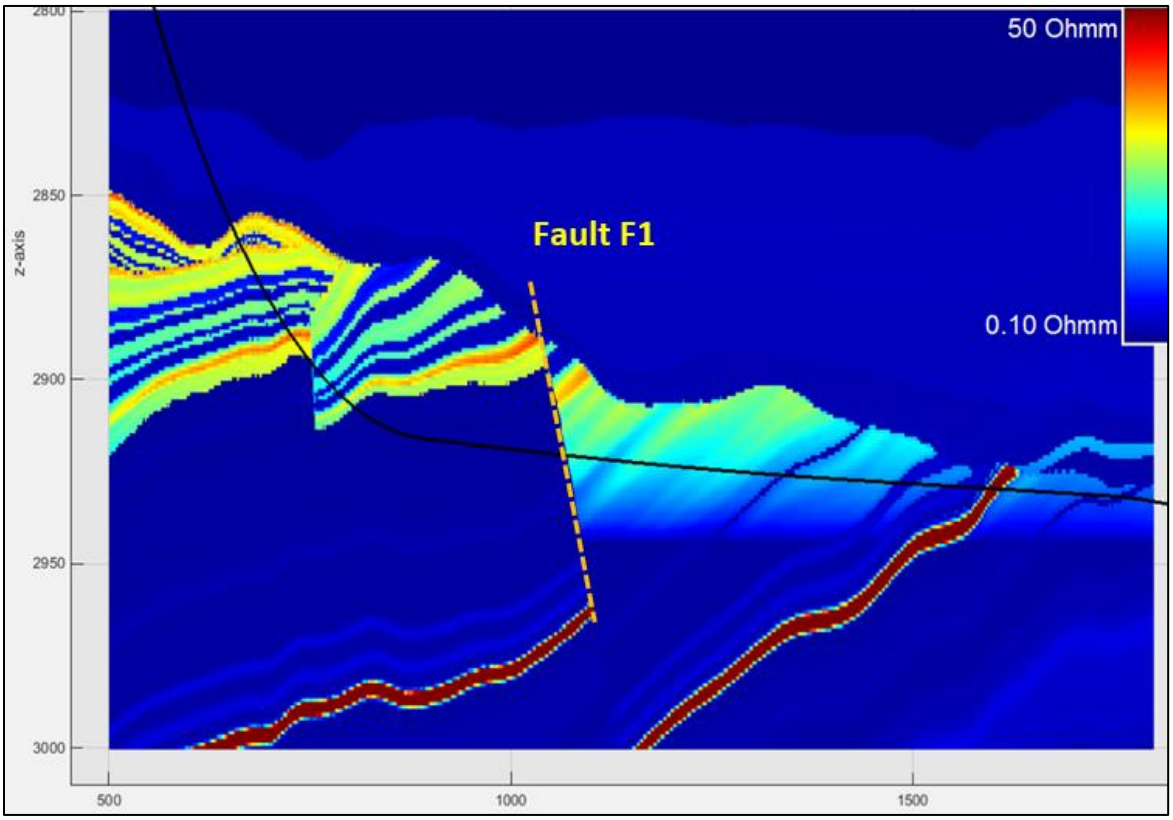

Figure 41: *Geomodel for the Sealing Fault Scenario in terms of resistivity, blue representing lower resistivity values (water zone) and red representing higher resistivity values (Ref. CES Software)*

In figure 41, the deep red features (approx. z= 2950 m to 3000 m) may be a result of cementation in the Lower Brent group as discussed in section 8.1 for figure 39.

8.3 Oil-Water contact depth position Scenarios

The oil-water contact (OWC) was expected to be at 2944 m TVD. The Communication scenario (section 8.1) was studied with variations in the OWC depth. Hence the resistivity inversion profiles were generated with OWC positioned at TVD 2934 m, 2939 m, 2959 m, 2964 m, 2969 m and 2974 m, i.e. above and below the regional OWC at 2944 m TVD.

The results obtained from these cases are presented in chapter 9 and are available in Appendix B.

9 Pre-job Scenarios Inversion Results

This chapter will present all the results obtained in this study for the scenarios and cases mentioned in chapter 8.

Fault F1 throw Scenarios

In order to justify the Fault throw of the main fault in consideration, namely F1, as 55 m, some cases were made with variations in the fault throw.

During **Restoration** process, keeping the fault throw constant at 55 m can be justified by the seismic image at that instant in time in restoration. Figure 42(a) clearly shows the horizons on the seismic line to the left of the fault F1 are in proper alignment with those to the right of the fault F1 when the fault throw is equal to 55 m. If this value is increased or decreased, the horizons will not be aligned well and therefore it would result in incorrect restoration process (figure 42(b)).

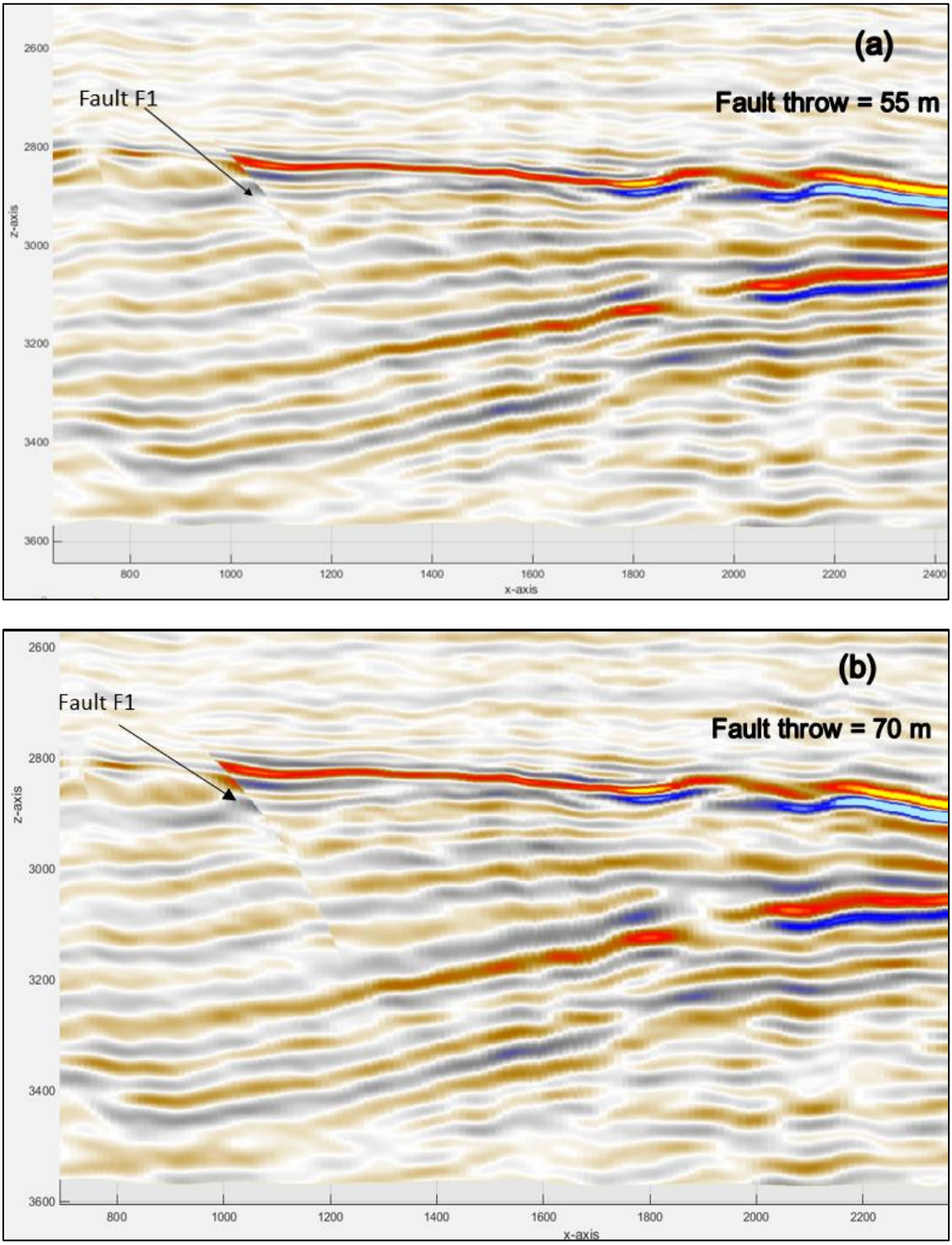

Figure 42: (a) *Seismic image after restoration of fault F1 showing proper alignment of horizons at fault throw equal to 55 m; (b) Seismic image after restoration of fault F1 at fault throw equal to 70 m showing improper alignment of horizons (Ref. CES Software)*

Therefore, the variation in the fault throw of the fault F1 was made only at the time of **Reconstruction.** The fault throw was changed to 45 m, 50 m, 60 m, 65 m and 75 m to appropriately demonstrate the changes caused due to variation in the fault throws.

The fault F1 is a normal fault with the hanging wall towards the East of the fault plane and the footwall towards the west of the fault plane (figure 43). Hence, with a change in the fault throw, we expect a change towards the hanging wall side of the fault on the synthetic seismic.

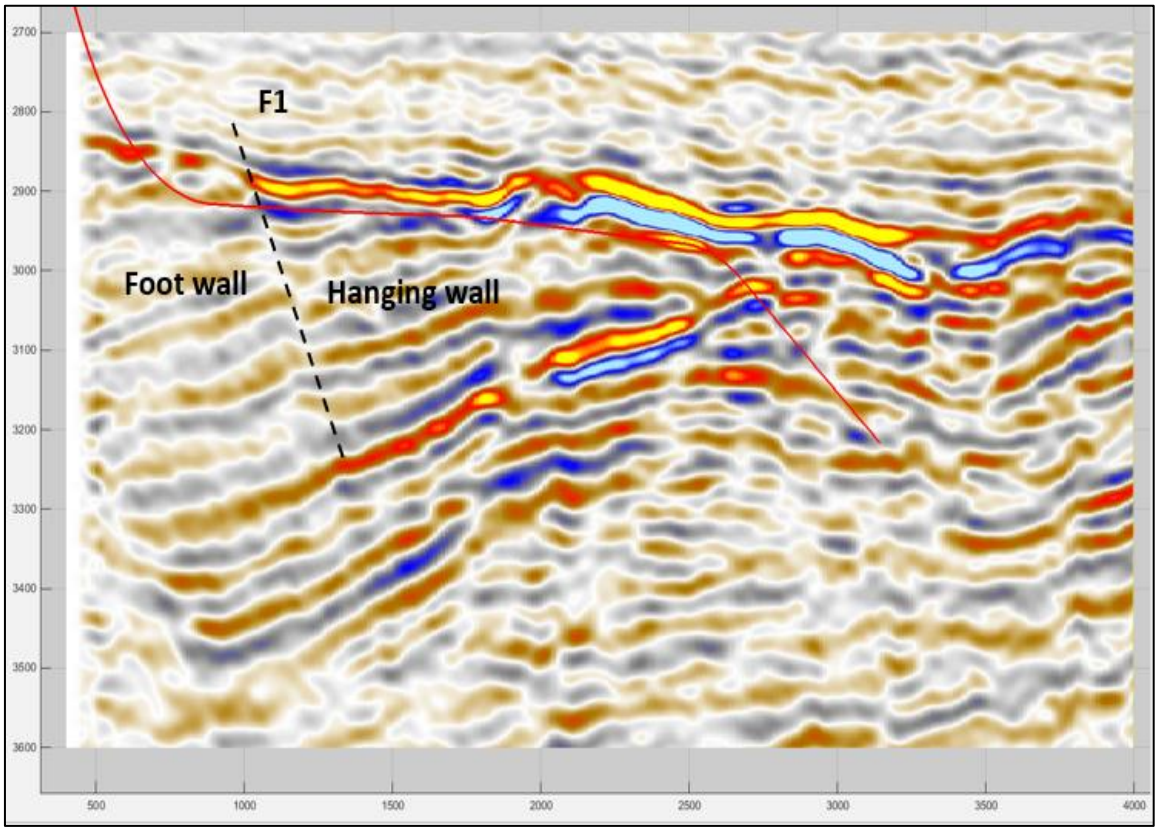

Figure 43: *Original Seismic image showing the position of fault F1 (Ref. CES Software)*

Appendix C summarizes the resulting synthetic seismic images generated from the variation in fault throws. For each image, the left side depicts the original seismic line and the right side depicts the synthetic seismic image. They have been put together in one window for one to one comparison of each reflector and therefore, for a better visualization. These images have been captured at two different positions on the x axis, namely, at x equal to 1205 m and 1250 m.

In this section, we discuss a few of these cases and make some important observations.

In figure 44, the seismic images at x=1205 m have been assembled. The synthetic seismic images clearly show that for cases with fault throw equal to 45 m, 50 m and 75 m, the reflectors in the seismic image as compared to the original seismic are not overlapping and hence are at incorrect positions. These mismatches are not acceptable.

Figure 45 shows the fault throw cases at x=1250 m. From these images, it is visible that for all fault throws except for fault throw = 55 m, the reflectors on the synthetic seismic are deviating from their actual position on the original seismic image.

Hence, we conclude that the fault throw equal to 55 m is justified. Although this is the best match, but we can say that fault throw equal to 60 m and 65 m is also acceptable at the reservoir level. The synthetic seismic with fault throw equal to 60 m and 65 m do not show much variation as compared to that at 55 m (figure 46 and figure 47). A difference of 10 m is acceptable since it is below the resolution of the seismic images (20 -30 m).

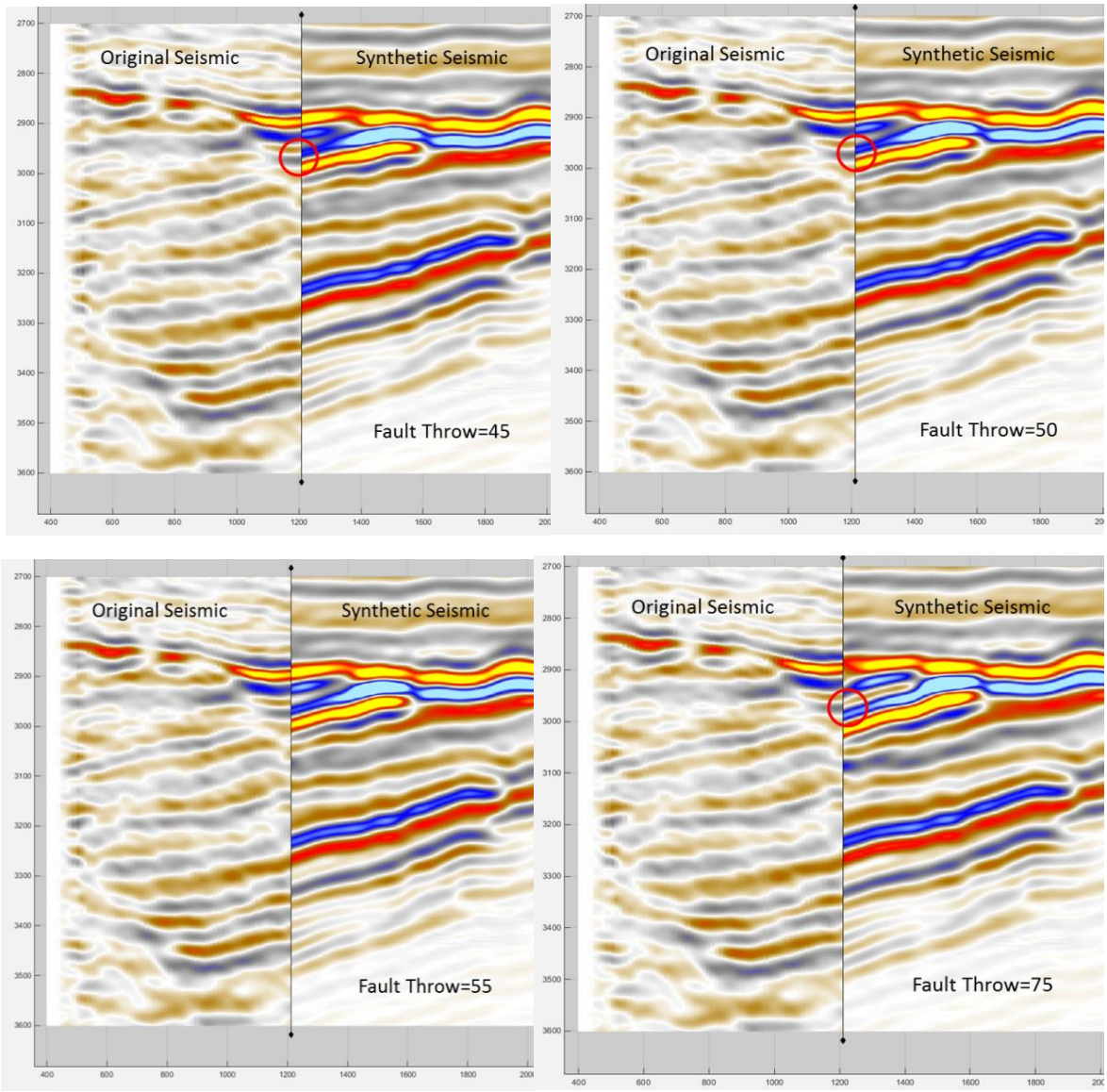

Figure 44: *Synthetic Seismic compared with Original Seismic Image for various fault throws at x=1205 m (Ref. CES Software)*

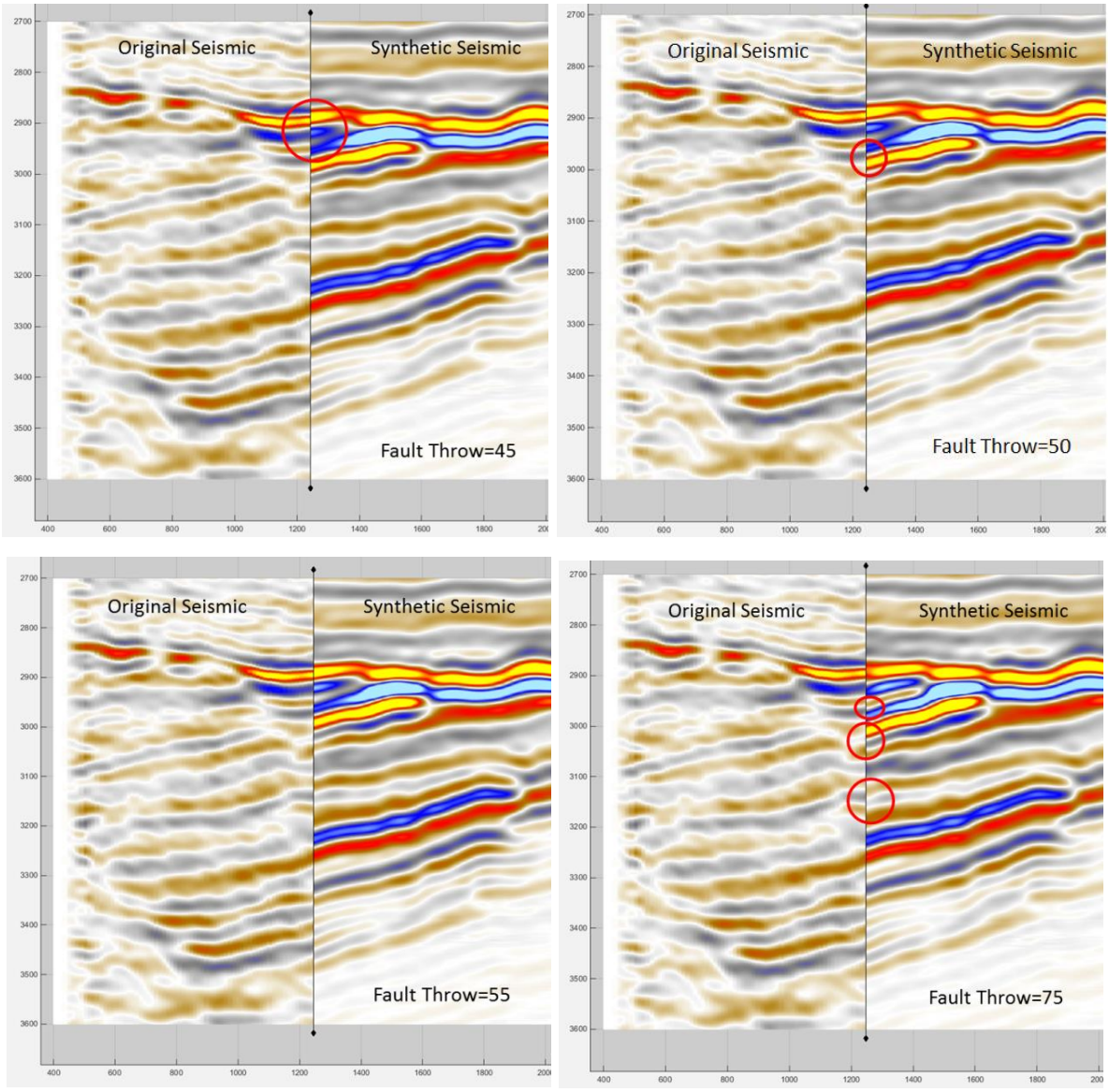

Figure 45: *Synthetic Seismic compared with Original Seismic Image for various fault throws at x=1250 m (Ref. CES Software)*

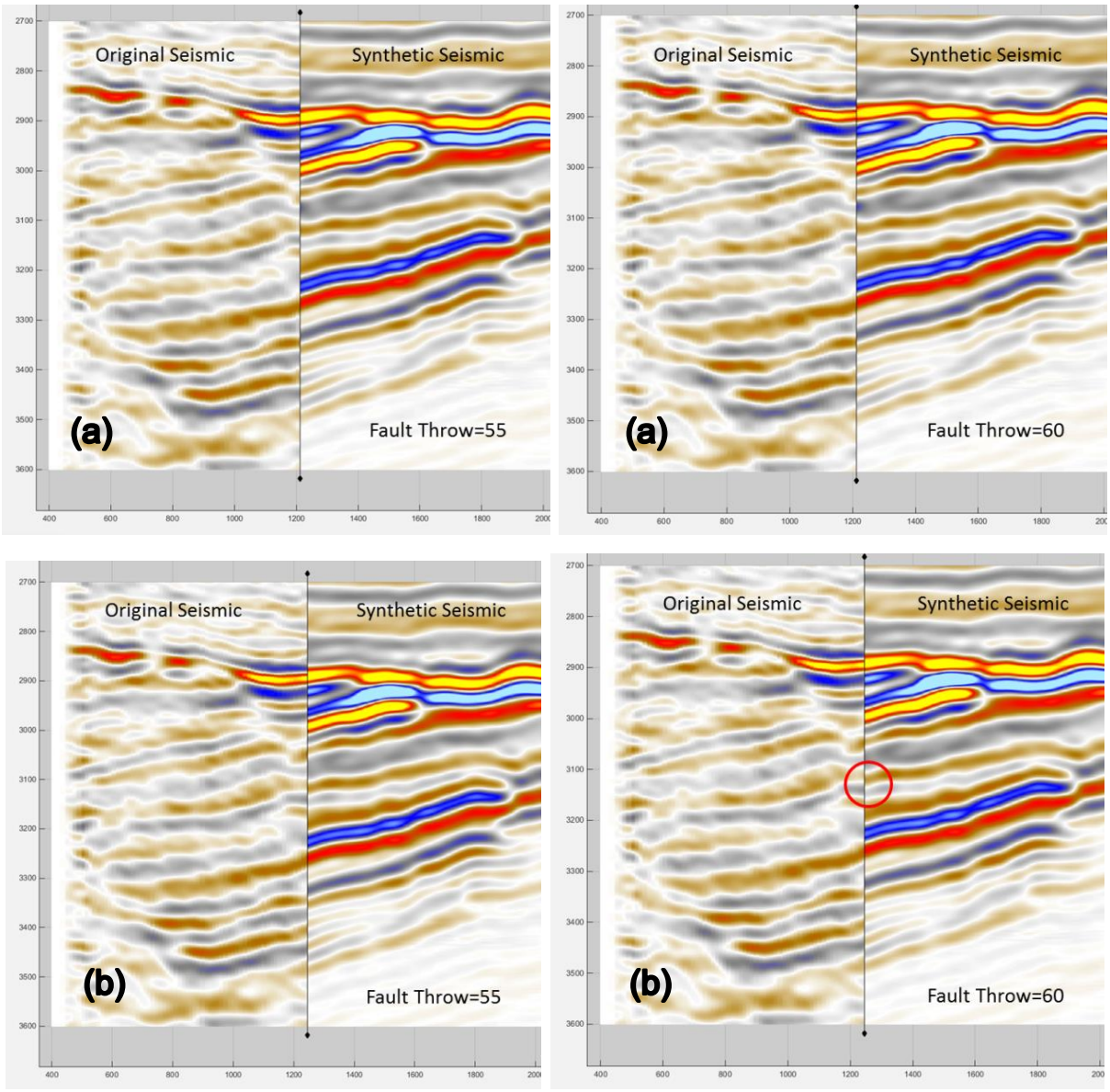

Figure 46: *(a) Synthetic Seismic compared with Original Seismic Image for fault throws = 55 m and 60 m at x= 1205 m; (b) and at 1250 m (below) (Ref. CES Software)*

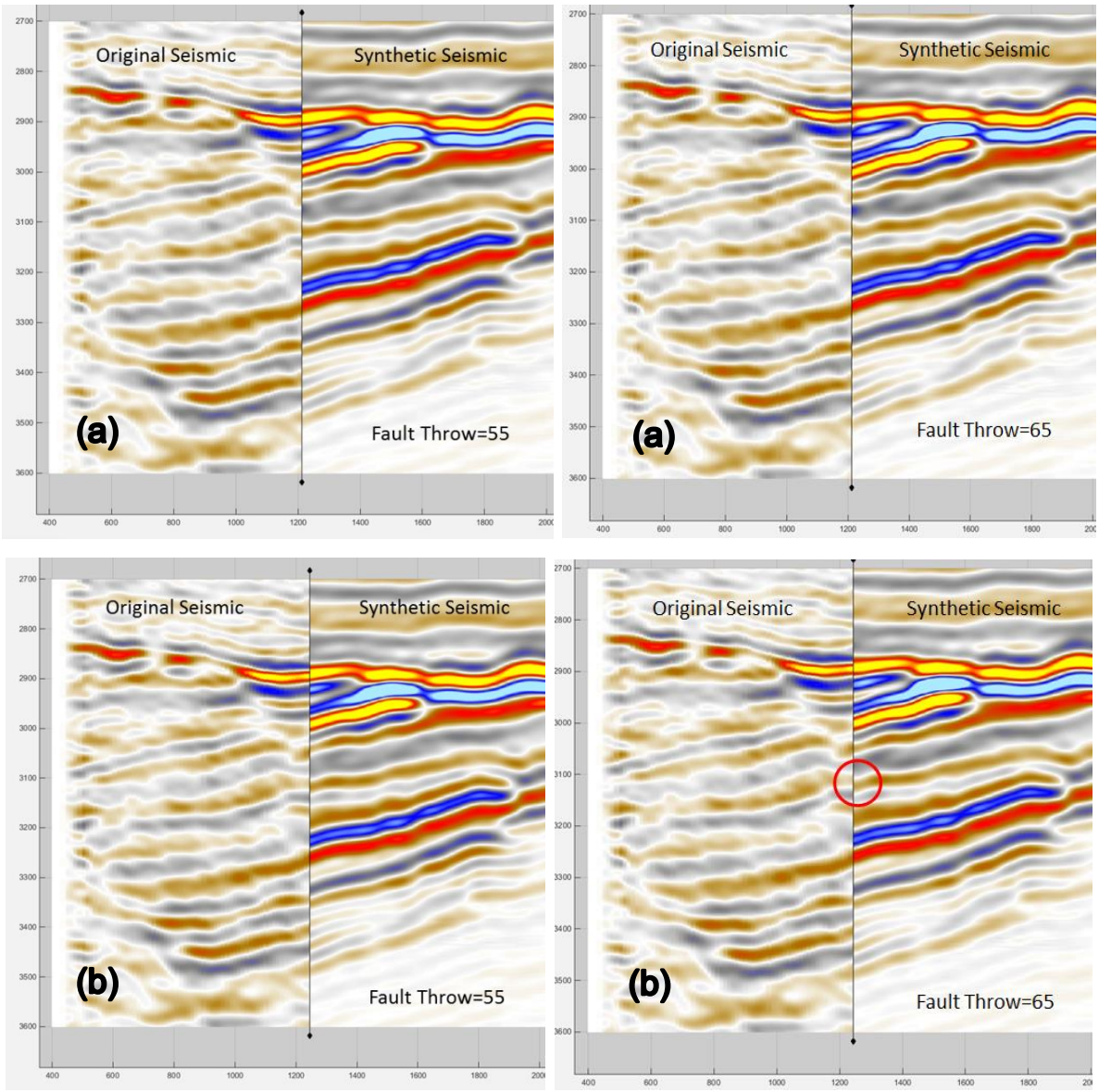

Figure 47: *(a) Synthetic Seismic compared with Original Seismic Image for fault throws = 55 m and 65 m at x= 1205 m; (b) and at 1250 m (Ref. CES Software)*

9.1 Communication Scenario

The geomodel for the Communication scenario was input into WebGS and the Forward and Inverse simulations were run in order to obtain a resistivity inversion profile for this case. Figure 48, shows this inversion image for both Geomodels A and B.

The colour scale in the figure represents that blue depicts the lower resistivity values (lowest is 0.01 Ohmm) and red depicts the higher resistivity value (highest is 50 Ohmm) range.

In the resistivity inversion profile in the figure, the oil-water contact is clearly visible. This is about 2944 m on the z axis (true vertical depth) for both the Geomodels A and B. It is depicted by a strong contrast in the colours. The bluish green colour below this level depicts low resistivity, i.e. water. The higher resistivity values above are shown in shades of red and yellow. This may indicate the presence of hydrocarbons. Hence the oil-water contact is identified for both geomodels.

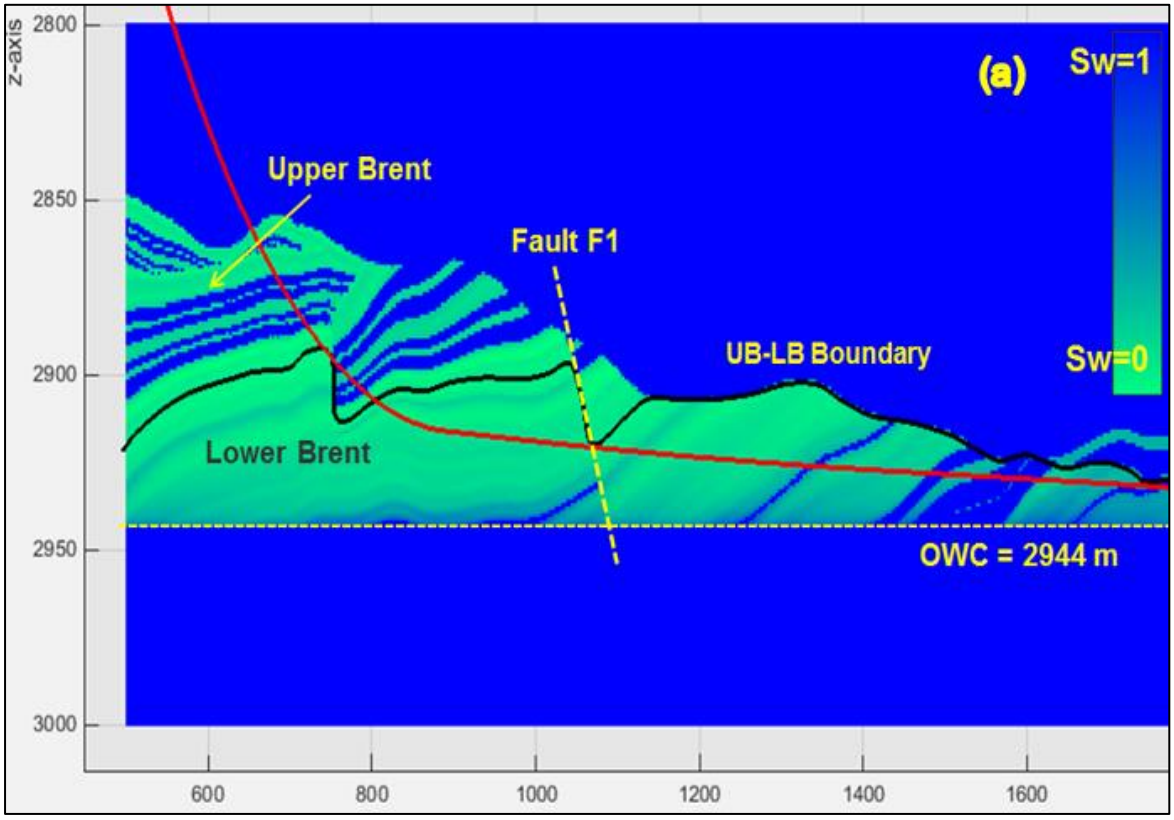
z-axis
2800
2850
2900
2950
3000
600
800
1000
1200
1400
1600
(a)
Sw=1
Sw=0
Upper Brent
Fault F1
UB-LB Boundary
Lower Brent
OWC = 2944 m

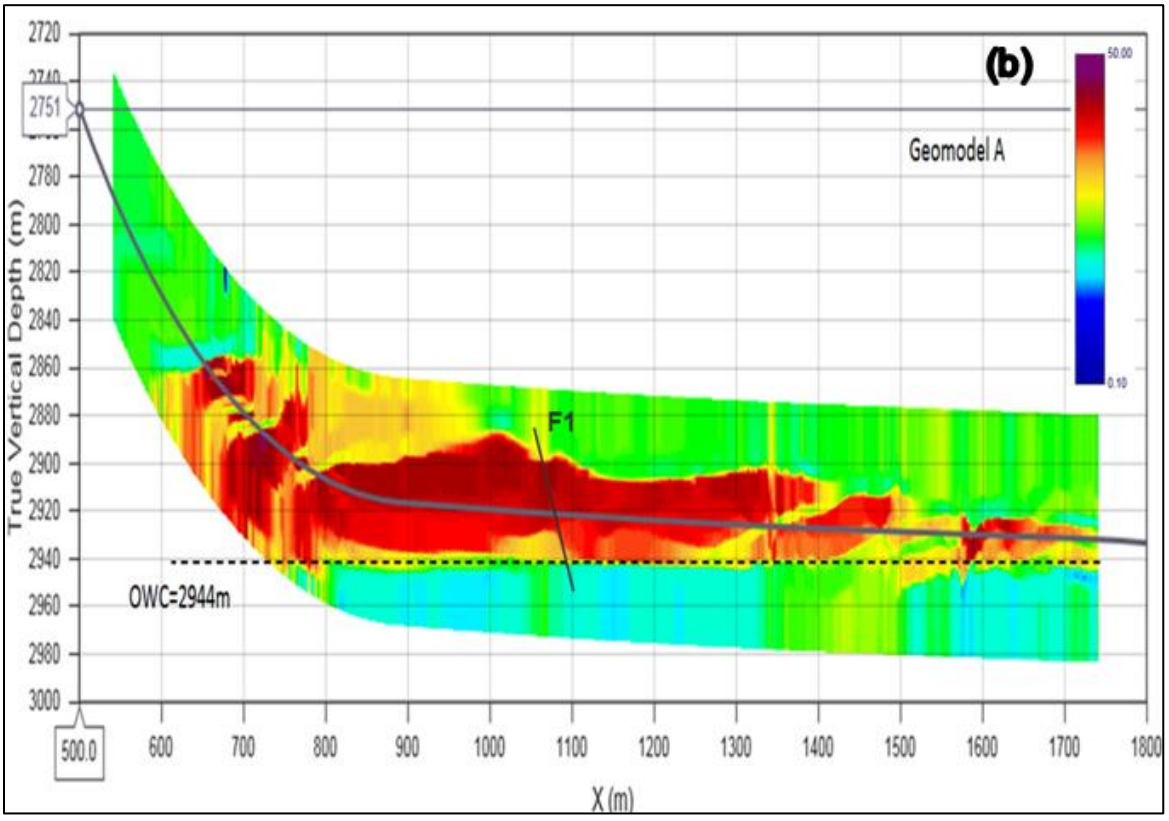
(b)
Geomodel A
50.00
0.10
2751
True Vertical Depth (m)
2720
2780
2800
2820
2840
2860
2880
2900
2920
2940
2960
2980
3000
F1
OWC=2944m
500.0
600
700
800
900
1000
1100
1200
1300
1400
1500
1600
1700
1800
X (m)

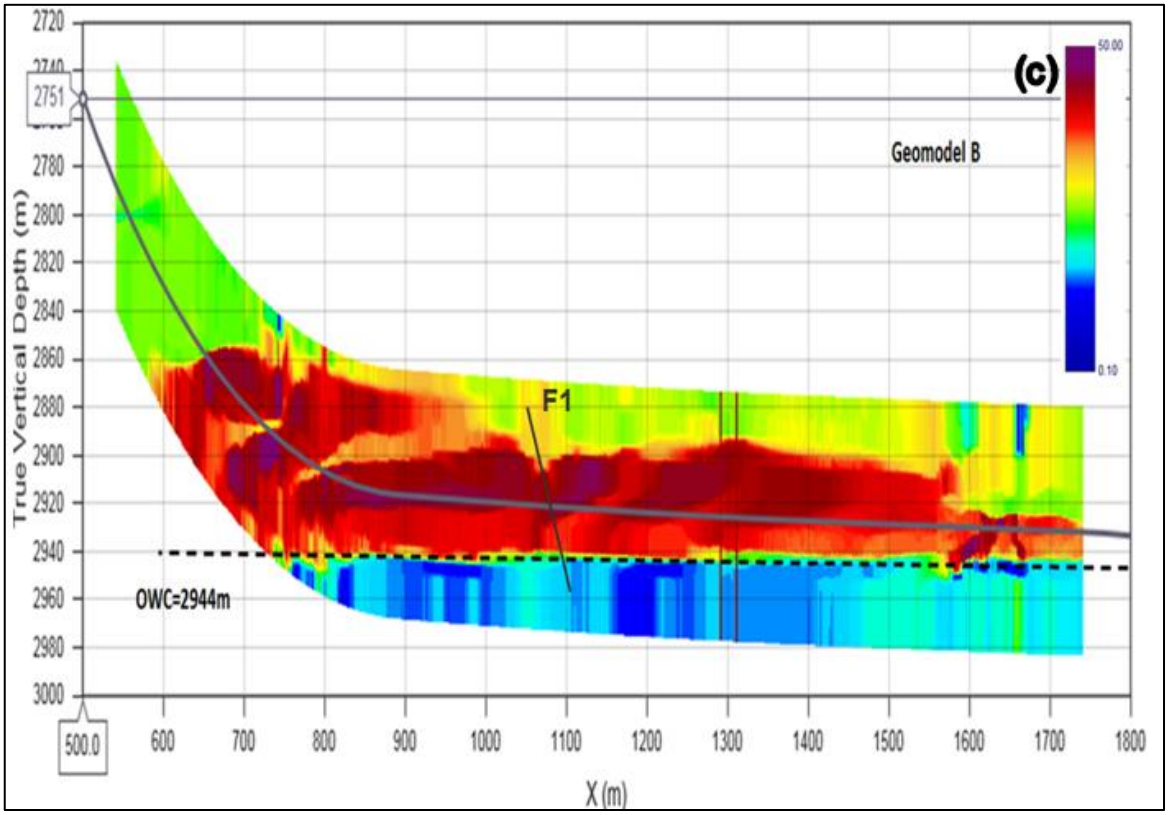

Figure 48: (a) *The Geomodel from CES in terms of water saturation; (b) the WebGS Resistivity Inversion for Communication scenario for Geomodel A; (c) the WebGS Resistivity Inversion for Communication scenario for Geomodel B; with blue depicting lower resistivity values and red depicting higher resistivity values (Ref. CES and WebGS Software)*

The fault F1 has been marked on the inversion images. However, this fault cannot be visually interpreted easily since the footwall and hanging wall cannot be well differentiated. In the inversion images from both Geomodels A and B we see high resistivity values on both sides of the fault plane. This may indicate that the communication of fluids through the fault plane exists, i.e. the Communication scenario.

The figure 48 also displays bluish green, i.e. low resistivity values, in the area above the Brent, at around 2900 m TVD on the z axis. This is possibly due to presence of shales in that area. This confirms what we know from the model and the offset wells that the Viking group shales are present above the Upper Brent.

9.2 Sealing Fault Scenario

The geomodel for the Sealing Fault scenario was input into WebGS and an inversion image was generated for both Geomodels A and B. This is shown in figure 49.

At the entrance of the well (landing and heel section) higher resistivity values are encountered. This may indicate the presence of hydrocarbons in the Upper Brent group.

In the resistivity inversion profile in figure 49, the oil-water contact is clearly visible to the right of fault F1. This is around 2944 m on the z axis (true vertical depth). It is depicted by a strong contrast in the colours. The bluish green colour below this level depicts low resistivity, i.e. water. The higher resistivity values above are shown in shades of red and yellow. This may indicate the hydrocarbons. Hence the oil-water contact is identified.

However, since the Lower Brent to the left side of fault F1 (approximately marked on the inversion images) is filled with water, the oil-water contact in this zone is not at 2944 m. This part of Lower Brent, to the left of the fault, shows lower resistivity values (blue-green).

In this inversion image, the fault F1 is clearly visible since the footwall and hanging wall can be well differentiated by the change in resistivities.

In the area above the Brent to the right of fault F1, at around 2900 m TVD on the z axis, presence of shales from the Viking group is depicted by lower resistivity values.

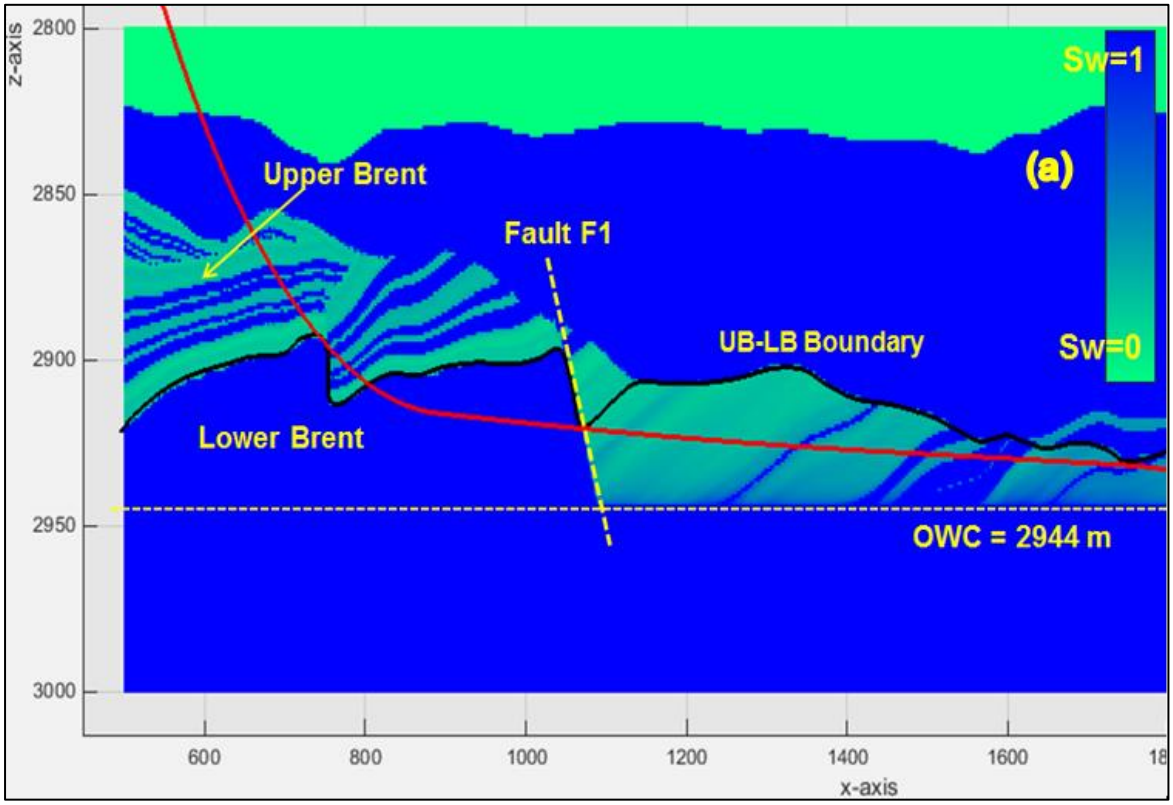
Z-axis
2800
2850
2900
2950
3000
600
800
1000
1200
1400
1600
x-axis
Sw=1
Sw=0
(a)
Upper Brent
Fault F1
UB-LB Boundary
Lower Brent
OWC = 2944 m

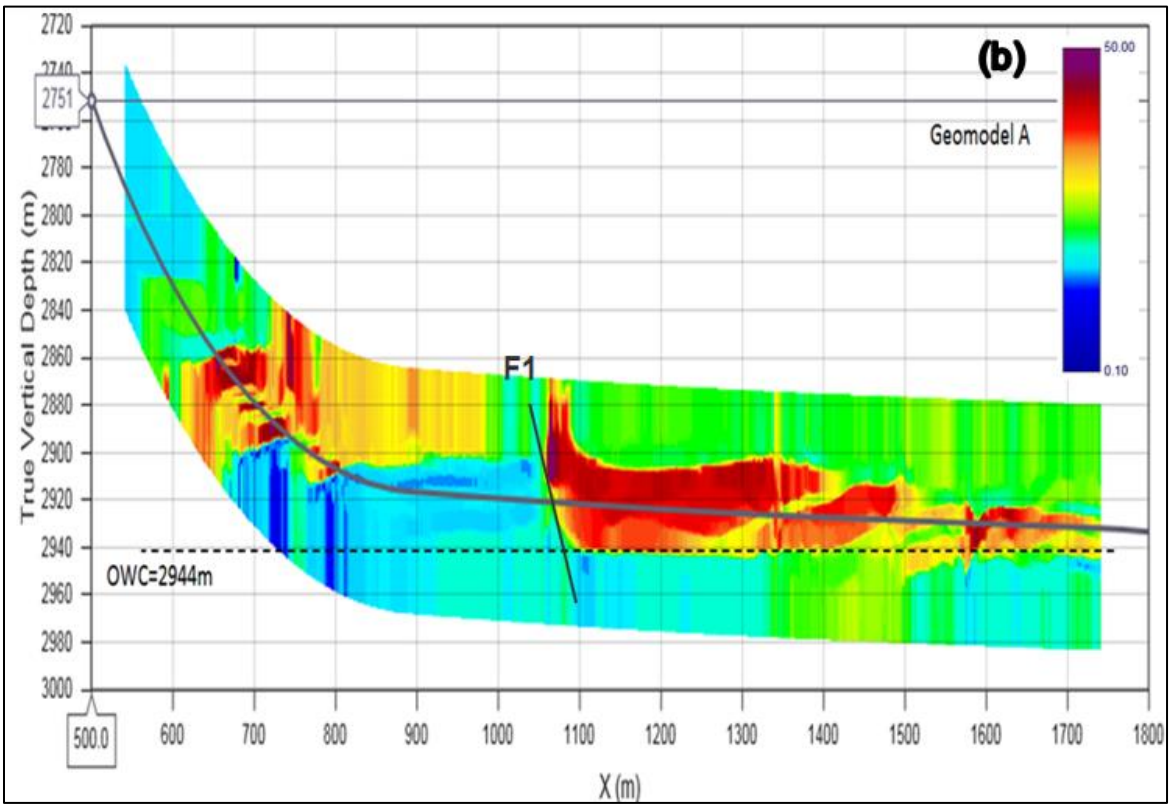
(b)
Geomodel A
50.00
0.10
True Vertical Depth (m)
2720
2751
2780
2800
2820
2840
2860
2880
2900
2920
2940
2960
2980
3000
F1
OWC=2944m
500.0
600
700
800
900
1000
1100
1200
1300
1400
1500
1600
1700
1800
X (m)

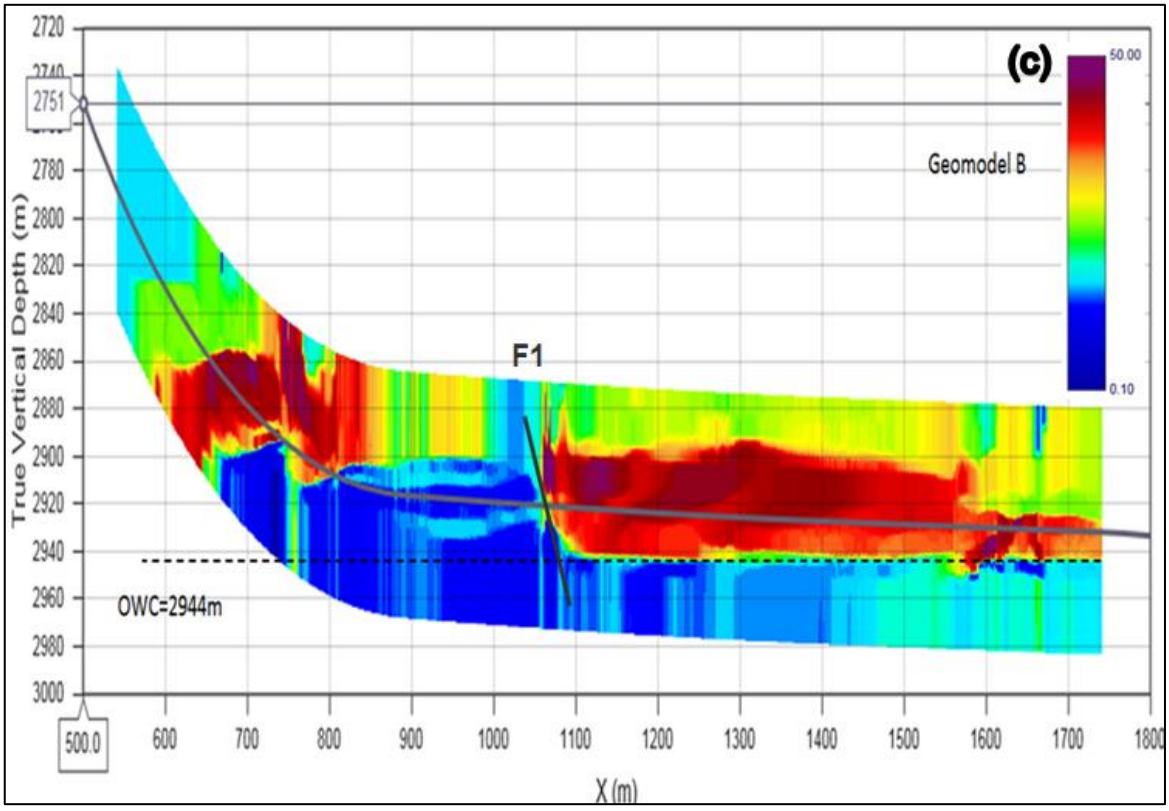

Figure 49: (a) *The Geomodel from CES in terms of water saturation; (b) the WebGS Resistivity Inversions for the Sealing Fault Scenario for Geomodel A; (c) the WebGS Resistivity Inversions for the Sealing Fault Scenario for Geomodel B; with blue depicting lower resistivity values and red depicting higher resistivity values (Ref. CES and WebGS Software)*

9.3 Oil-Water contact depth position Scenarios

The oil-water contact was expected to be present at 2944 m TVD (refer section 3.4). A few cases were run with shifts of 5 m in the position of the OWC above and below its expected position. These were run in order to study the effects of variation in the OWC depth on the inversion answer product generated by WebGS.

The results for all the cases of shifts in the oil-water contact can be found in Appendix B. These were studied only for Geomodel B for the Communication scenario.

For all the inversion images, the depth of investigation from the wellbore to the OWC was picked at a constant location on the x axis (approximately x = 1120 m). This was done to pick good measurements when the well trajectory is horizontal and make all the DOI results consistent with each other. For some cases, the OWC may be detected before this picking point. But for other cases, some artefacts exist, for example, those in the heel section of the well that follow the curvature of the well trajectory, as marked in figures 51 and 52.

The base case, i.e. OWC at 2944 m TVD is shown in figure 50. The oil-water contact is detected at 20 m away from the well trajectory.

The oil-water contacts at 2934 m, 2939 m, 2944 m, 2959 m and 2964 m TVD were detected as can be seen in the resistivity inversion profiles in Appendix B. However, the oil-water contacts beyond 2964 m TVD, i.e. OWC at 2969 m and 2974 m were not detected.

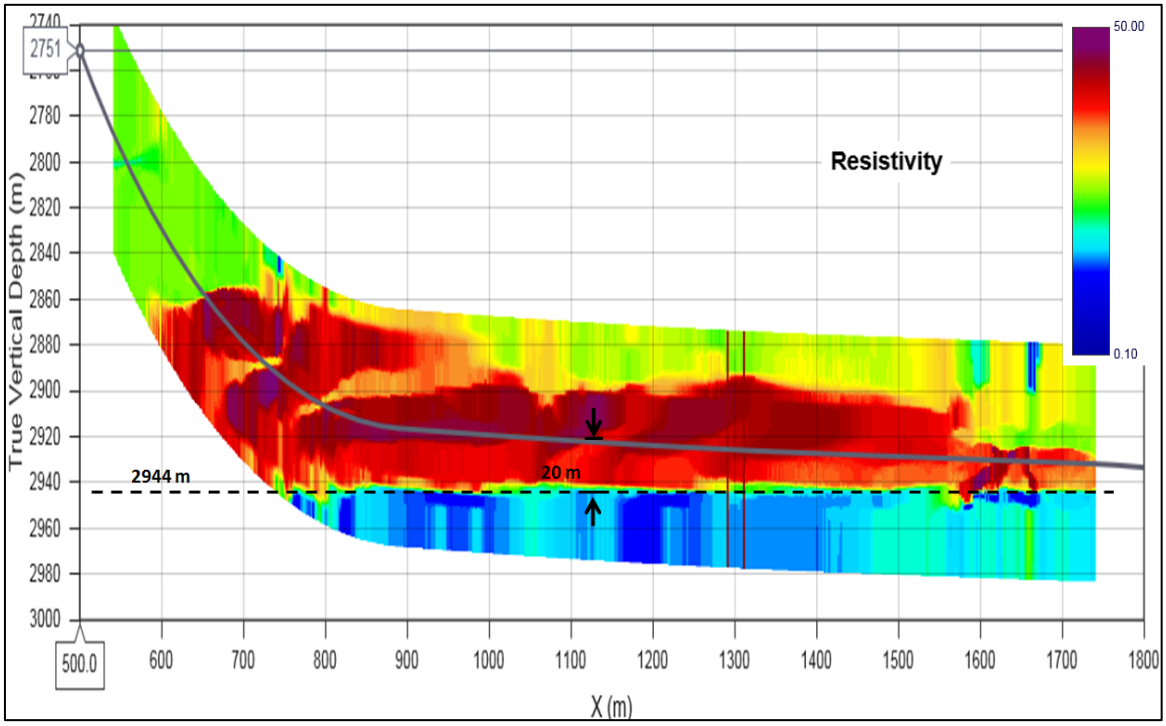

Figure 50: *WebGS Resistivity Inversion image for OWC = 2944 m TVD, OWC detected 20 m away from the borehole (Ref. WebGS Software)*

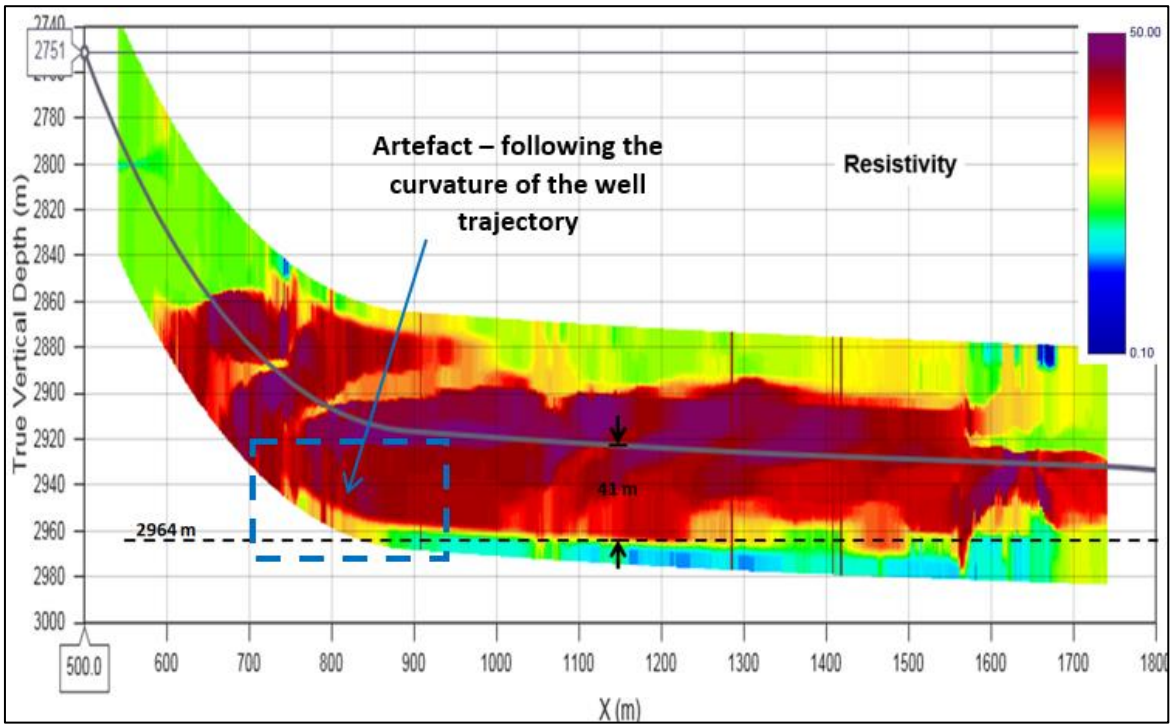

Figure 51: *WebGS Resistivity Inversion image for OWC = 2964 m TVD, OWC detected 41 m away from the borehole (Ref. WebGS Software)*

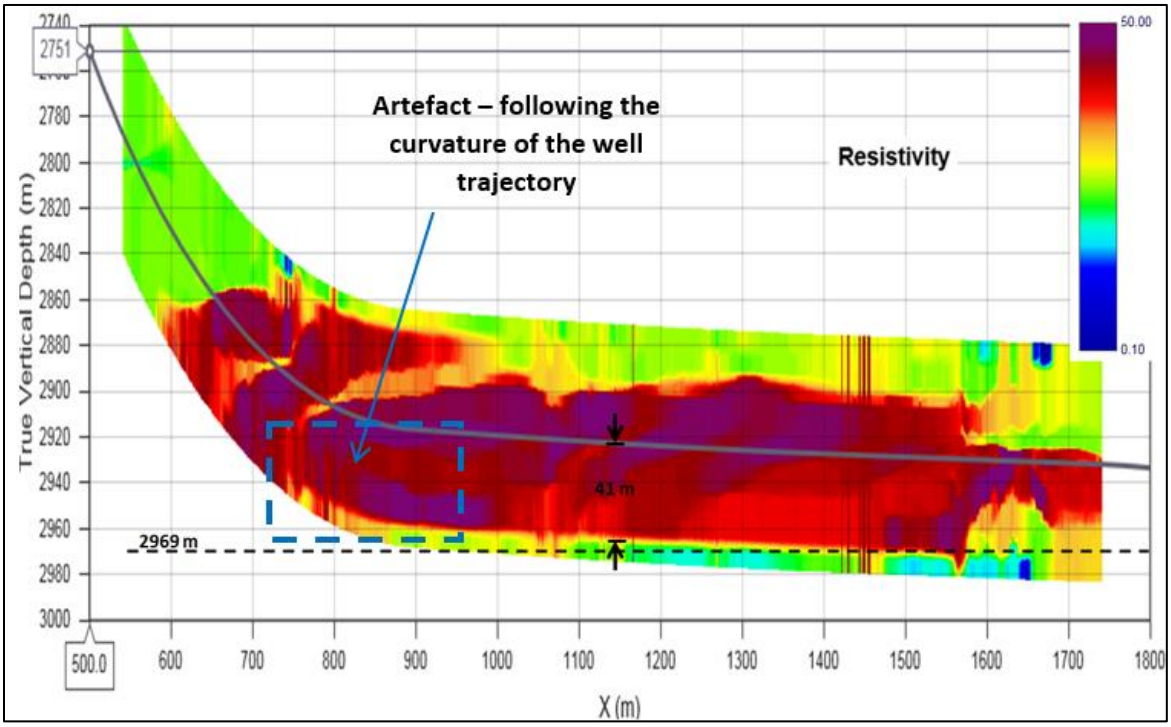

Figure 52: *WebGS Resistivity Inversion image for OWC = 2969 m TVD, OWC not detected at the appropriate location (Ref. WebGS Software)*

When the OWC is at 2964 m TVD, the distance between the Geosphere tool (in the wellbore) and the OWC is 41 m TVD (figure 51). Figure 52 shows the resistivity inversion profile for OWC at 2969 m TVD. However, this is not detected at 2969 m on the z axis, but is above it (about z = 2964 m). This implies that the OWC is at a distance that is beyond the scope of the tool and therefore we conclude that in this scenario, the deep reading tool can detect up to about 40 m away from the borehole.

This can also be confirmed by the results obtained during the semester thesis titled *Software Simulations of an Ultra Deep Resistivity Tool using Synthetic Geo-models, December 2015, NTNU* (Arora P., 2015). In this study, it was concluded that the maximum depth of investigation of the deep reading Geosphere tool was about 38 m TVD for a scenario in which the tool is present in a high resistivity environment and is investigating into a low resistivity environment (water), for given frequencies and Transmitter – Receiver spacings.

An interesting observation is that during the semester thesis work, three-receiver configuration for the GeoSphere tool was used, while in this study, two-receiver configuration for GeoSphere is used. The results from both the studies are comparable because the deepest reading is dependent on the farthest Transmitter-Receiver (T-R) spacing and the frequencies used by the farthest receiver. The farthest T-R spacing for both the studies was similar (nearly 32 m) and the frequencies that this receiver works with are same for both the studies (2 kHz, 6 kHz and 12 kHz).

It is important to keep in mind that when using the WebGS software to generate inversion images, no noise is taken into consideration. The presence of noise in real time environment will alter these results and will reduce the depth of investigation.

10 Discussions

We divide the entire trajectory into four zones in order to discuss and compare each part of the inversion images from various scenarios with the real time results obtained at the time of drilling. This will help us evaluate how close to the real situation and beneficial these pre-job modelling scenarios are and how they can improve reservoir understanding while drilling which can be applied to improve the well placement.

It must be kept in mind that in case of real time inversions, noise considerations are taken into account whereas, the WebGS inversion images for the pre-job models do not take into account tool noise. Hence, some differences between the real-time and synthetic pre-job modelling inversions must be expected.

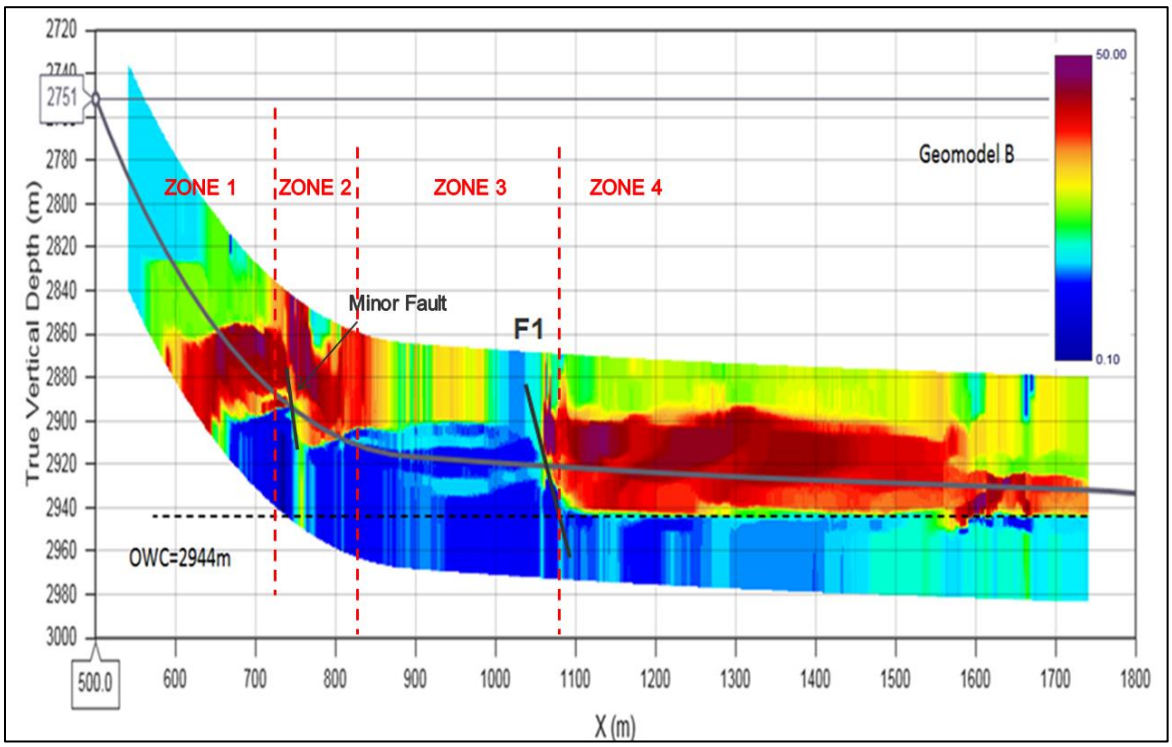

Figure 53: *Four zones of the trajectory for discussion purposes (Ref. WebGS Software)*

The four zones of the trajectory are (figure 53) – Landing zone (zone 1), Heel section zone (zone 2), Left of Fault F1 zone (zone 3) and Right of Fault F1 zone (zone 4).

The real time resistivity inversion image obtained for the well 34/8 A-16 H is displayed in figure 54. The colour scale in this image is consistent with the colour scale of WebGS and represents blue depicting lower resistivity values (lowest is 0.1 Ohmm) and red depicting the higher resistivity value range (highest is 50 Ohmm).

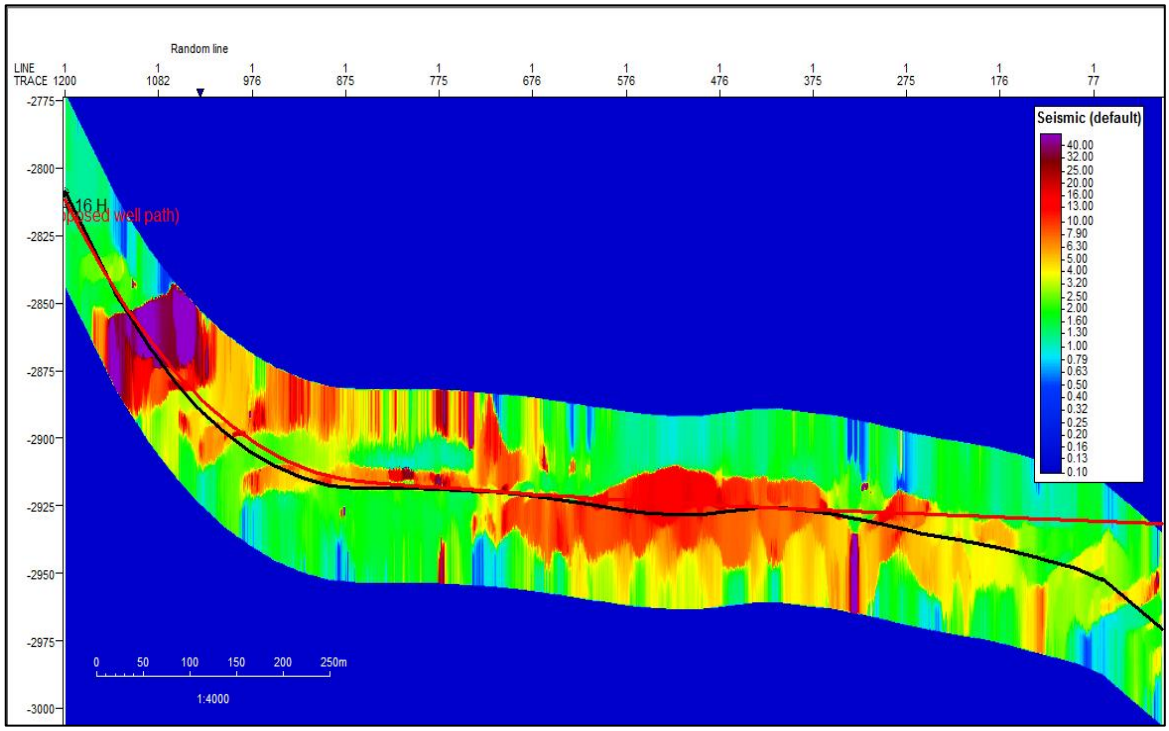

Figure 54: *Real time resistivity inversion image for well 34/8 A-16 H, blue depicting low resistivity zones and red depicting higher resistivity zones, red solid line shows the proposed well path and the black solid line represents the actual well path (Statoil ASA)*

10.1 Zone 1 – Landing zone

The first part of discussion is for the Landing of the well. This is when the well trajectory first enters the Upper Brent formation.

The top of the reservoir is first visible in this case. In the real time inversion image (figure 55(a)), the top of reservoir is very clearly identifiable by the sudden increase in resistivity values. This is detected at a distance of 22 m TVD from the wellbore.

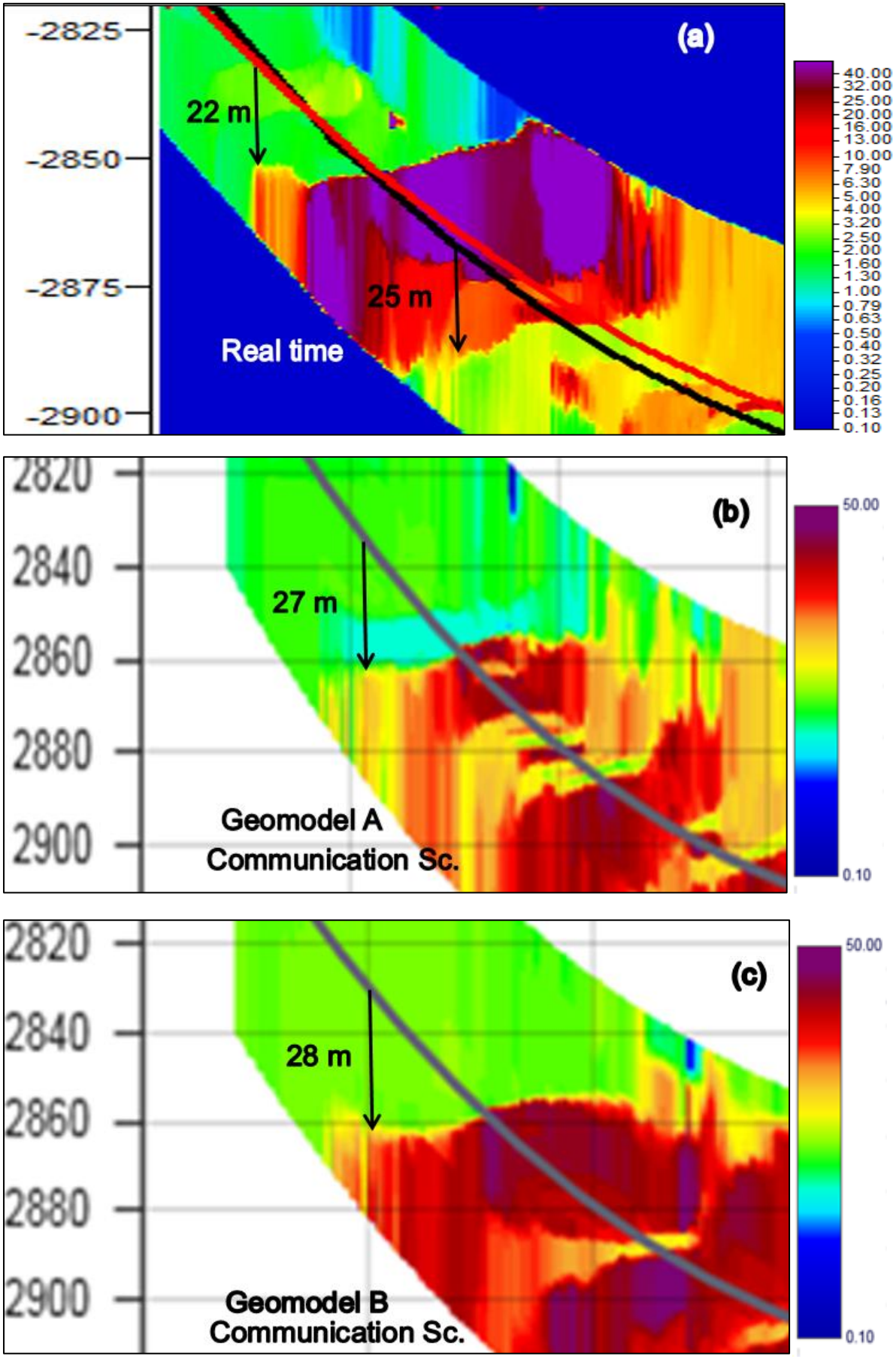
-2825
-2850
-2875
-2900
(a)
22 m
25 m
Real time
40.00
32.00
25.00
20.00
16.00
13.00
10.00
7.90
6.30
5.00
4.00
3.20
2.50
2.00
1.60
1.30
1.00
0.79
0.63
0.50
0.40
0.32
0.25
0.20
0.16
0.13
0.10
2820
2840
2860
2880
2900
(b)
27 m
Geomodel A
Communication Sc.
50.00
0.10
2820
2840
2860
2880
2900
(c)
28 m
Geomodel B
Communication Sc.
50.00
0.10

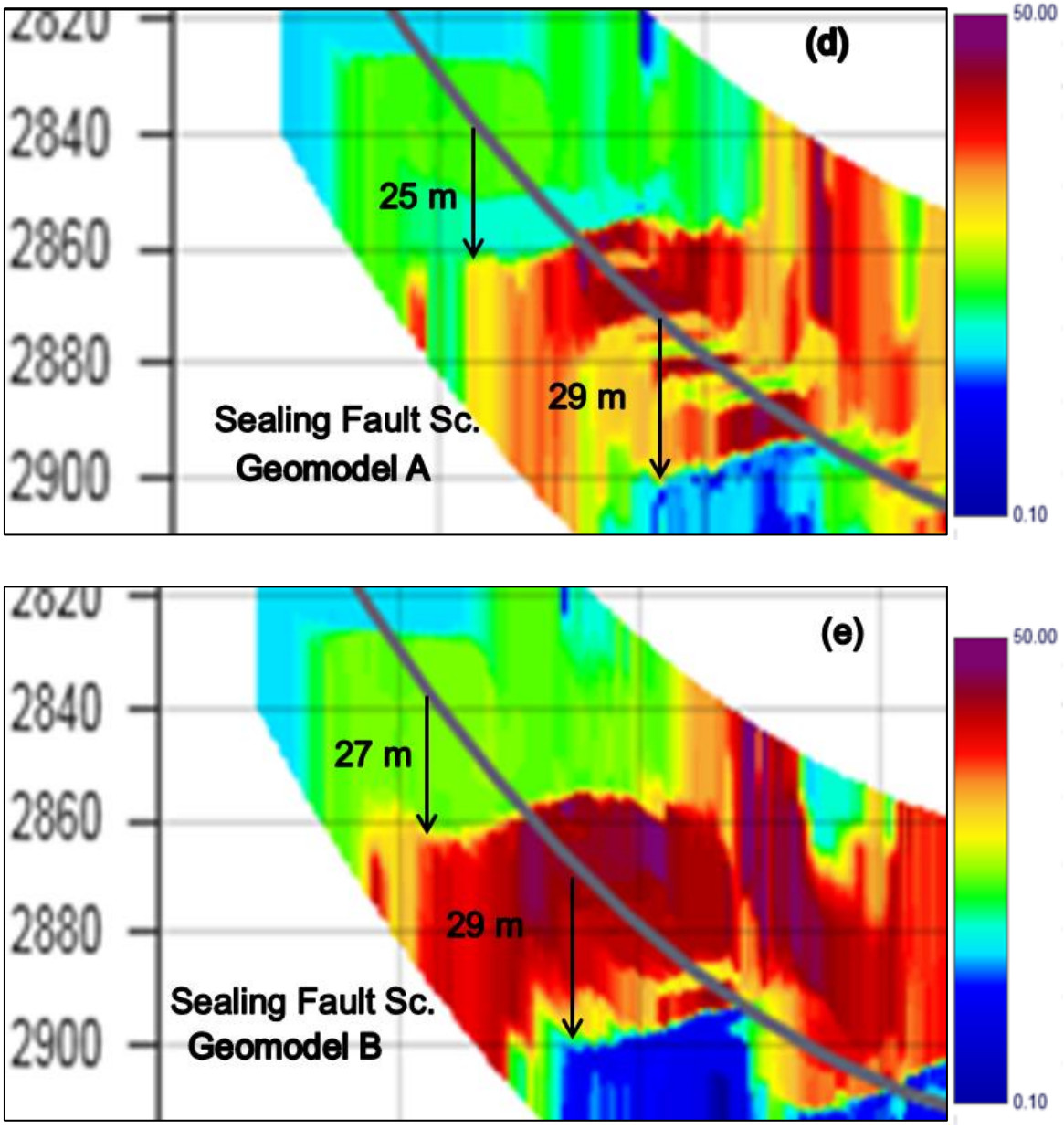

Figure 55: *Zone 1 – Landing: (a) Real time resistivity inversion image, black solid line represents the actual well path; (b) Resistivity inversion image for Communication scenario with Geomodel A; (c) Resistivity inversion image for Communication scenario with Geomodel B; (d) Resistivity inversion image for Sealing Fault scenario with Geomodel A; (e) Resistivity inversion image for Sealing Fault scenario with Geomodel B (Statoil ASA, WebGS Software)*

In the resistivity inversion images obtained from Geomodels A and B for both, the Communication scenario and the Sealing Fault scenario, the top of the reservoir is clearly identifiable as well. For Geomodel A, these are detected at 27 m and 25 m TVD for the Communication scenario and Sealing Fault scenario respectively. For Geomodel B, these are detected at 28 m and 27 m TVD for the Communication scenario and Sealing Fault scenario respectively.

The difference in the depth of investigation for the real-time image and synthetic inversion images is due a number of factors. The WebGS images do not consider any noise but there is an effect of noise on real-time images. The WebGS inversion algorithm (Gauss-Newton algorithm) and Real-time inversion algorithm (Monte-Carlo algorithm) are different and may generate slightly different images. The synthetic models were isotropic whereas anisotropy is present and included in the real-time images, which reduces the DOI.

The higher depth of investigations for Geomodel B (figure 55(c) and (e)) as compared to those for Geomodel A (figure 55(b) and (d)) can be explained by the presence of more homogeneous sands in Geomodel B and therefore higher resistivity contrast. The Geomodel B uses the offset well 34/8-11 in the Brent formation and this offset well has more sand in comparison to well 34/8-8 which is used in Geomodel A. Higher resistivity contrast leads to greater depth of investigation. These observations are confirmed by the results obtained during the semester thesis titled *Software Simulations of an Ultra Deep Resistivity Tool using Synthetic Geo-models, December 2015, NTNU* (Arora P., 2015).

Beneath this high resistivity zone of a finite thickness, a conductive layer is visible on the real-time inversion image (figure 55(a)). The Communication scenario inversion images do not show this conductive layer (figure 55 (b) and (c)). However, this conductive layer is clearly visible on the Sealing Fault scenario inversion images (figure 55 (d) and (e)). This implies that the geomodel for the Communication scenario is not a good representation of the geological conditions in that area. The depth of investigation to the conductive layer from the wellbore is 25 m on the real-time inversion images and is 29 m for the Sealing Fault scenario inversion images.

The detection of the top reservoir and the conductive layer beneath it, at similar distances from the wellbore, on both the real-time inversion image and the synthetic inversion image, confirms that the synthetic model is showing realistic values. Hence, these modelling results can be used with confidence. The early detection of the top reservoir, in case of a depleted reservoir, gives an early warning and hence casing above the reservoir can be set before drilling into it. This highlights the benefits of pre-job modelling and they assist in a more appropriate planning of the well trajectory.

10.2 Zone 2 – Heel Section zone

This part of discussion is for the heel section of the well when it steers through a minor fault in the Brent formation. This fault has been marked approximately in the images in figure 56.

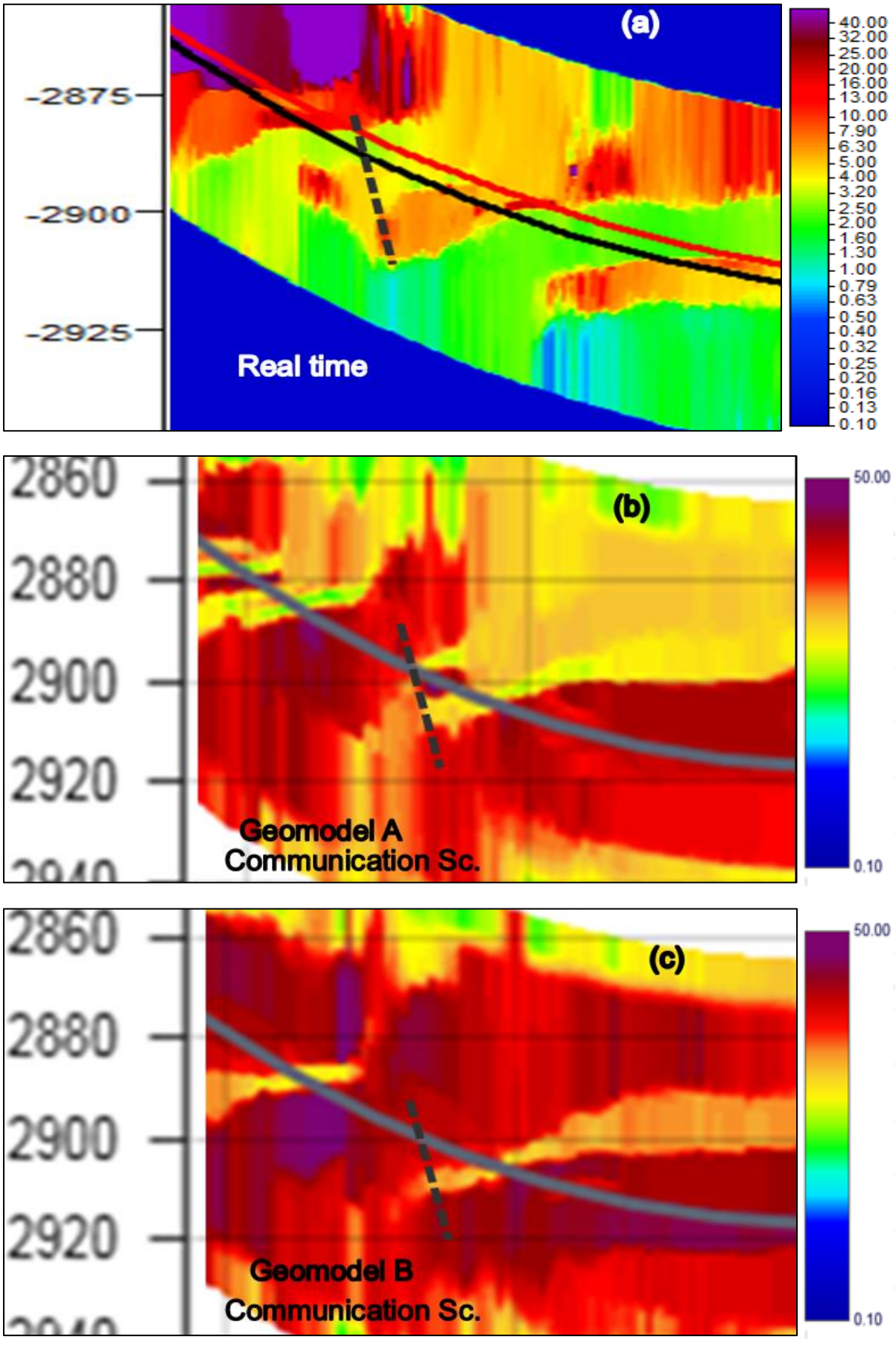
(a)
-2875
-2900
-2925
Real time
40.00
32.00
25.00
20.00
16.00
13.00
10.00
7.90
6.30
5.00
4.00
3.20
2.50
2.00
1.60
1.30
1.00
0.79
0.63
0.50
0.40
0.32
0.25
0.20
0.16
0.13
0.10
(b)
2860
2880
2900
2920
Geomodel A
Communication Sc.
50.00
0.10
(c)
2860
2880
2900
2920
Geomodel B
Communication Sc.
50.00
0.10

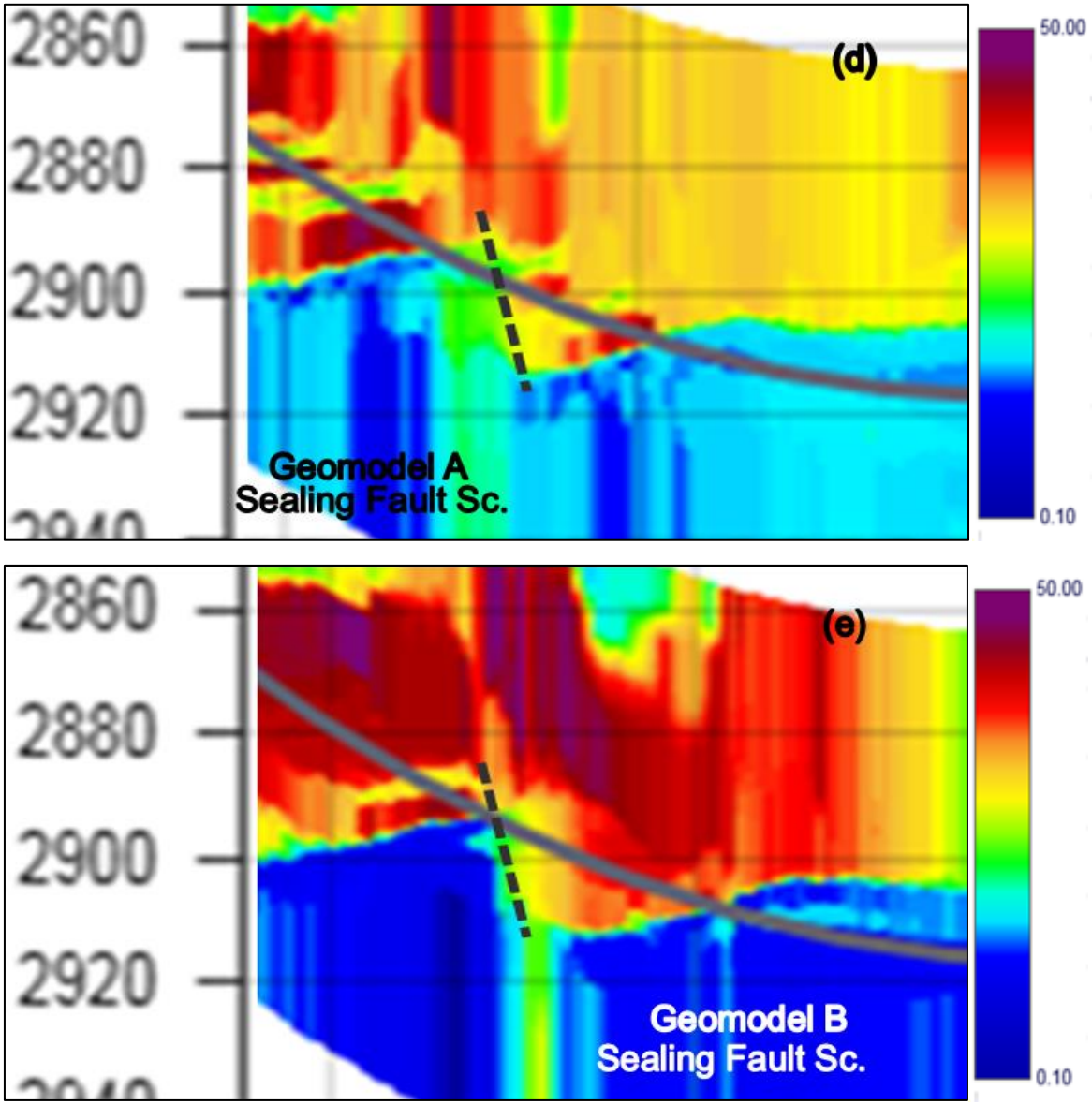

Figure 56: *Zone 2 – Heel Section: (a) Real time resistivity inversion image, black solid line represents the actual well path; (b) Resistivity inversion image for Communication scenario with Geomodel A; (c) Resistivity inversion image for Communication scenario with Geomodel B; (d) Resistivity inversion image for Sealing Fault scenario with Geomodel A; (e) Resistivity inversion image for Sealing Fault scenario with Geomodel B (Statoil ASA, WebGS Software)*

On the real time inversion image (figure 56(a)), this minor fault is visible. It is possible to distinguish between the left (lower resistivity values) and right side (higher resistivity values) of the minor fault plane. However, the minor fault is not visible on the resistivity inversion images for the Communication scenario (figure 56(b) and (c)). The left and right of the fault show similar resistivity values, i.e. communication of fluids through the minor fault. Hence, it is unable to identify the fault visually.

On the Sealing Fault scenario resistivity inversion images for Geomodels A and B (figure 56(d) and (e)), this minor fault is visually identifiable. The fluid to the left of the fault is different to that on the right of the fault, in terms of the resistivity values.

The sands in Geomodel B are more homogeneous and have higher resistivity values as compared to Geomodel A. This is because of the well 34/8-11 being sandier than the offset well 34/8-8, which causes this difference in resistivity values. The sand in Geomodel A shows a more layered structure and is inhomogeneous.

We conclude that for zone 2, the pre-job Sealing fault scenarios depict the minor faults as on the real time inversion image more appropriately.

10.3 Zone 3 – Left of fault F1 zone

This part of discussion is for the zone to the left of Fault F1. This zone was considered to have higher resistivity for the Communication scenario model and was water flooded (low resistivity) for the Sealing Fault scenario in the Lower Brent formation.

The real time inversion image (figure 57(a)), shows that this zone consists of water filled sands in the Lower Brent, depicted by the lower resistivity values in that region. The well was steered very closely above the water filled sands.

The Communication scenario model (figure 57(b) and (c)) is clearly not a good representation of this zone as there is no high resistivity fluid present in the Lower Brent, according to the real time inversion image. Also, the fault F1 cannot be identified on the pre-job Communication scenario images whereas it is clearly identifiable on the real time inversion image.

The Sealing Fault scenario inversion images (figure 57(d) and (e)), however, show a similar fluid (based on resistivity values) in the Lower Brent as that in the real time inversion image.

The fault F1 position is identifiable on the inversion images of the Sealing Fault scenario as the left of the fault has fluids with lower resistivity and the right of the fault has higher resistivity fluids.

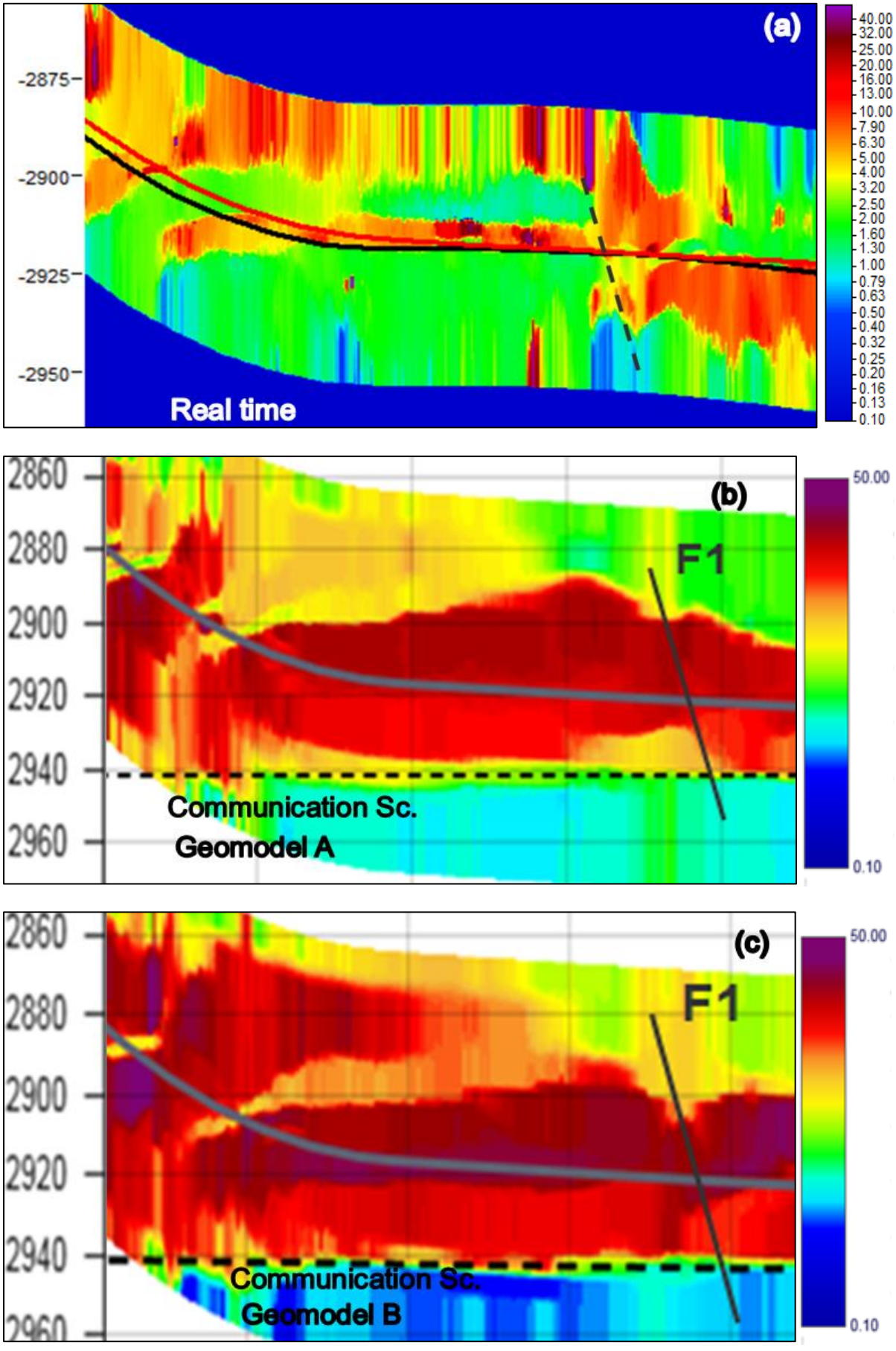
(a)
-2875
-2900
-2925
-2950
Real time
40.00
32.00
25.00
20.00
16.00
13.00
10.00
7.90
6.30
5.00
4.00
3.20
2.50
2.00
1.60
1.30
1.00
0.79
0.63
0.50
0.40
0.32
0.25
0.20
0.16
0.13
0.10
(b)
F1
Communication Sc.
Geomodel A
2860
2880
2900
2920
2940
2960
50.00
0.10
(c)
F1
Communication Sc.
Geomodel B
2860
2880
2900
2920
2940
2960
50.00
0.10

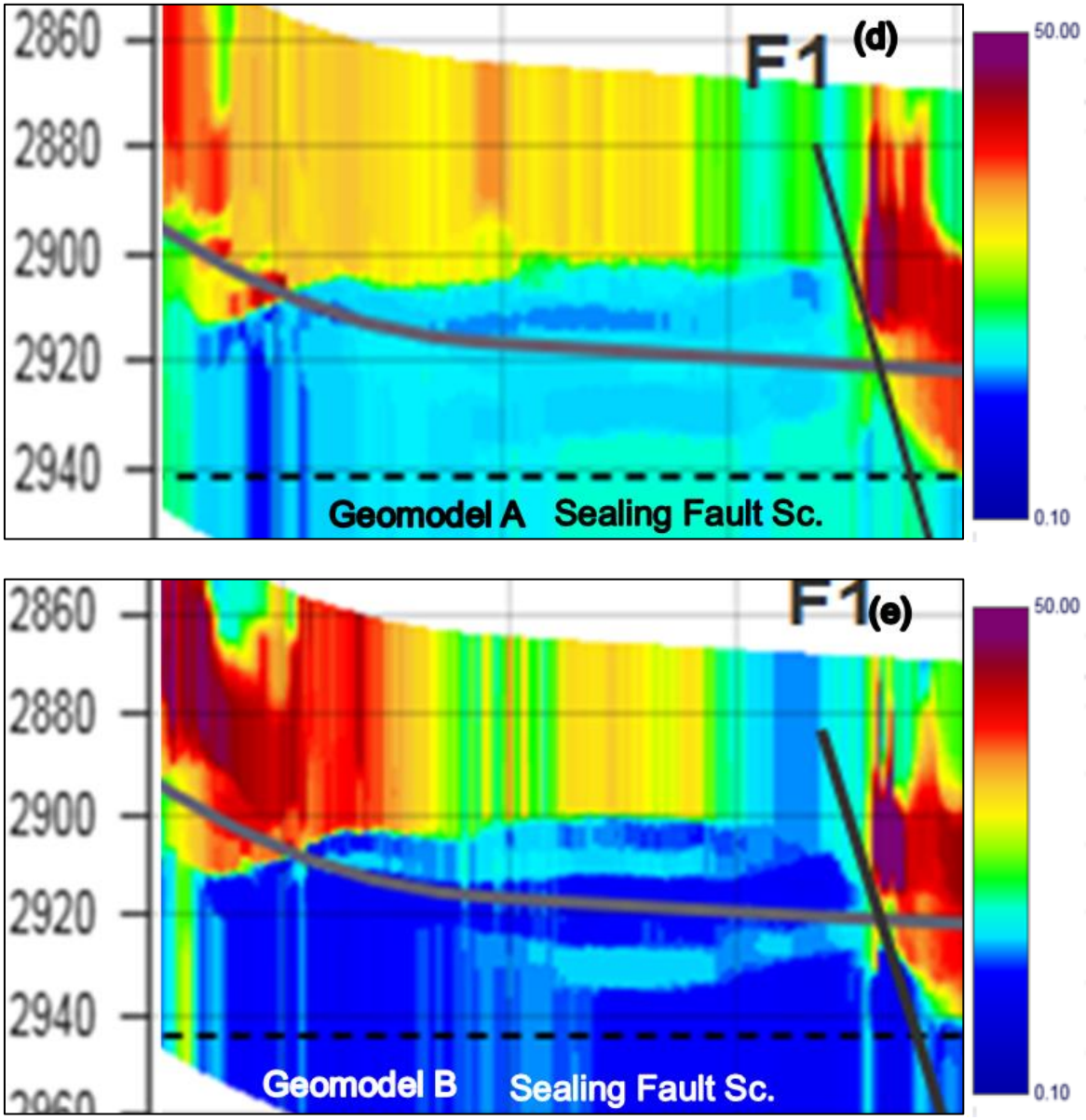

Figure 57: *Zone 3 – Left of Fault F1: (a) Real time resistivity inversion image, black solid line represents the actual well path; (b) Resistivity inversion image for Communication scenario with Geomodel A; (c) Resistivity inversion image for Communication scenario with Geomodel B; (d) Resistivity inversion image for Sealing Fault scenario with Geomodel A; (e) Resistivity inversion image for Sealing Fault scenario with Geomodel; black-dashed horizontal line shows the regional OWC at 2944 m TVD (Statoil ASA, WebGS Software)*

The Geomodel B shows better quality sand due to lower resistivity values, distributed in a homogeneous way as compared to Geomodel A (figure 57(d) and (e)). However, the numerical value of resistivity in that zone is very similar for both geomodels. This visual difference is mainly because of the default resistivity scale, which is very sensitive to small changes in the resistivity values. This slight variation may also be due to the offset well 34/8-11, used in Geomodel B, being sandier as compared to offset well 34/8-8, used in Geomodel A. Hence the Geomodel B shows darker blue in that area, depicting higher conductivity due to presence of more sand and therefore more porosity.

In figure 57(a), a high resistivity fluid is visible and the well was steered at the base of it, just above the water filled sand. This is possibly indicating the presence of more silty-sand with some remnant oil. This high resistivity feature is not visible in the synthetic inversion images (figure 57(d) and (e)) because the Lower Brent to the left of fault F1 was forced to be filled with water using the petrophysical equations when the geomodels were created. Further development in the technology to generate geomodels can be made by the including the possibility of flooding the target areas and hence making the process more dynamic.

10.4 Zone 4 – Right of fault F1 zone

This part of discussion is for the zone to the right of Fault F1. This zone was considered to have higher resistivity for both the Communication scenario as well as for the Sealing Fault scenario in the Brent formation. This is the most important section of the entire trajectory because this is the expected producing zone and is the main target of the well.

In the real time inversion image (figure 58(a)), high resistivity fluids are visible and the well is steered through this zone.

All the pre-job model inversion results have a high resistivity fluid in this zone. However, we know from the discussions in the zones above that the Communication scenario is not acceptable.

In the Sealing Fault scenario (figure 58(d) and (e)), the Geomodel B inversion image shows more homogeneous sand with very high resistivity values. The sand in Geomodel A has some low resistivity features as well. Geomodel B seems to be more promising in terms of presence of hydrocarbons. It uses the offset well 34/8-11 in the Brent formation and this offset well has more sand in comparison to well 34/8-8. This explains the more high-resistivity features on the inversion image obtained from Geomodel B.

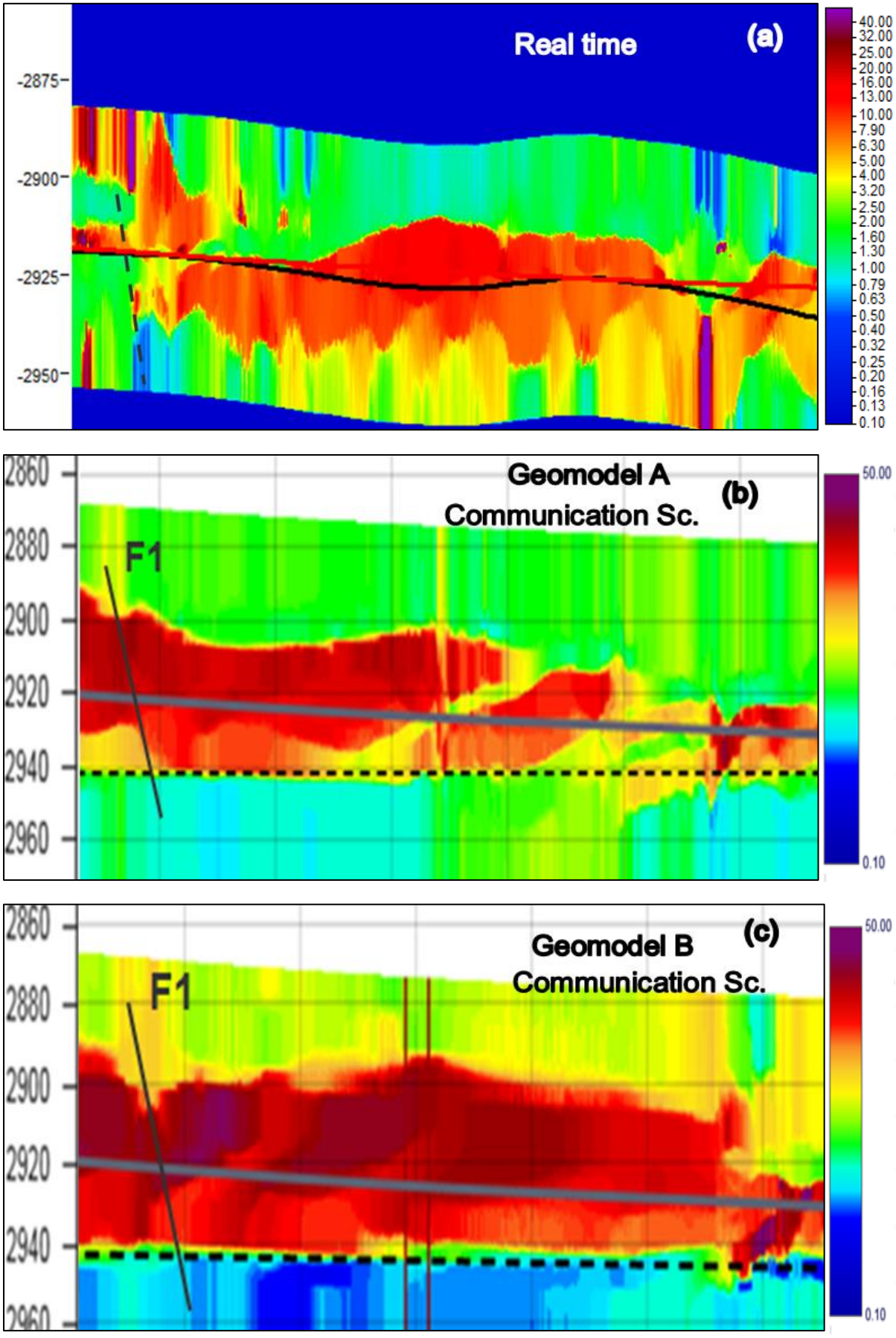
Real time
(a)
-2875
-2900
-2925
-2950
40.00
32.00
25.00
20.00
16.00
13.00
10.00
7.90
6.30
5.00
4.00
3.20
2.50
2.00
1.60
1.30
1.00
0.79
0.63
0.50
0.40
0.32
0.25
0.20
0.16
0.13
0.10
Geomodel A
Communication Sc.
(b)
F1
2860
2880
2900
2920
2940
2960
50.00
0.10
Geomodel B
Communication Sc.
(c)
F1
2860
2880
2900
2920
2940
2960
50.00
0.10

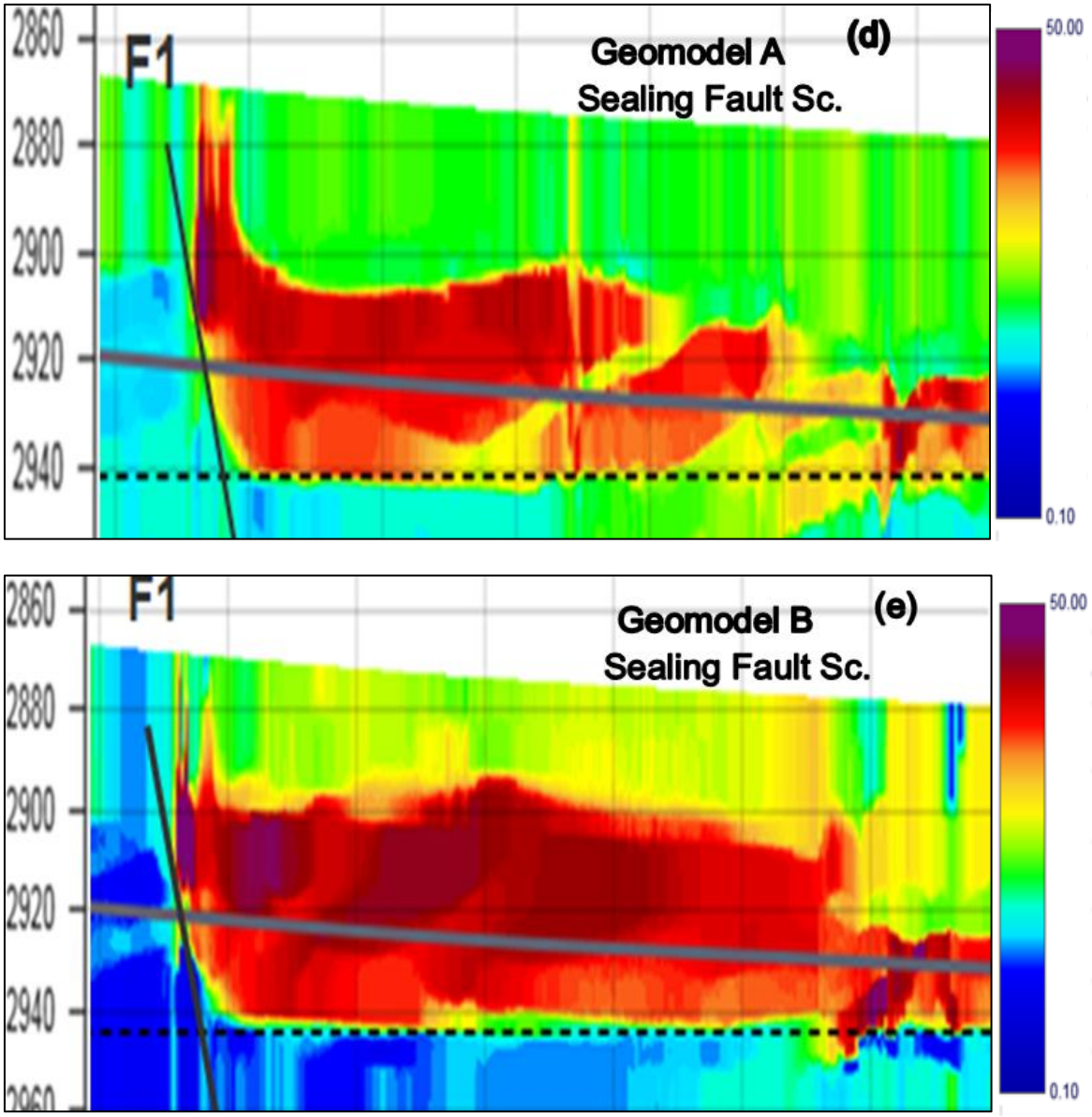

Figure 58: *Zone 4 – Right of Fault F1: (a) Real time resistivity inversion image, black solid line represents the actual well path; (b) Resistivity inversion image for Communication scenario with Geomodel A; (c) Resistivity inversion image for Communication scenario with Geomodel B; (d) Resistivity inversion image for Sealing Fault scenario with Geomodel A; (e) Resistivity inversion image for Sealing Fault scenario with Geomodel B; black-dashed horizontal line shows the regional OWC at 2944 m TVD (Statoil ASA, WebGS Software)*

10.5 Discussion Summary

From the discussions on the four zones, we know that the Communication scenario inversion images are not comparable to real time inversion images.

The Sealing Fault scenario inversion images show similar features such as detection of the top of the reservoir and conductive layer below it, presence of water-flooded sands in the Lower Brent, detection of the minor fault and fault F1 etc., as those on the real-time inversion images. However, it must be noted that the Sealing Fault scenario geomodel is not an exact representation of the actual geological conditions.

We compare the real-time inversion image (figure 59(a)) with the Sealing Fault scenario inversion images for both Geomodels A and B (figure 59(b) and (c)).

The expected producing zone which was the main target of this well, i.e. to the right of fault F1, shows high resistivity fluid in the real-time as well as the synthetic model inversion images. However, the architecture and shape of this high resistivity sand is not similar in these cases. On the real-time inversion images, the top of this reservoir is not similar in shape and is lower in depth, than that on the synthetic inversion images. This implies the possibility of more erosion over this formation and the shale above the Brent was lower and more towards the wellbore.

This also indicates that the actual fault throw was higher than that in the synthetic model, since on the real-time inversion image, the top of reservoir to the right of fault F1 is lower in depth.

The oil-water contact on the real-time inversion image cannot be identified (figure 59(a)). But, the OWC on the synthetic model inversion images (figures 59(b) and (c)) are very appropriately identified and is sharp and distinguishable at 2944 m TVD. This suggests that if the OWC was present at 2944 m TVD, it should be detected on the real-time inversion image. Hence, we conclude that the actual OWC is deeper than the regional OWC (2944 m TVD) and is beyond the DOI of the tool and is therefore not detected. We know from personal communication with the asset that the OWC is present at around 2960 m TVD.

The synthetic geomodels with varying OWCs that were studied suggest that when the OWC was at 2964 m TVD, it was 41 m away from the borehole and was the maximum distance detected on the inversion images. During real-time inversion, considering noise, anisotropy and other factors as discussed before, this DOI is expected to be decreased.

Hence we conclude that Sealing Fault scenario geomodel in not the best representation of the actual geological conditions and further updates need to be made on the model in order to make it a better match. This is a part of the post-job interpretation workflow and is not a part of this study.

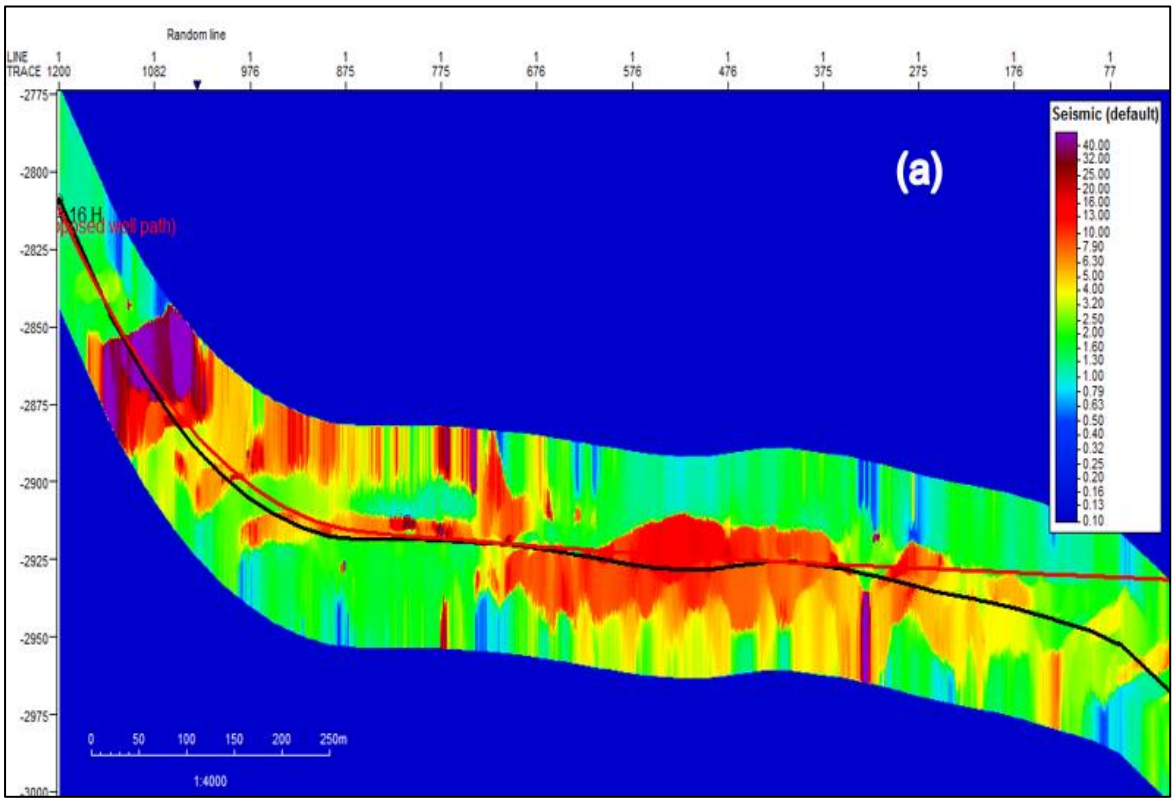
Random line
LINE
TRACE
Seismic (default)
(a)
0 50 100 150 200 250m
1:4000

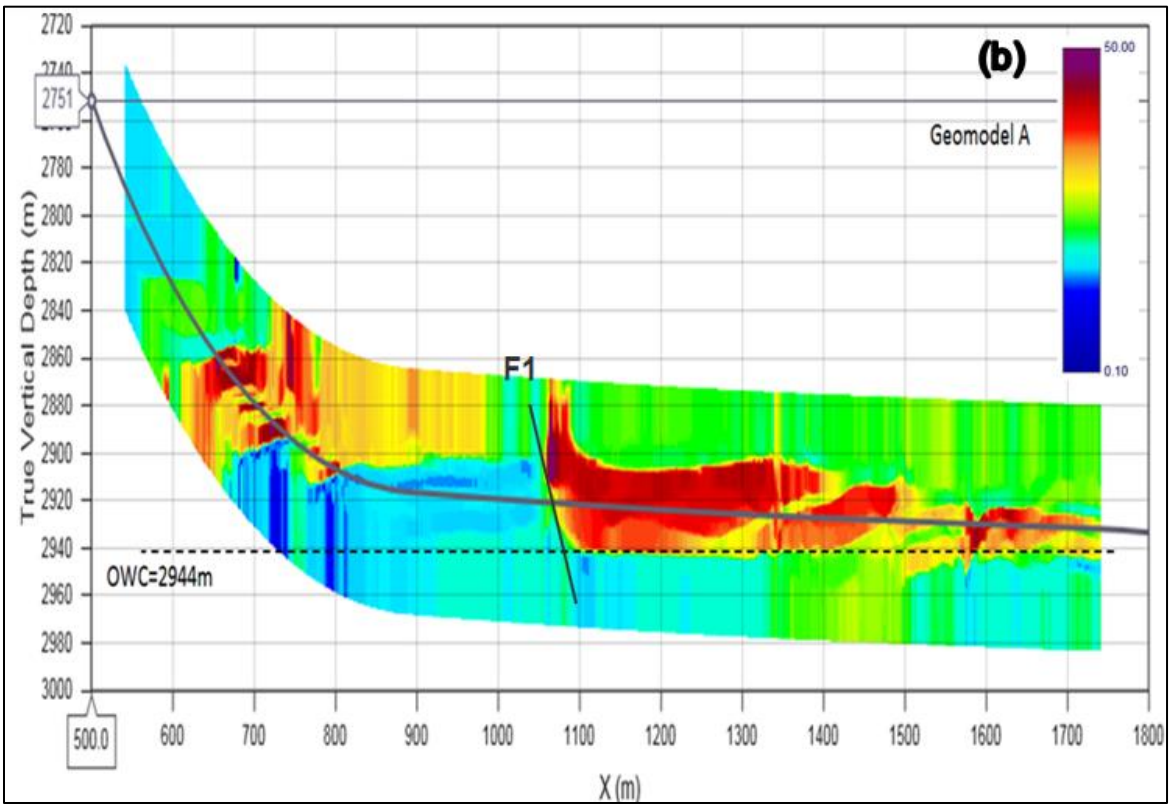
(b)
Geomodel A
F1
OWC=2944m
True Vertical Depth (m)
X (m)

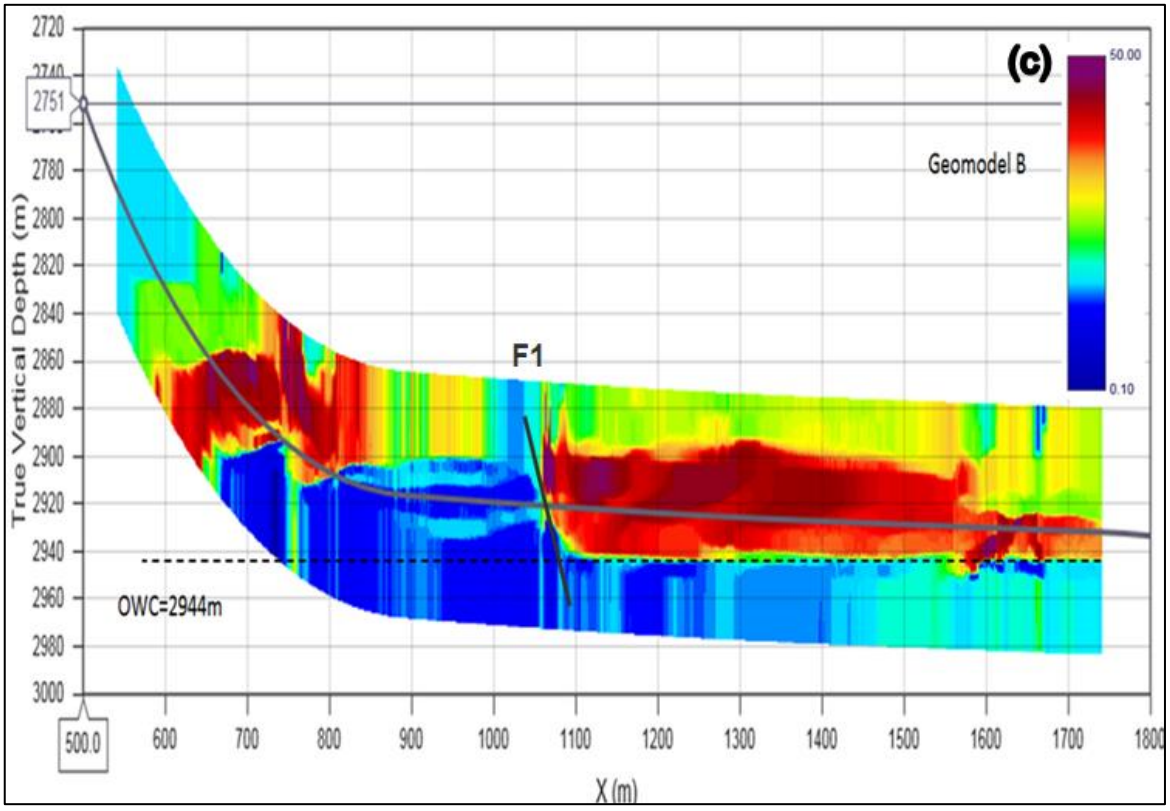

Figure 59: *(a) Real-time resistivity inversion image for well 34/8 A-16 H, red solid line shows the proposed well path and the black solid line represents the actual well path; (b) Sealing Fault scenario inversion image for Geomodel A; (c) Sealing Fault scenario inversion image for Geomodel B (Ref. WebGS Software)*

When several possible pre-job models are available, the variations encountered at the time of drilling can be updated more swiftly. The perforations and completion operations based on the Sealing Fault scenario can be applied real-time to a certain extent, during drilling and therefore this increased understanding of the subsurface conditions makes the process faster and more accurate.

Studying varied fault throws and oil-water contact depth positions will also assist in being prepared beforehand when any variations are encountered to the expected depths and to predict the expected responses in such cases.

The pre-job resistivity inversion profiles help the asset to better interpret the real-time GeoSphere inversion results. In the absence of pre-job models, the uncertainty in the interpretation of the GeoSphere inversion images increases because they could be interpreted as a range of possibilities. To narrow the possibilities, the geomodels are built and their inversions are studied.

The pre-job planning phase geomodels, therefore, provide an increased understanding of the geological conditions in the subsurface. Studying a good representation of the actual geological conditions during the pre-job planning phase makes the team very well prepared and gives a head-start to the operations. It makes the evaluation of the uncertainties possible, increases the ability to react pro-actively and leads to better geosteering decisions and planning leading to optimized well placement.

The GeoSphere tool plays a major role to link the LWD data to the Seismic scale data. The conventional LWD tools can look up to only 1-2 m around the borehole. The Periscope tool, a previous version of the directional EM tool that operates on high frequencies (100 kHz and above), can look up to about 5 m around the borehole. However the GeoSphere tool can look about 30 m around the wellbore, depending on the resistivity, transmitter-receiver spacing in the tool and frequencies it operates upon. Figure 60 highlights this fact based on images. If the Periscope tool was used, it would not have been easy to be able to estimate many important features such as find the OWC depth while entering the top of reservoir, estimate the fault throws, find an appropriate direction to avoid the water-filled sands etc. On the image from the Geosphere tool, the OWC, fault location, high resistivity zones that are prospective production zones, water filled zones etc. can be easily identified visually.

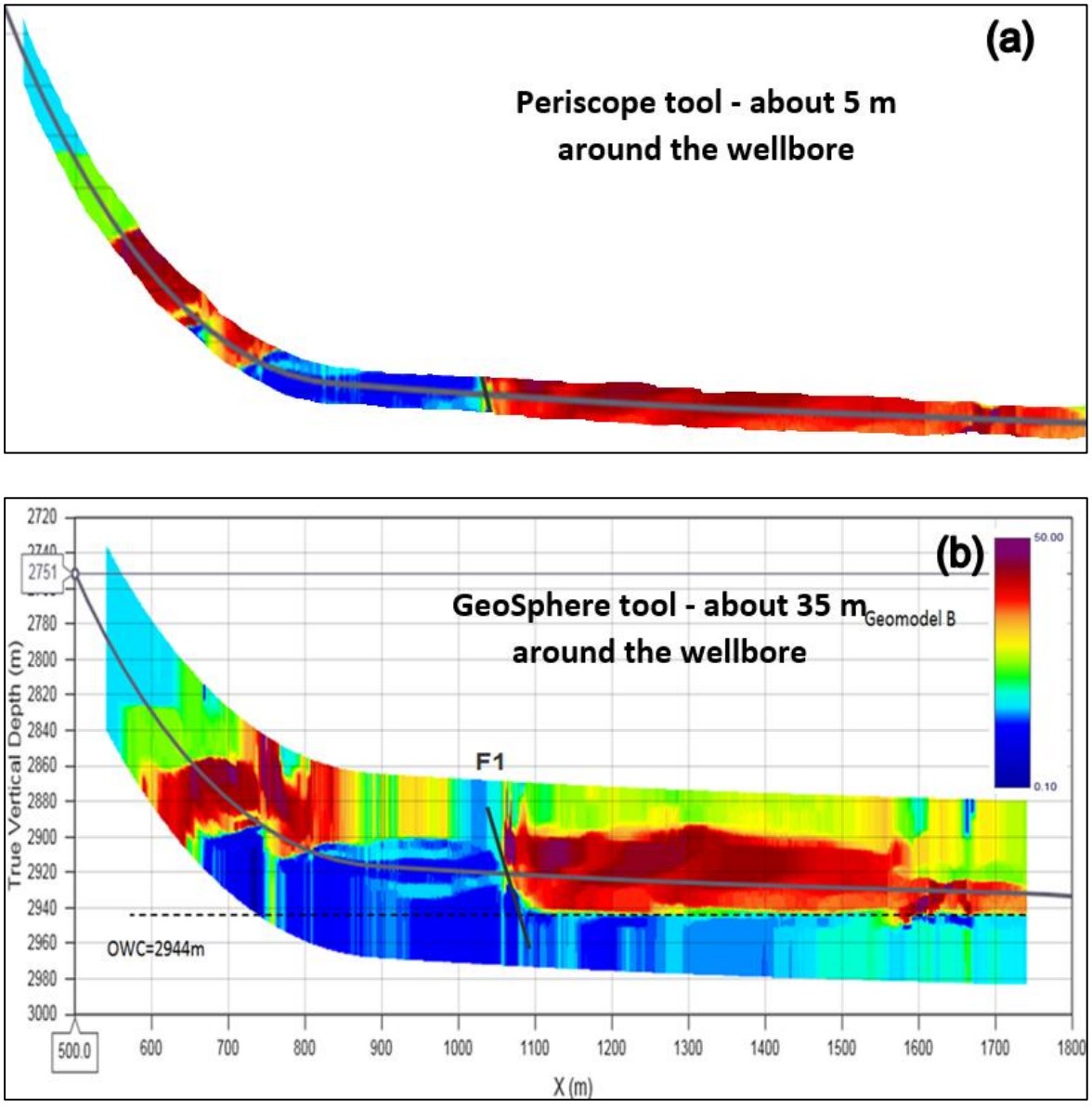

Figure 60: *(a) An image representing the images obtained from Periscope tool, looking up to 5 m around the borehole; (b) An image obtained by the use of GeoSphere tool, looking about 35 m around the wellbore (Ref. WebGS Software)*

11 Conclusions

This study highlights the importance of the pre-job planning phase in order to investigate the geological conditions to achieve optimized well placement. The main objective is to link the geological interpretation to the synthetic models generated before drilling and study various scenarios on it to be well prepared to face the uncertainties while drilling.

The Ultra-Deep Electromagnetic measurements play a key role to link LWD-measurements to seismic and hence prove their importance.

The pre-job modelling inversions help in understanding and interpreting the real-time inversions and measurements better. They have the capability to investigate the sensitivity to top reservoir, assist in the robust interpretation of the fluid contacts, possible flooding scenarios and formation structures while drilling.

They give an improved understanding of the subsurface and reservoir conditions and result in better completion and perforation operations on the well.

Any variations that may be encountered at the time of drilling can be compensated for, more swiftly, with these pre-job models available on different scenarios, avoiding errors and wrong decisions. Thus, the pre-job model inversions increase the ability to react pro-actively and help in geosteering decision making process.

12 Suggestions for Further Study

After the pre-job planning is completed and the well is drilled, the post job evaluation phase begins. The post-job evaluation phase involves the comparison of well logs (Gamma Ray, Density, Neutron, Resistivity) generated from the synthetic model with the real time LWD logs obtained. This is done in order to verify if the synthetic geomodel is a good representation of the real geological conditions or not, and to steer the changes required in the synthetic geomodel to bring it as close as possible to the real measurements.

Also, the real time inversion data obtained by using the GeoSphere tool is compared with the synthetic model inversion results to make the necessary adjustments in the model. The synthetic models are built or updated to verify with the real measurements.

Finally, necessary adjustments are made in the model to match the synthetic seismic with the real seismic line. The geomodel is consistent with the real geological conditions at the LWD measurement scale, GeoSphere scale and the seismic scale and is a result of the integration of all the available knowledge and data. This post-job phase has not been a part of this study.

Technological advancement such as real-time update of the geomodel can be very challenging but it has the capacity to push for improved reservoir understanding of more complex targets in the future.

The WebGS forward and inverse simulations do take into consideration any noise. Advancement in the WebGS software that would add noise to the forward and inverse simulation results could generate synthetic inversion images closer and comparable to the real-time inversion images.

The inversion algorithm used in WebGS as well as Real-time inversion software is 1D. 2D and 3D inversion algorithms are already in development phase and they would give a better representation of complex geological structures such as faults, folds etc.

References

Adda, G. W., 2012. *Hydrocarbon generation and migration from Jurassic source rocks in the northern North Sea*. Master Thesis, Department of Geology and Mineral Resources Engineering, NTNU, Norway.

Faleide, J. I., Bjørlykke, K. and Gabrielsen, R. H., 2010. *Geology of the Norwegian continental shelf.* In: Bjørlykke K. (ed.), Petroleum Geoscience: From Sedimentary Environments to Rock Physics. Springer Science, pp 467 – 499.

Fraser, S.I., Robinson, A.M., Johnson, H.D., Underhill, J.R., Kadolsky, D.G.A., Connel, R., Johannessen, P. and Ravnas, R., 2002. Upper Jurassic. In: Evans, D., Graham, C., Armour, A. and Bathurst, P (eds.), *The Millennium Atlas: petroleum geology of the central and northern North Sea*, pp. 157-189.

Færseth, R.B., Knudsen, B.E., Liljedahl, T., Midbøe, P.S. and Søderstrøm, B., 1997. *Oblique rifting and sequential faulting in the Jurassic development of the northern North Sea.* Journal of Structural Geology, v.19 (10); pp. 1285- 1302.

Glennie, K.W., Underhill, J.R., 1998. *Origin, development and evolution structural styles*. In: Glennie, K.W. (ed.), Petroleum geology of the North Sea: Basic concepts and recent advances (4th Ed.). Oxford: Blackwell Science, pp. 42-84.

Oliveira, M. E., Petersen, S. A. and Riste, P., 2015. *Oseberg South (J) - CES material for 4D analysis contractor-evaluation.* Internal: Statoil ASA.

Omeragic, D., Bayraktar, Z., Thiel, M., Habashy, T., Wu, P., Shray, F., Antezana, V., 2015. *Triaxial Induction Interpretation in Horizontal Wells: Mapping Boundaries, and Characterizing Anisotropy and Fractures*. SPWLA, CA.

Seydoux, J., Legendre, E., Mirto, E., Dupuis, C., Denichou, J., Bennett, N., Kutiev, G., Kuchenbecker, M., Morriss, C., Yang, L., 2014. *Full 3D Deep Directional Resistivity Measurements Optimize Well Placement and provide Reservoir-Scale Imaging while Drilling*. SPWLA, UAE.

Toxopeus, G., Thorbecke, J., Wapenaar, K., Petersen, S., Slob, E. and Fokkema, J., 2008. *Simulating migrated and inverted seismic data by filtering a geologic model*. Geophysics, v.73, no.2.

Vollset, J., and Dore, A.G. (eds.), 1984. *A revised Triassic and Jurassic lithostratigraphic nomenclature for the Norwegian North Sea.* Bulletin of the Norwegian Petroleum Directorate, No.3.

Zanella, E. and Coward, M.P., 2003. *Structural framework.* In: Evans, D., Graham, C., Armour, A. and Bathurst, P (eds.), The Millennium Atlas: petroleum geology of the central and northern North Sea, pp.45-59.

Other Sources:

Arora, P., 2015. *Software Simulations of an Ultra Deep Resistivity Tool using Synthetic Geo-models.* Semester Thesis, Norwegian University of Science and Technology (NTNU), December 2015. Unpublished.

Brent Study, Statoil ASA Wikipedia, Internal, Revised: July, 2015, Link: https://wiki.statoil.no/wiki/index.php/BRENT:Regiona

Concept Selection Report, NO 34/8-A-16 H & NO 34/8-A-16 AH, Internal: Statoil ASA, September 2015.

Concept Phase Report, GeoSphere, WebGS and CES, Internal: Statoil ASA, January 2016.

Norsk Petroleum AS, Revised: June, 2016, Link: http://www.norskpetroleum.no/en/production/field/visund/

Offshore Technology, Revised: June, 2016, Link: http://www.offshore-technology.com/projects/visund/

Statoil ASA, Published: September, 2007, Updated: January, 2015, Link: http://www.statoil.com/en/OurOperations/ExplorationProd/ncs/visund/Pages/default.aspx

Visund Field Study, Statoil ASA Wikipedia, Internal, Revised: June, 2015, Link: https://wiki.statoil.no/wiki/index.php/BRENT:Visund

www.npd.no

Appendix A

Information Retrieval

Information Retrieval plays a very important role in any research work. Good background information is one of the prerequisites before the work is begun. For any technical work, such as this, information about the background geology, thorough awareness about the data and resources available and the alternate methodology or previous work done, associated with the task is very important to be known.

Hence, before beginning with the actual task, a thorough literature study was done. This was done with the help of tools such as Oria, an online library made available by the NTNU University library. Oria is a search engine that gives access to a variety of the library's printed and digital resources. Also, scientific databases such as OnePetro, Scopus and Compendex were used to find technical articles related to the previous work done in relation to this study.

Internal literature and reports were made available by Statoil ASA which formed the backbone of this work.

Appendix B

OWC Cases Results

Geomodel B – Communication Scenario

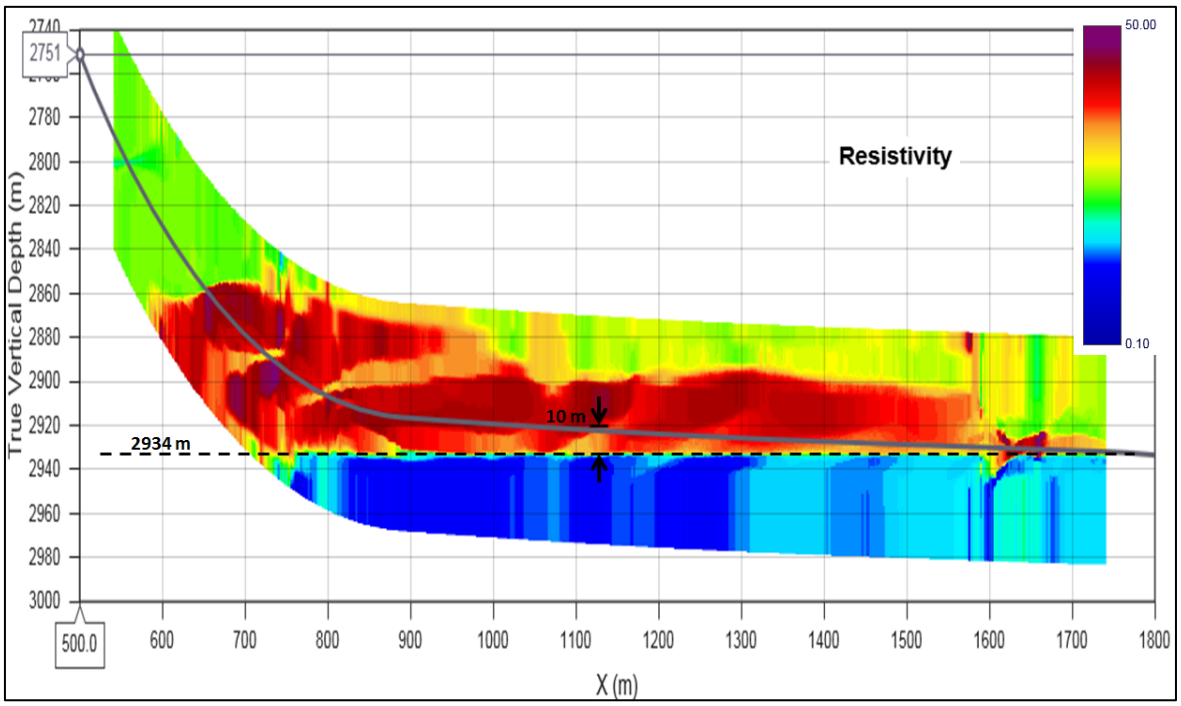

Figure 61: *Resistivity Inversion profile for Oil-Water Contact scenarios when OWC is at 2934 m, i.e. -10 m from Base Case (2944 m). It is detected at 10 m away from the borehole (Ref. WebGS Software)*

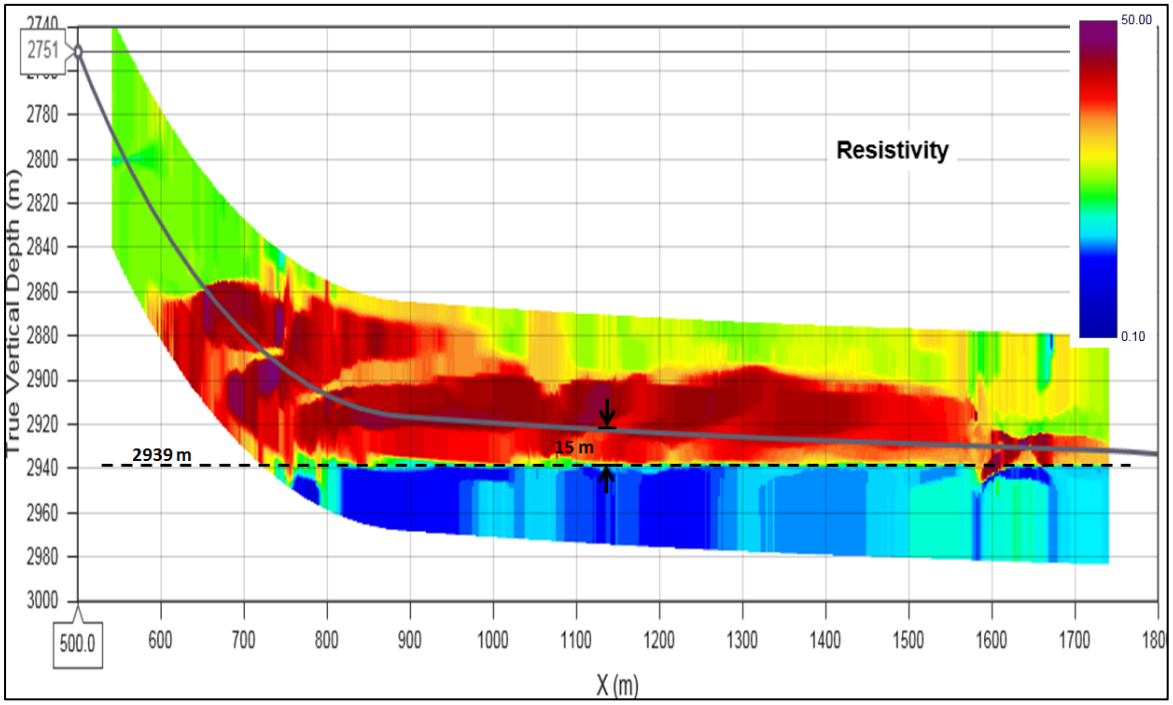

Figure 62: *Resistivity Inversion profile for Oil-Water Contact scenarios when OWC is at 2939 m, i.e. -5 m from Base Case (2944 m). It is detected at 15 m away from the borehole (Ref. WebGS Software)*

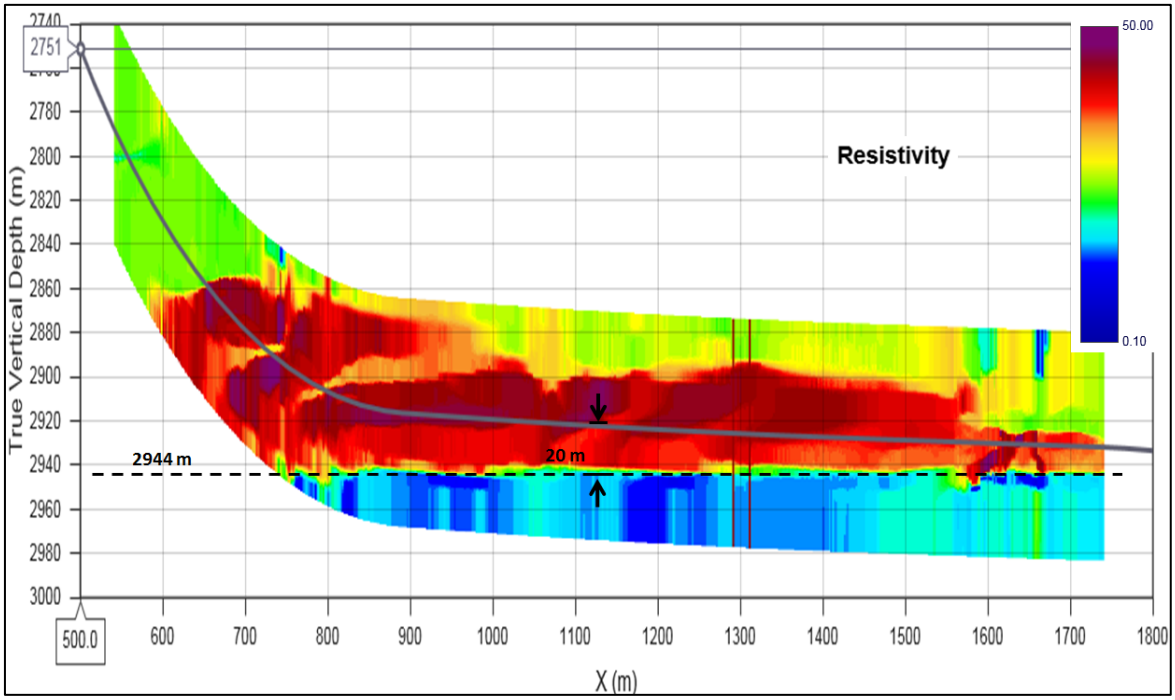

Figure 63: *Resistivity Inversion profile for Oil-Water Contact scenarios when OWC is at 2944 m, i.e. the Base Case. It is detected at 20 m away from the borehole (Ref. WebGS Software)*

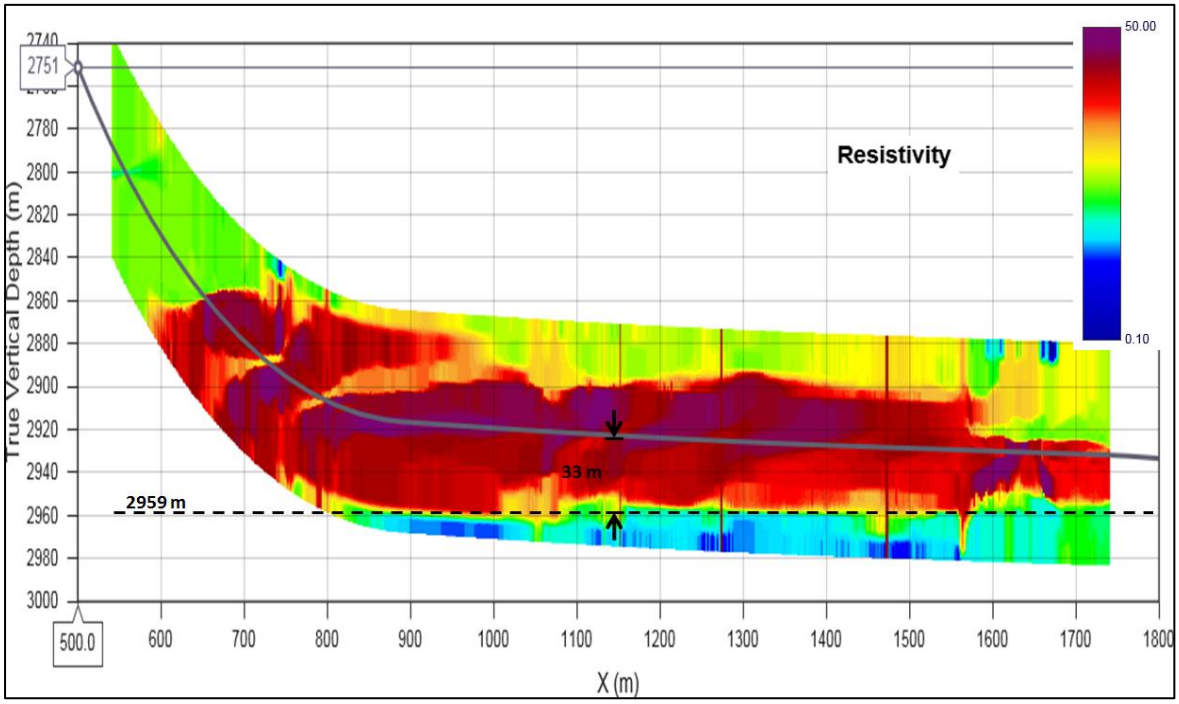

Figure 64: *Resistivity Inversion profile for Oil-Water Contact scenarios when OWC is at 2959 m, i.e. +15 m from Base Case (2944 m). It is detected at 33 m away from the borehole (Ref. WebGS Software)*

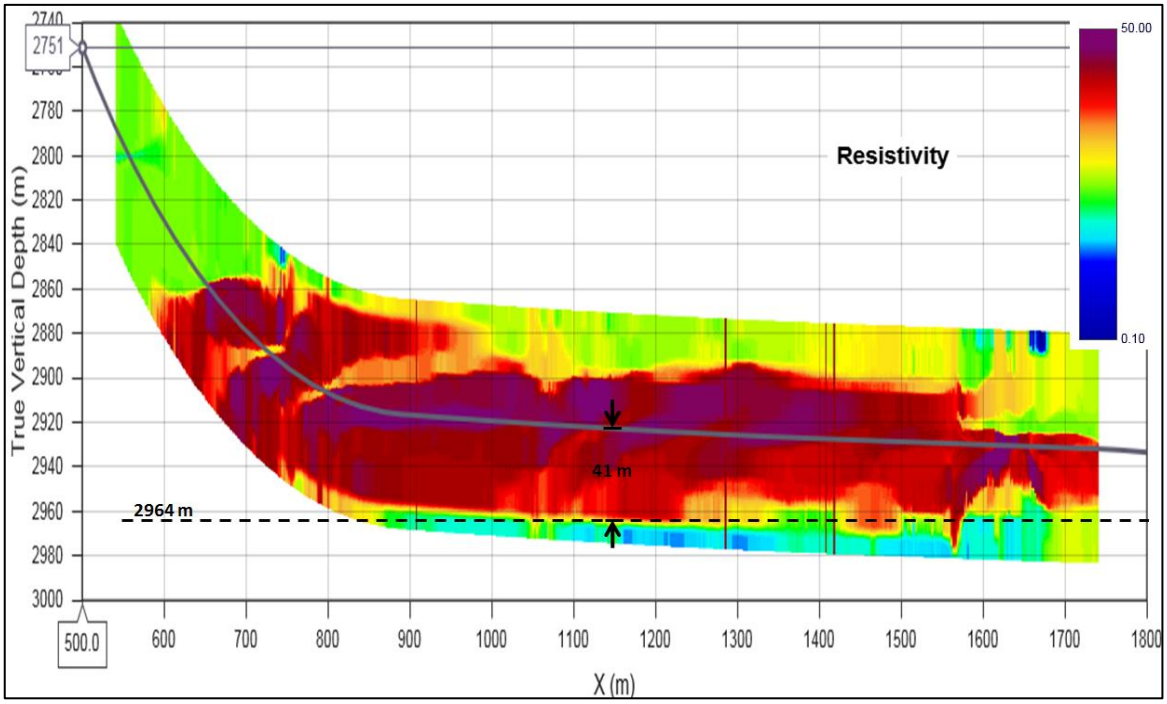

Figure 65: *Resistivity Inversion profile for Oil-Water Contact scenarios when OWC is at 2964 m, i.e. +20 m from Base Case (2944 m). It is detected at 41 m away from the borehole (Ref. WebGS Software)*

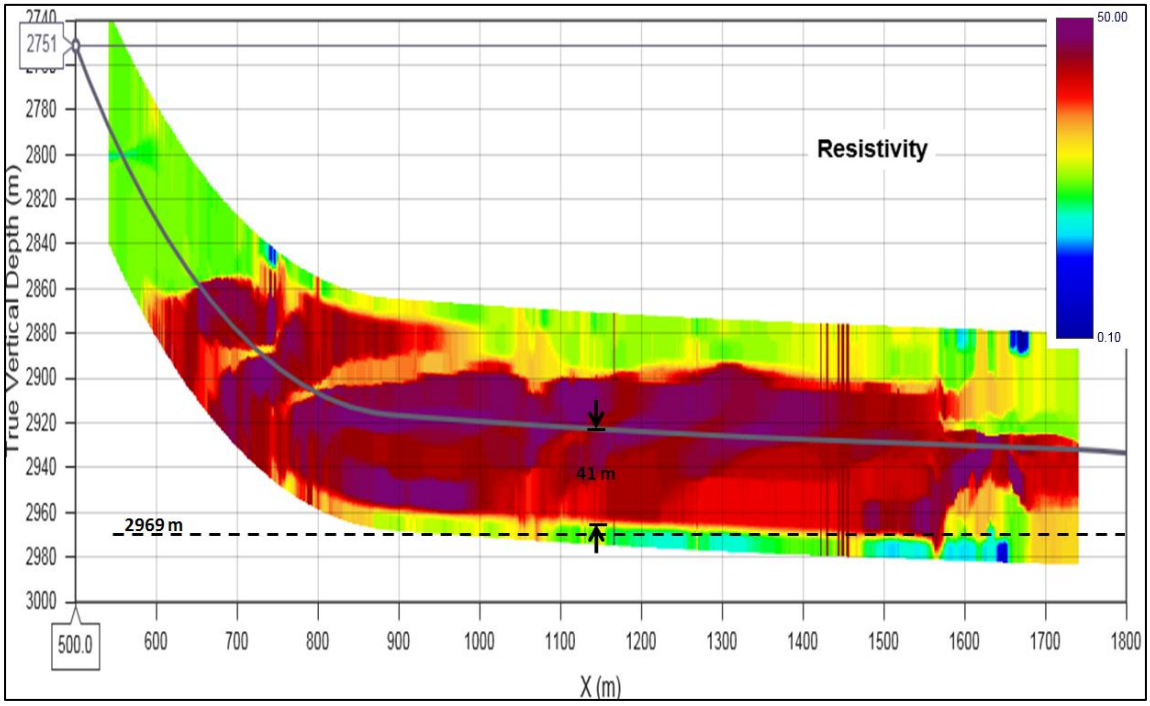

Figure 66: *Resistivity Inversion profile for Oil-Water Contact scenarios when OWC is at 2969 m, i.e. +25 m from Base Case (2944 m). It is detected at 41 m away from the borehole, which is not the true OWC position (Ref. WebGS Software)*

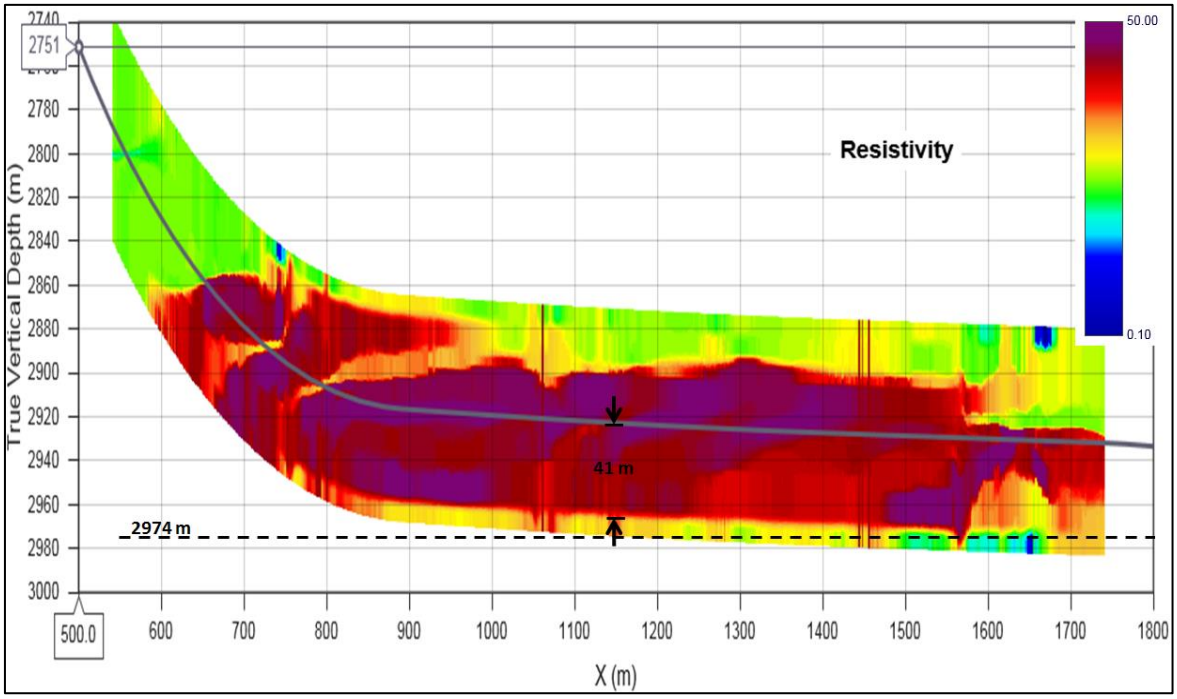

Figure 67: *Resistivity Inversion profile for Oil-Water Contact scenarios when OWC is at 2974 m, i.e. +30 m from Base Case (2944 m). It is detected at 41 m away from the borehole, which is not the true OWC position (Ref. WebGS Software)*

Appendix C

Fault Throw Cases Results

Comparison between Original Seismic line and Synthetic Seismic at X= 1205 m, for Fault Throw= 45 m, 50 m, 55 m (base case),60 m, 65 m and 75 m

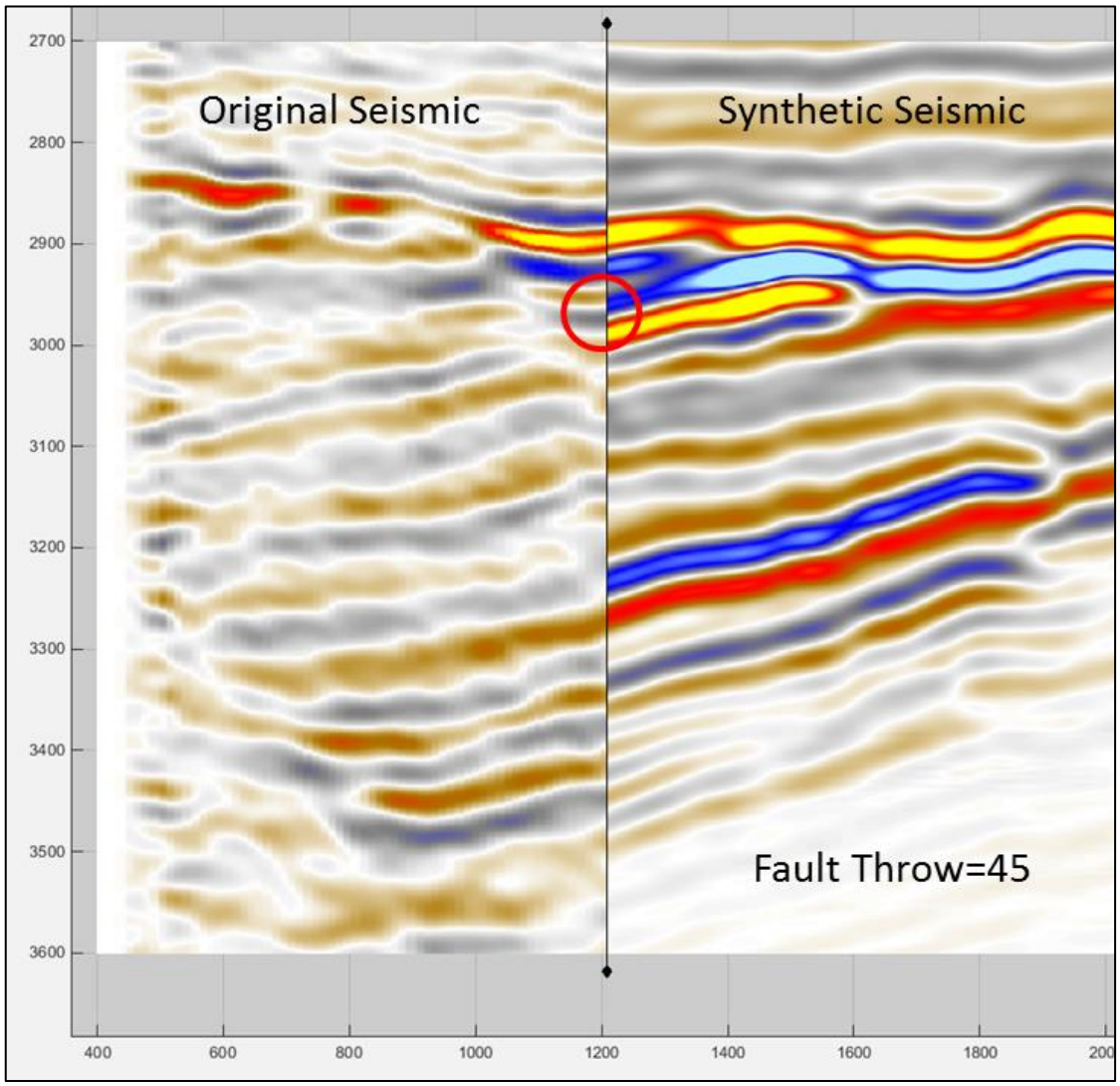

Figure 68: *Comparison between Original Seismic line (left) and Synthetic Seismic (right) at X= 1205 m for Fault Throw= 45 m. The reflectors do not overlap perfectly (Ref. CES Software)*

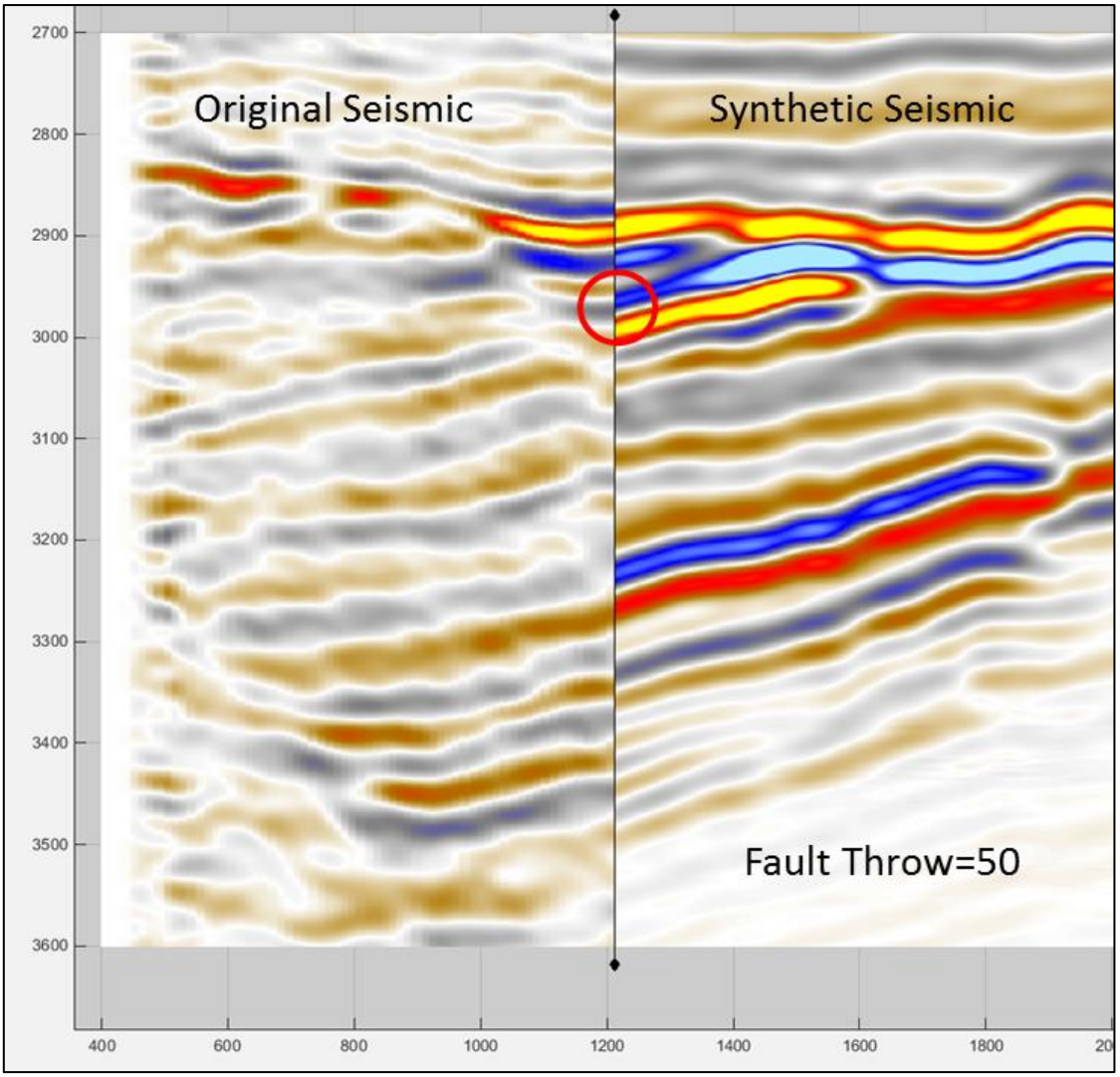

Figure 69: *Comparison between Original Seismic line (left) and Synthetic Seismic (right) at X= 1205 m for Fault Throw= 50 m. The reflectors do not overlap perfectly (Ref. CES Software)*

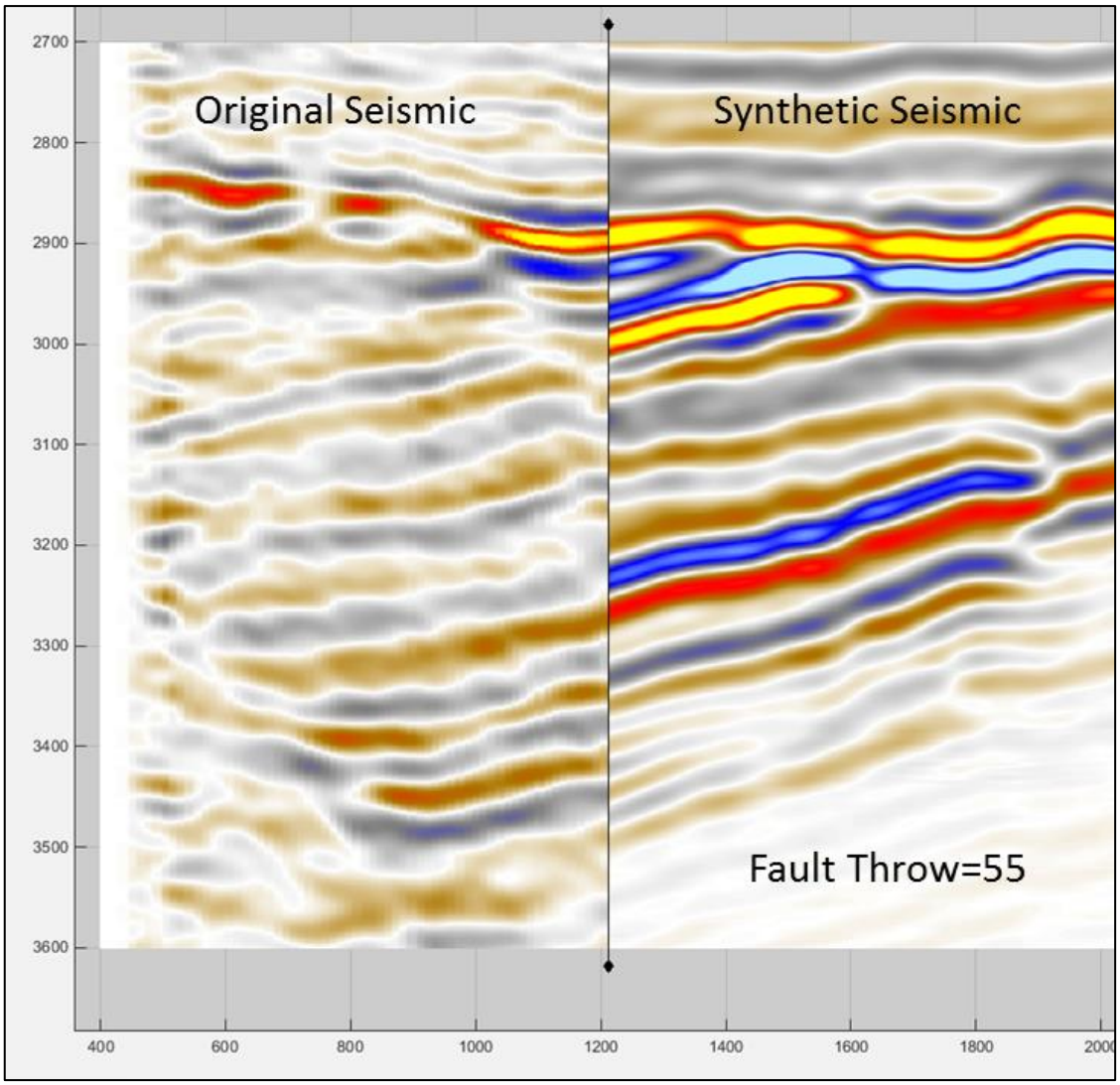

Figure 70: *Comparison between Original Seismic line (left) and Synthetic Seismic (right) at X= 1205 m for Fault Throw= 55 m (Base Case). The reflectors overlap perfectly (Ref. CES Software)*

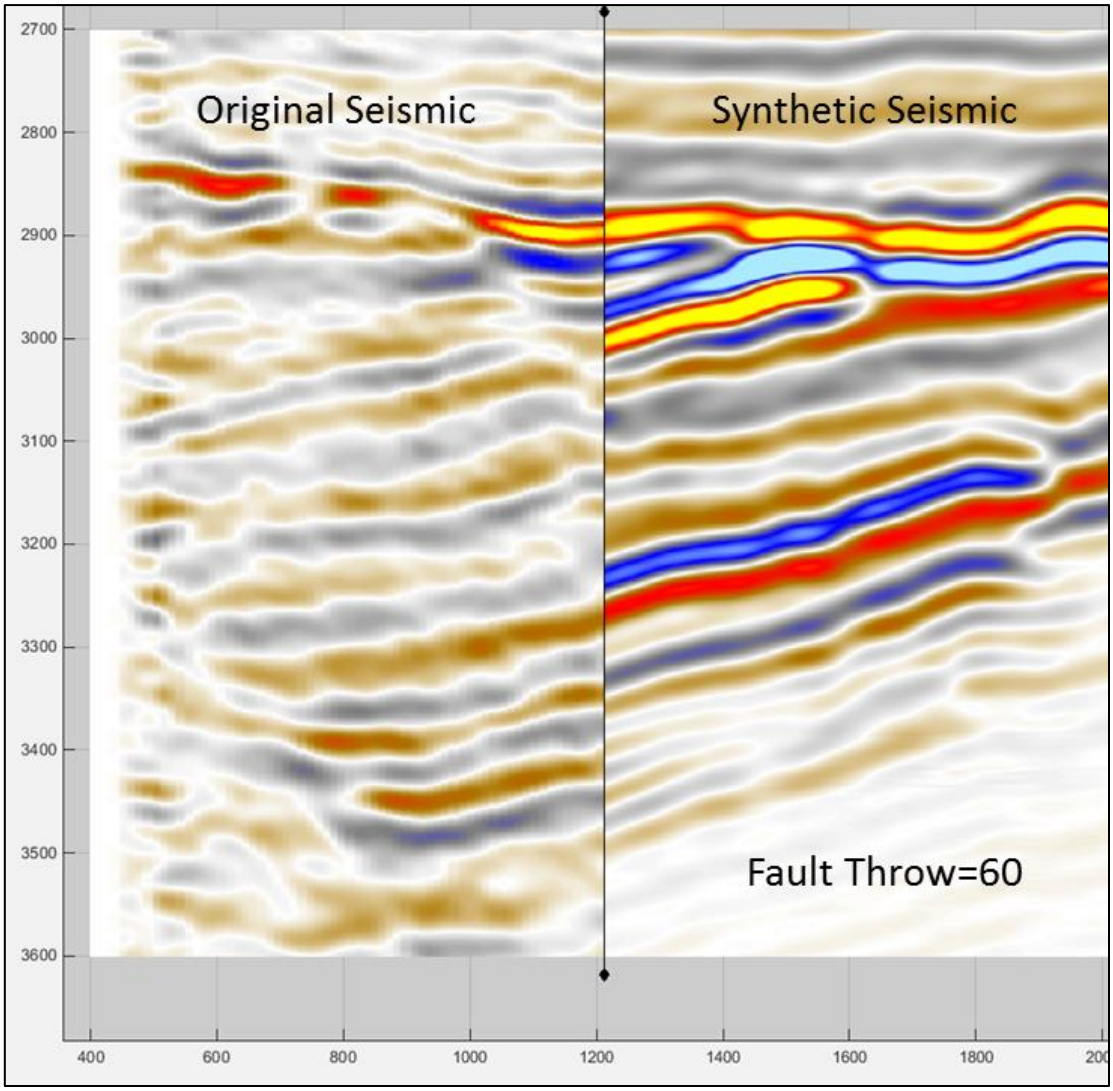

Figure 71: *Comparison between Original Seismic line (left) and Synthetic Seismic (right) at X= 1205 m for Fault Throw= 60 m. The reflectors overlap perfectly (Ref. CES Software)*

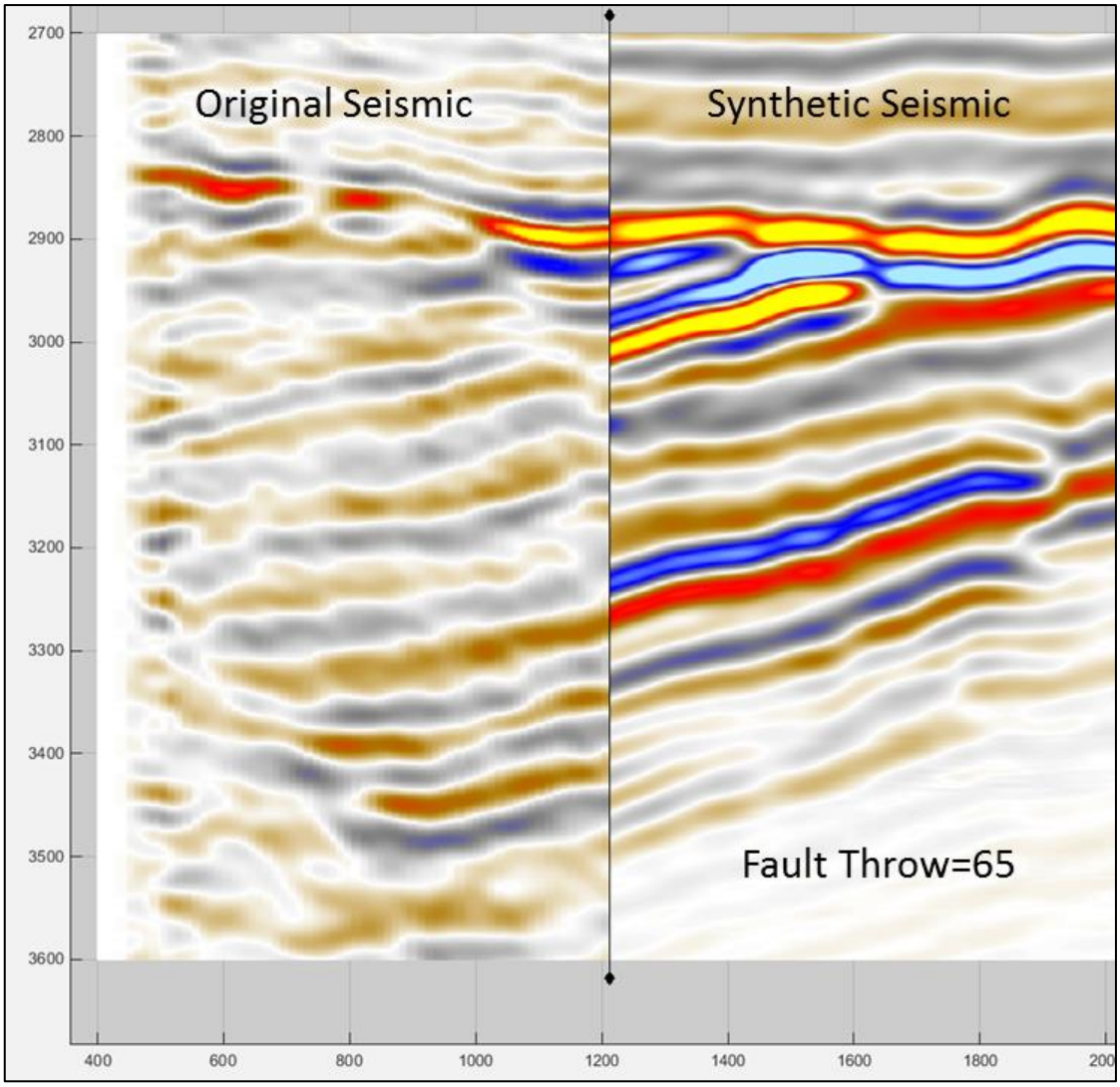

Figure 72: *Comparison between Original Seismic line (left) and Synthetic Seismic (right) at X= 1205 m for Fault Throw= 65 m. The reflectors overlap perfectly (Ref. CES Software)*

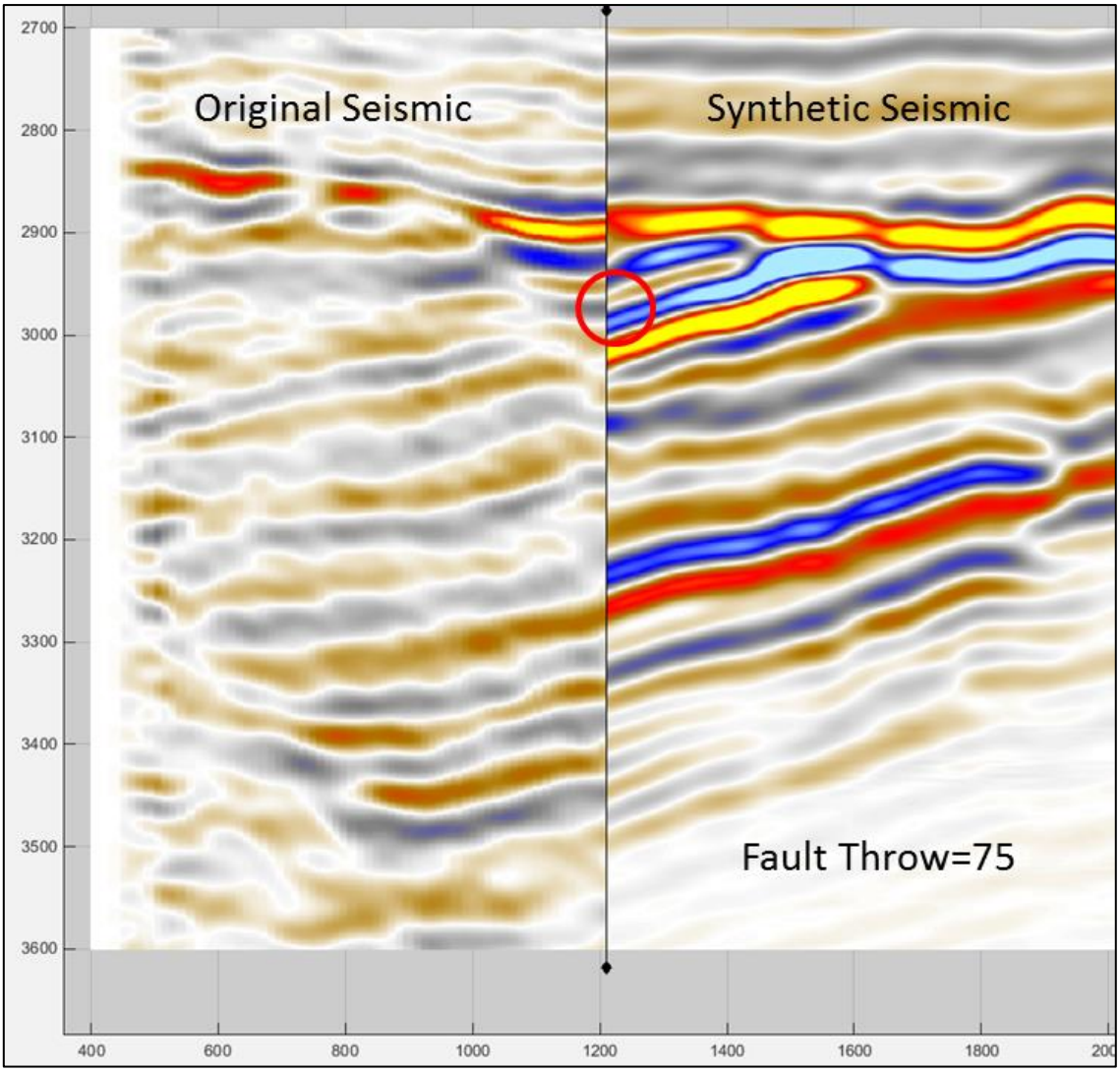

Figure 73: *Comparison between Original Seismic line (left) and Synthetic Seismic (right) at X= 1205 m for Fault Throw= 75 m. The reflectors do not overlap perfectly (Ref. CES Software)*

Comparison between Original Seismic line and Synthetic Seismic at X= 1250 m, for Fault Throw= 45 m, 50 m, 55 m (base case),60 m, 65 m and 75 m

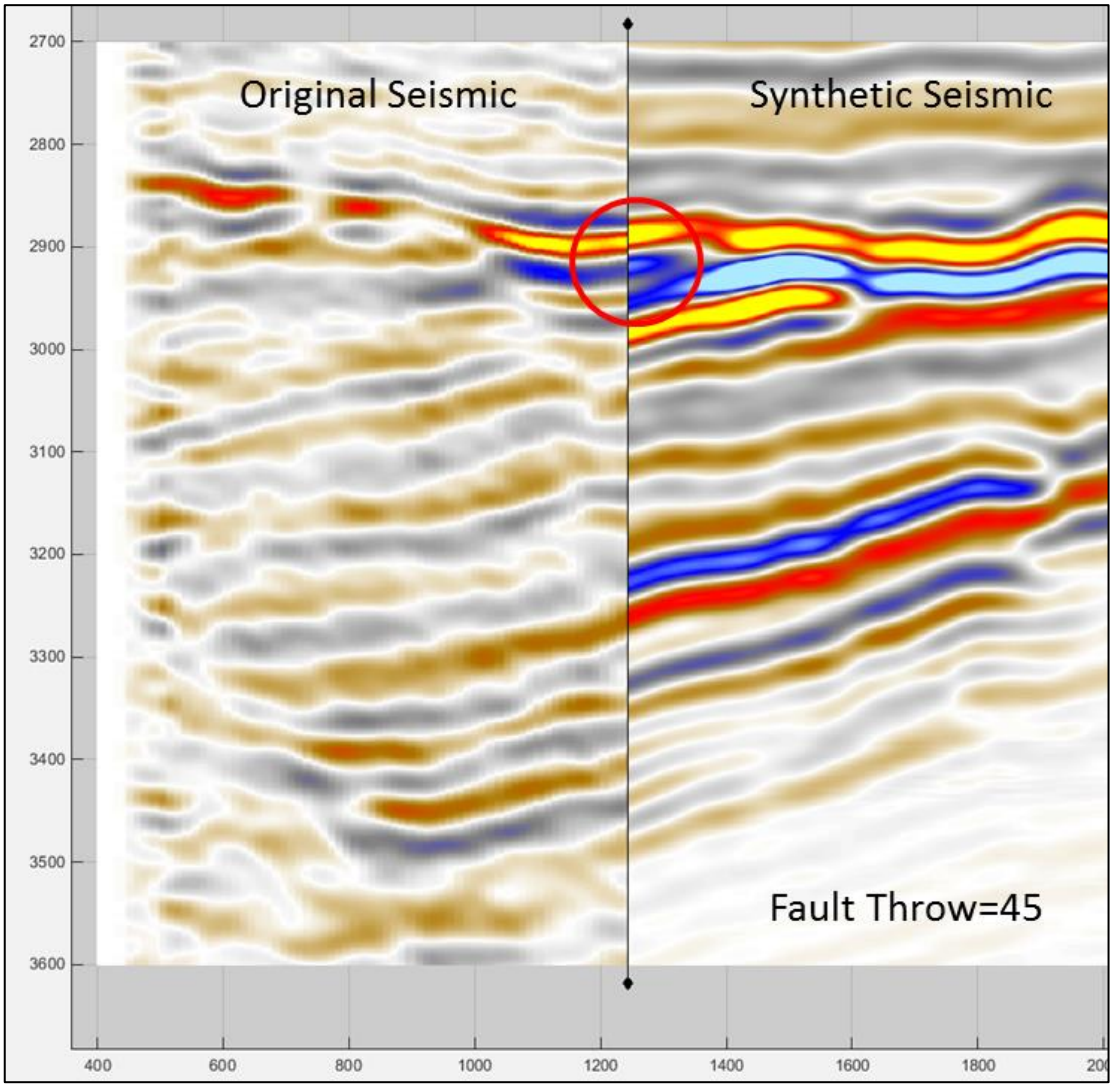

Figure 74: *Comparison between Original Seismic line (left) and Synthetic Seismic (right) at X= 1250 m for Fault Throw= 45 m. The reflectors do not overlap perfectly (Ref. CES Software)*

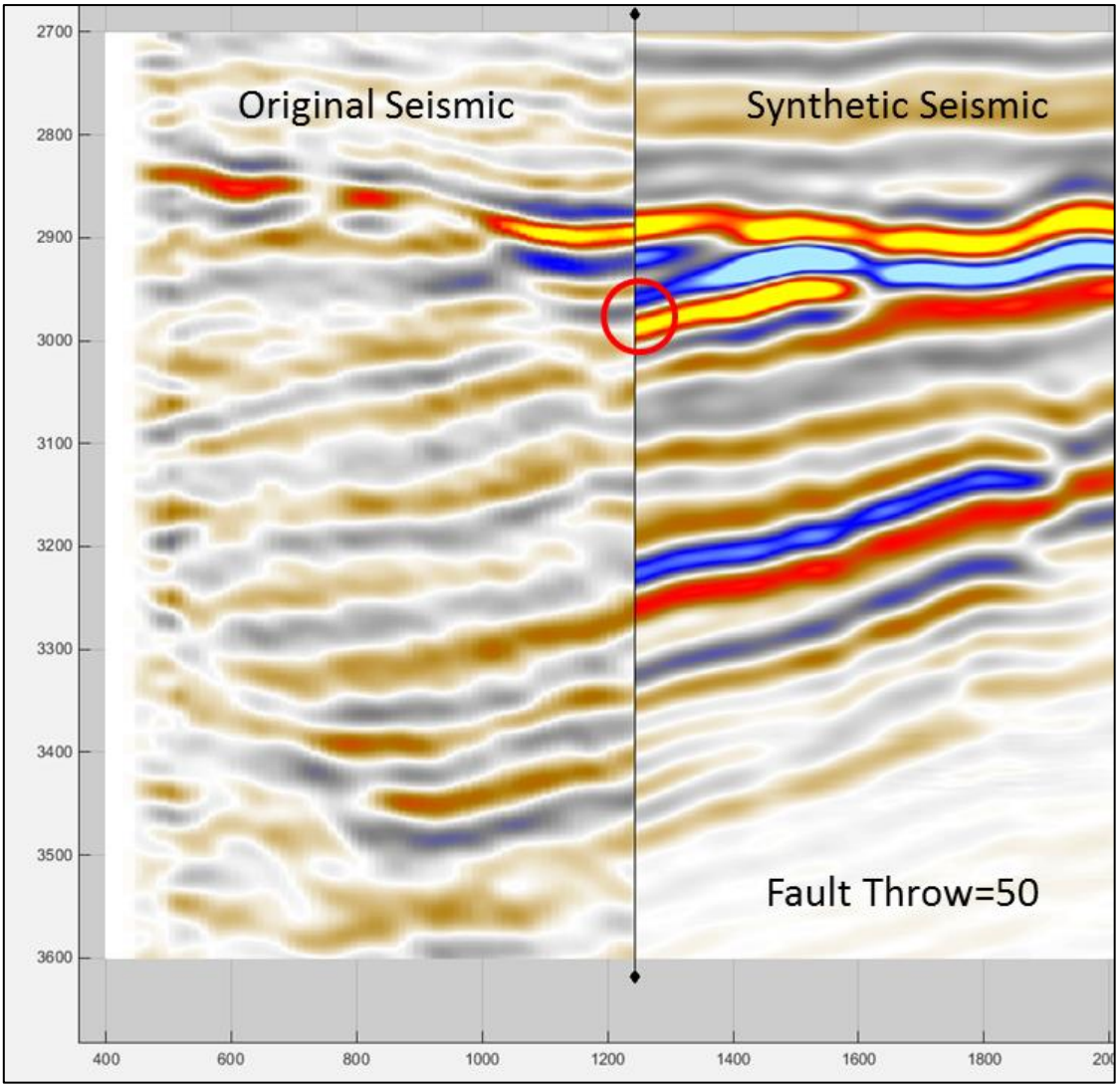

Figure 75: *Comparison between Original Seismic line (left) and Synthetic Seismic (right) at X= 1250 m for Fault Throw= 50 m. The reflectors do not overlap perfectly (Ref. CES Software)*

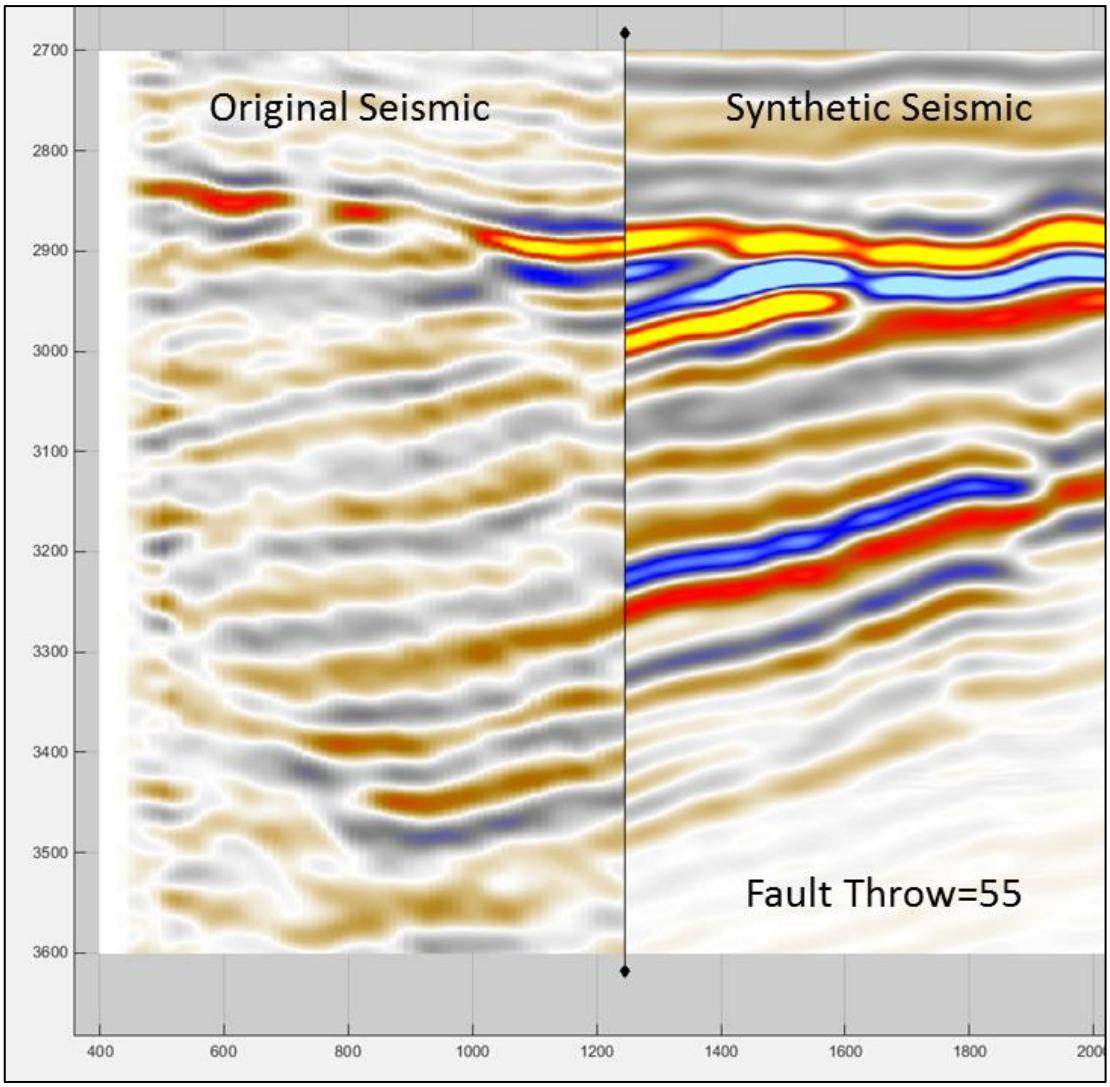

Figure 76: *Comparison between Original Seismic line (left) and Synthetic Seismic (right) at X= 1250 m for Fault Throw= 55 m (Base Case). The reflectors overlap perfectly (Ref. CES Software)*

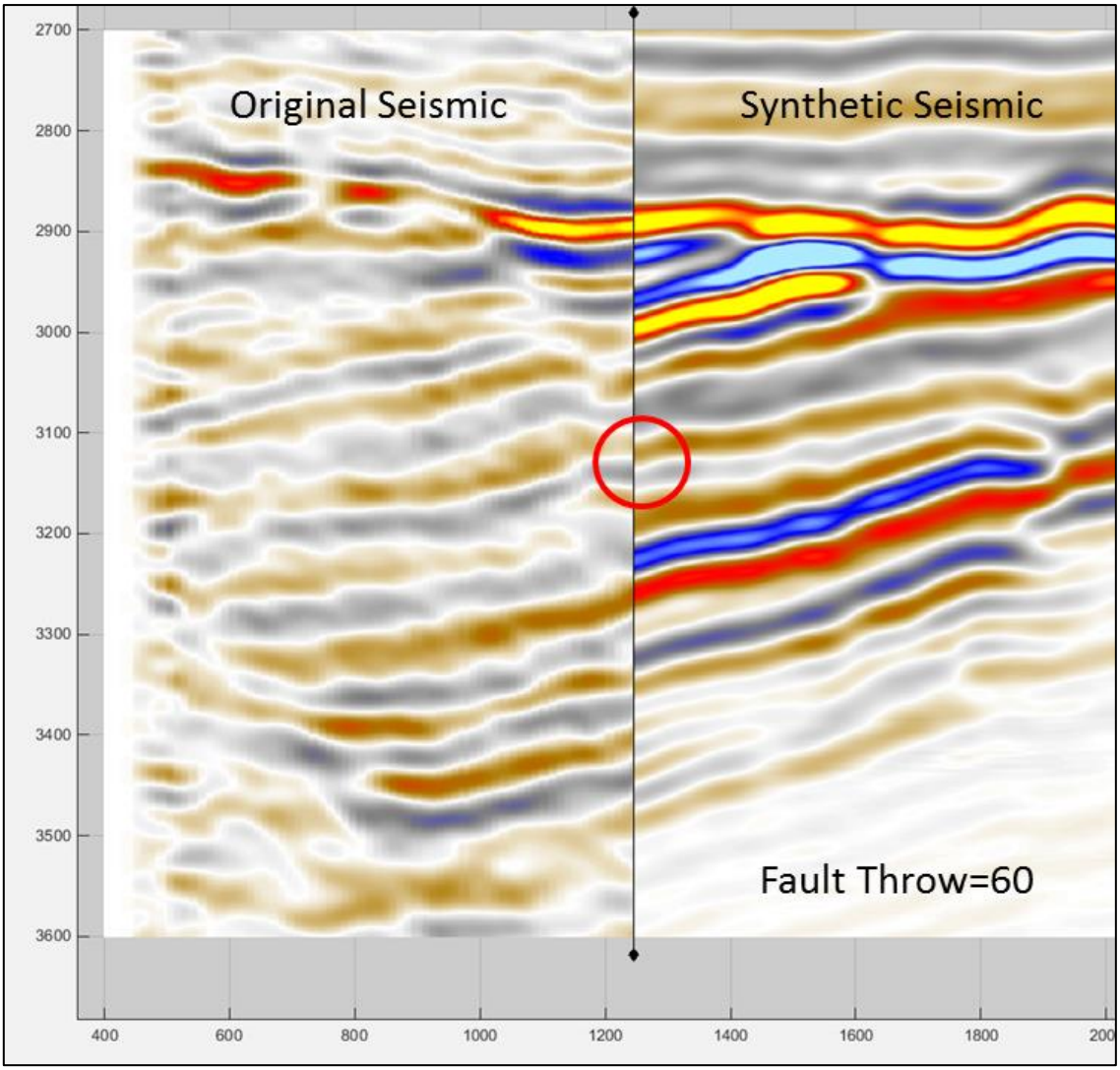

Figure 77: *Comparison between Original Seismic line (left) and Synthetic Seismic (right) at X= 1250 m for Fault Throw= 60 m. (Ref. CES Software)*

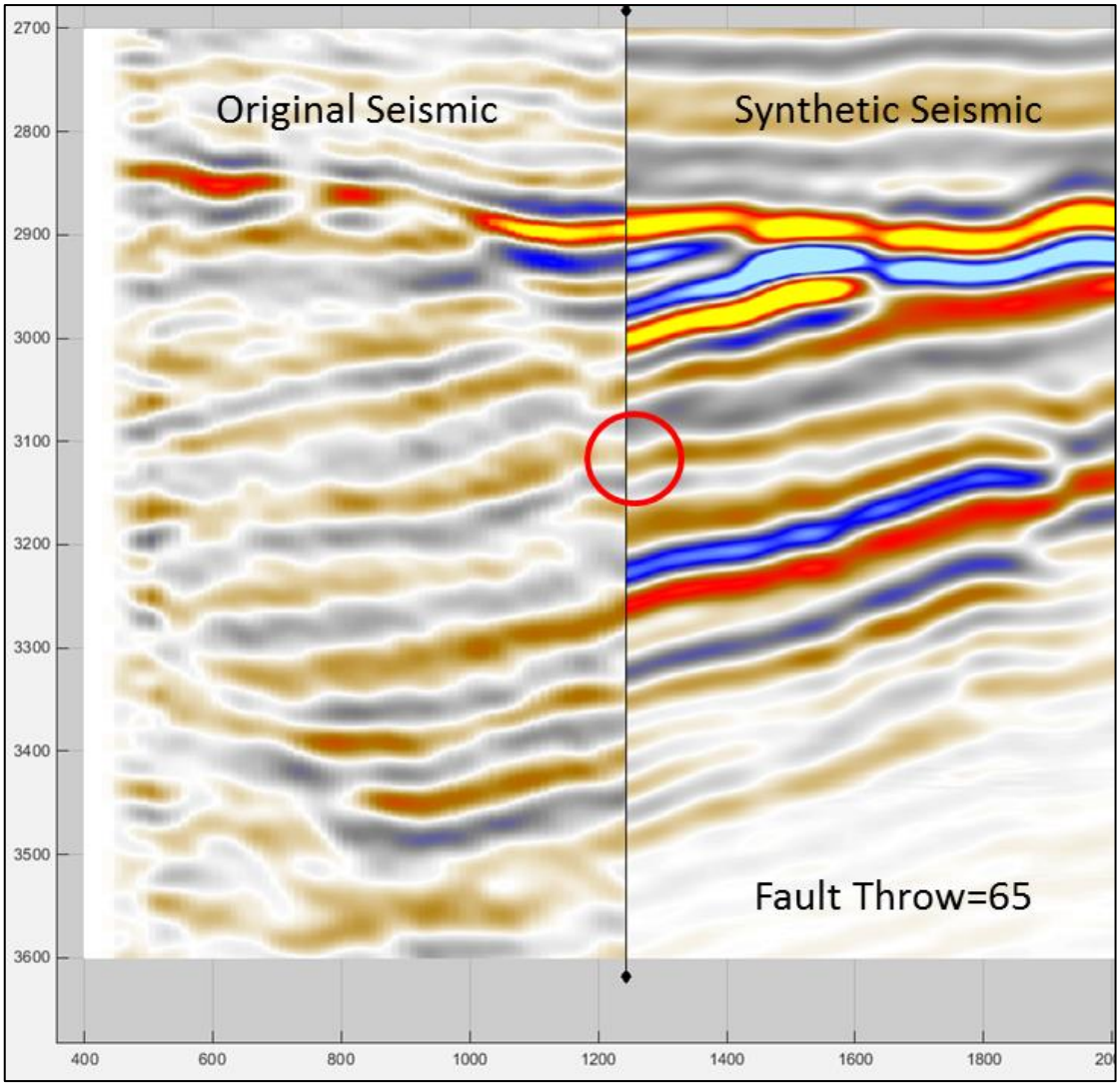

Figure 78: *Comparison between Original Seismic line (left) and Synthetic Seismic (right) at X= 1250 m for Fault Throw= 65 m. (Ref. CES Software)*

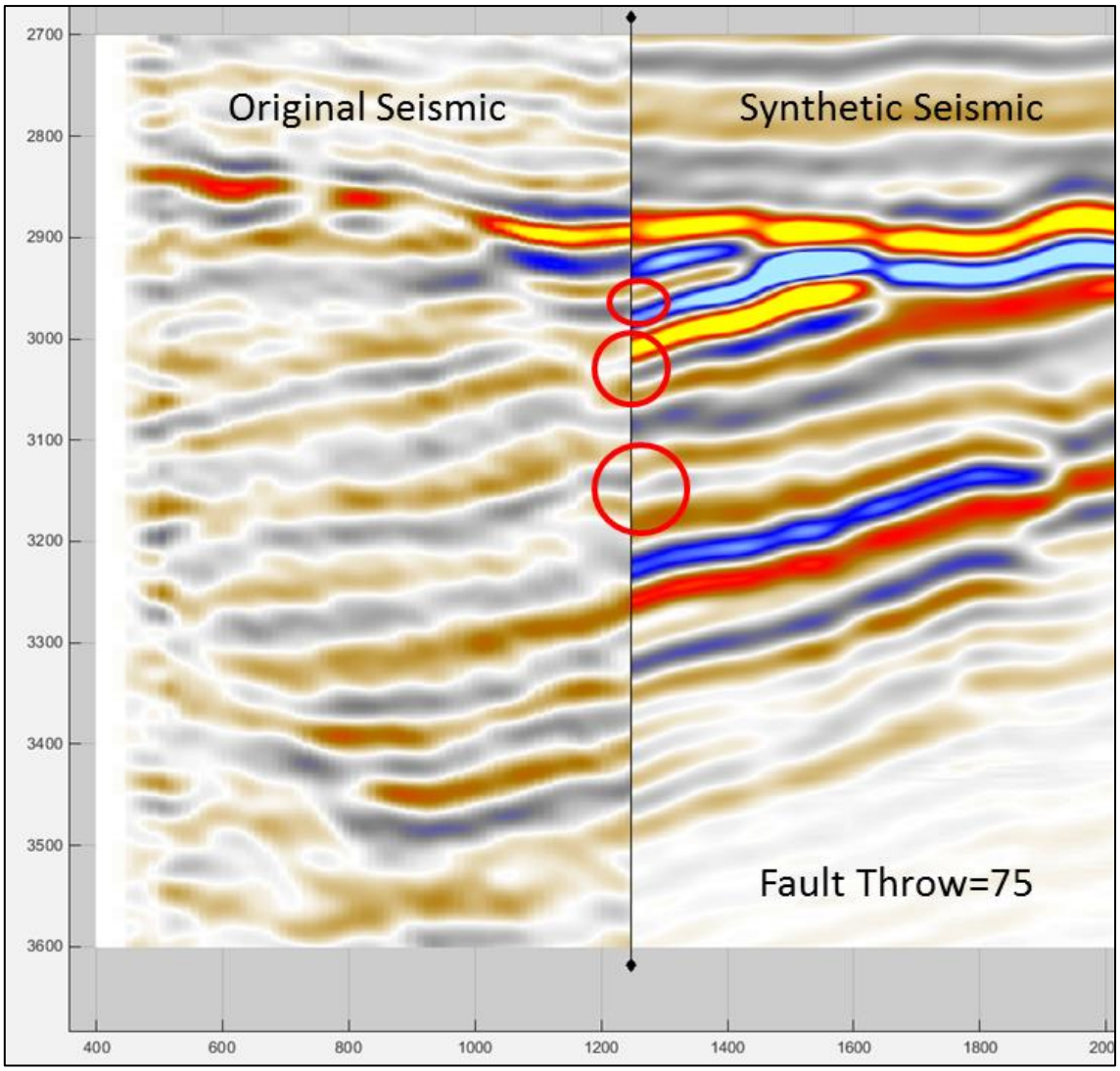

Figure 79: *Comparison between Original Seismic line (left) and Synthetic Seismic (right) at X= 1250 m for Fault Throw= 75 m. The reflectors do not overlap perfectly (Ref. CES Software)*

Appendix D

WebGS Input Parameters

Forward Simulations

For the forward simulations, the parameters that were used as input are in figure 80.

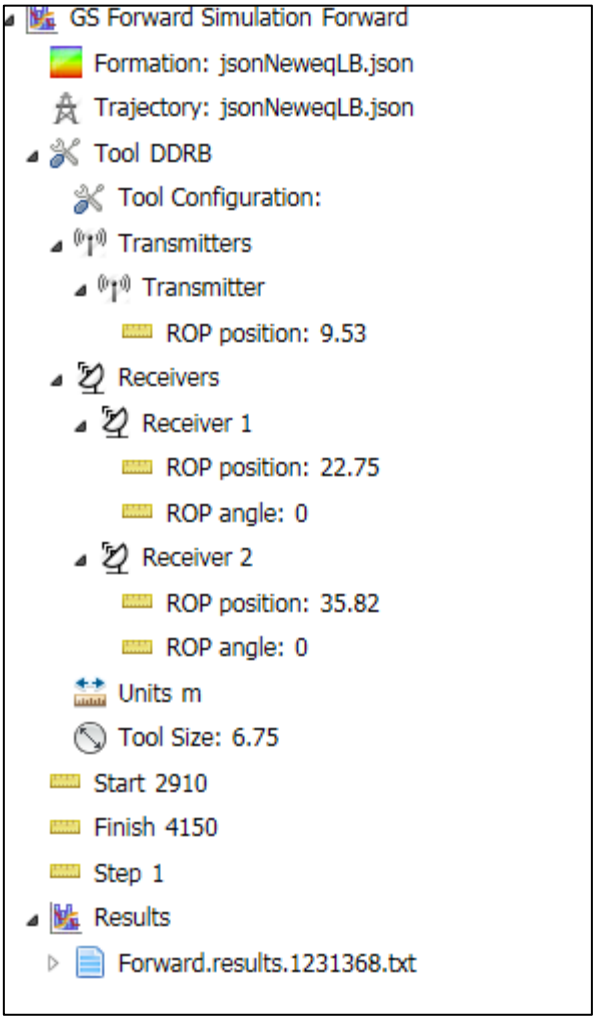

Figure 80: *Input parameters during Forward simulation in WebGS (Ref. WebGS Software)*

The json file containing the geomodel from CES is given as input in Formation and Trajectory.

The tool is called the DDRB[4] tool. Only two receiver configuration was used in this study. The position of the transmitter and the two receivers was given as inputs. This was based upon the tool configuration used real time at the time of drilling the 34/8-A-16 H well. The transmitter-receiver spacing is 13.22 m and 26.29 m for receivers 1 and 2 respectively.

The Start and Finish was decided based on the trajectory and the area under consideration for this study. The Start was set to 2910 m and the Finish was set to 4150 m. This is the measured depth on the trajectory that remains within the zone of interest.

The Step size is the size interval at which the simulations would be performed. This represents the interval at which each simulation will take place, on the measured depth. This was set to a value of 1 m.

The frequencies for which each receiver would work can be made to vary from the various frequencies that the tool operates upon, namely, 2 kHz, 6 kHz, 12 kHz, 24 kHz, 48 kHz and 96 kHz. For the forward simulations, all receivers were set to work with all frequencies.

[4] GeoSphere tool representation in WebGS

Inverse Simulations

For the Inverse simulations, the parameters that were used as input are shown in figure 81.

The json file containing the geomodel from CES and the forward simulation results are given as inputs.

The tool configuration does not change and is the same for both Forward and Inverse simulations. Hence, only two receivers were used and the transmitter-receiver spacing is 13.22 m and 26.29 m for receivers 1 and 2 respectively.

The start and finish remain the same as in case of forward simulation.

The Step size was set to a value of 2 m. This represents the distance on the measured depth at which each inversion would be performed.

The frequencies for which each receiver would work are made to vary during the Inversion. The first receiver operated with 6 kHz, 12 kHz and 24 kHz. The second receiver operated with 2 kHz, 6 kHz and 12 kHz. This was based upon the tool setting real time at the time of drilling of the well.

The results obtained during the semester thesis titled *Software Simulations of an Ultra Deep Resistivity Tool using Synthetic Geo-models, December 2015, NTNU,* suggest that the lower frequency values (2 kHz, 6 kHz) go deeper into the formation, whereas, higher frequency values (24 kHz, 48 kHz, 96 kHz) go shallower into the formation but give a better resolution (Arora P., 2015).

Hence, this setting of restricted frequencies is justified and must give a good image and overview of the surrounding formation.

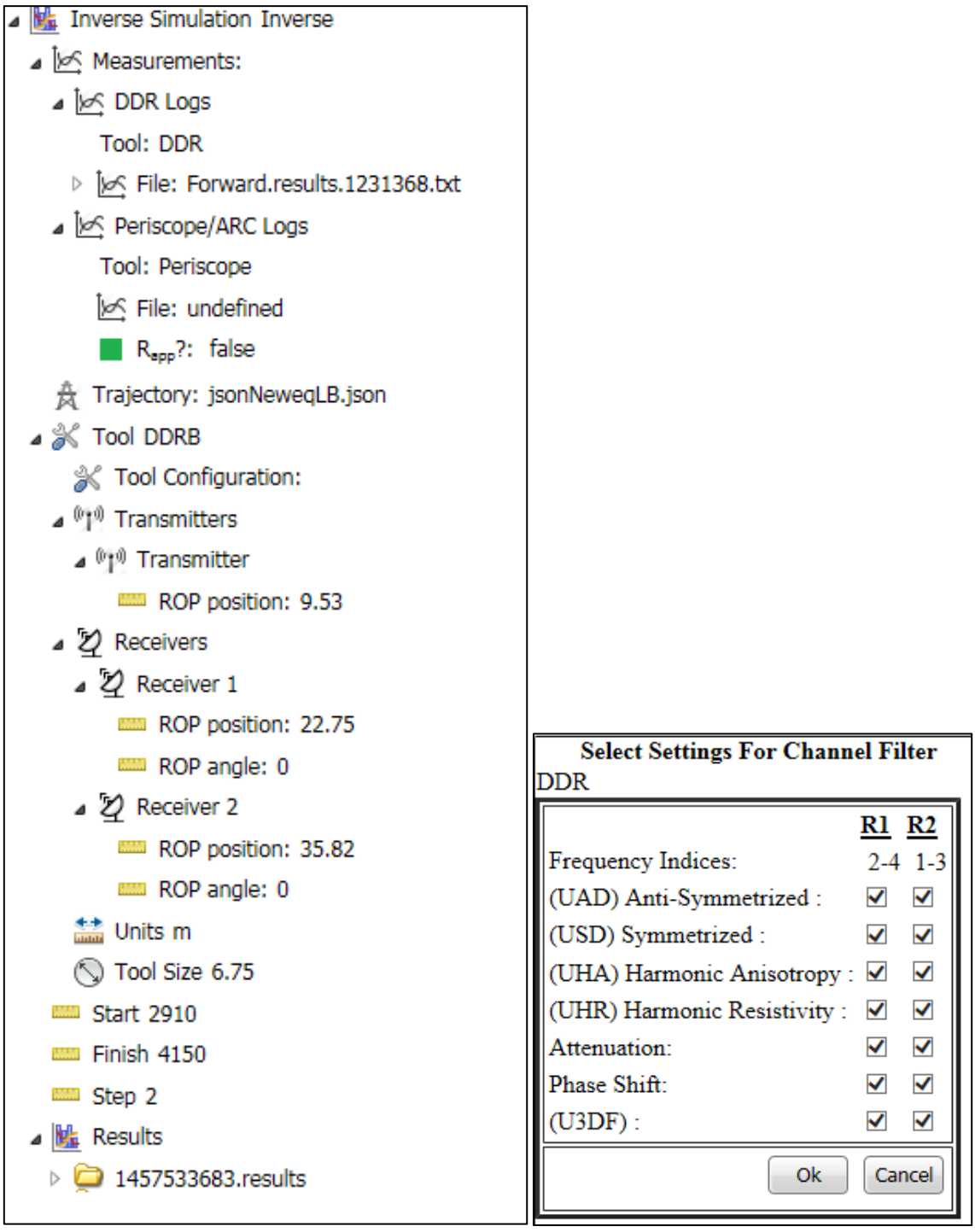

Figure 81: *Input parameters during Inverse simulation in WebGS (Ref. WebGS Software*